Microscopic Theory of Photon Bose-Einstein Condensation

Dissertation
zur
Erlangung des Doktorgrades (Dr. rer. nat.)
der
Mathematisch-Naturwissenschaftlichen Fakultät
der
Rheinischen Friedrich-Wilhelms-Universität Bonn

von
Michael Rolf Otto Kajan
aus
Troisdorf, Deutschland

Bonn, 22.05.2024

Angefertigt mit Genehmigung der Mathematisch-Naturwissenschaftlichen Fakultät der Rheinischen Friedrich-Wilhelms-Universität Bonn

1. Gutachter:	Prof. Dr. Johann Kroha
2. Gutachter:	Prof. Dr. Corinna Kollath
Tag der Promotion:	22.05.2024
Erscheinungsjahr:	2024

Abstract

We introduce a novel approach for analysing light-matter interactions within driven-dissipative environments. Our study centres on the interaction between dye molecule solutions and photonic cavity modes, mediated by Jaynes-Cummings coupling. These dye molecules exhibit discrete electronic and rovibrational energy levels influenced by the surrounding thermal environment imposed by the solvent.

The principal contribution of this work lies in the development of a mapping that links the discrete-level structure of dye molecules to auxiliary bosons, subject to an additional operator constraint. This mapping facilitates the application of field theory methods, particularly leveraging the Schwinger-Keldysh formalism to address general non-equilibrium scenarios. Especially, this framework allows for the exact implementation of the operator constraint. It enables us to consider Markovian and non-Markovian baths coupled to the molecules. Including non-Markovian baths is of significant importance in achieving thermalisation beyond the occupation of levels and allowing to imprint the thermal fluctuation-dissipation relation onto the spectra.

The main goal of this work is to investigate the emergence of phase coherence in the photon field. Our method enables a unified treatment of photon field fluctuations and coherence dynamics, allowing the spontaneous breaking of the $U(1)$ symmetry inherent in the Jaynes-Cummings interaction. The large dye reservoir is incorporated via a simplified Dynamical-Mean-Field Theory leveraging an expansion in the dye molecule density. We investigate the implications of broken $U(1)$ symmetry in an open-driven context and validate the corresponding Ward identity in the phase of the Bose-Einstein condensate. This sheds light on the intricate interplay between coherence, fluctuations, and symmetry in light-matter coupled systems within driven-dissipative environments.

Acknowledgements

This thesis would not have been possible without the countless people who supported me and I want to express my gratitude for their support here.

I want to thank my supervisor, Hans, for the opportunity to work on this fascinating and challenging topic. His group is full of talented people, and working with them was an amazing experience. I want to thank here some of them in particular. This work would not have been possible without my Keldysh-comrades Tim, Francisco and Michael. The various and long talks and fiddling around with Keldysh/2-PI/DMFT were invaluable, and I feel this work is the culmination of these. My thanks also go out to the current photon BEC practitioners, Sayak and Aya. The discussions about it helped me tremendously to understand the key ingredients. I also want to thank our equilibrium team, Marvin and Ulli. Discussing Fermions with you and organising the various lectures was a great pleasure!

The Fachschaft Physik has been my second home over my studies, and seeing it flourish fills me with joy. Johann Ostmeyer and Kevin Lukas in particular made my studies so much more enjoyable and insightful.

The experiments in the Weitz group in Bonn are at the heart of this thesis. The tremendous inside and intuition they have for this system is stunning. I want to thank here in particular Frank Vewinger, Julian Schmitt and Martin Weitz for the discussions and explanation of their marvelous experiments. My thanks also go to my fellow ML4Q colleague Andreas Redmann for the discussions and back-and-forth bouncing of ideas.

I have been part of the SFB OSCAR now for quite some time and i want to extend by gratitude to this amazing collaboration. In particular, I want to thank Enrico Stein and Axel Pelster from Kaiserslautern for the many discussions over the years.

The support from my parents and my brothers over the years was invaluable. A special thanks goes to my girlfriend Rieka. Without you, I could not have done this.

Contents

Preface

The study of light-matter interactions is at the heart of modern condensed matter physics. New experimental platforms are being discovered continuously, moving ever closer to the realm of Quantum optics. We will focus here on organic materials coupled to light in micro-cavities. Organic molecules, with their diverse electronic structures and optical properties, offer the opportunity to study a broad range of phenomena. They can reach from weak to strong coupling, and from their intrinsic driven-dissipative nature, life at the border between equilibrium and non-equilibrium. This allows these platforms to show a diverse set of phenomena, from lasers [1] and photon Bose-Einstein condensates (BEC) [2–4] over exciton-polariton condensates [5, 6] to single-photon sources [7]. The inherent open nature makes these systems a perfect testing field for studying the competition of coherent and incoherent processes.

We will focus on dye molecule solutions in a cavity. This system was demonstrated to form a BEC of light [2]. The dense liquid leads to rapid thermalisation of the dye, imprinting thermal equilibrium properties onto the emission and absorption spectra of the solution. This translates to a thermalisation of the emitted light, such that a Bose-distributed photon spectrum can be observed. The BEC state also shows strong temporal coherence [8]. The emergence of this coherence has not been tackled in conjunction with the fluctuation spectrum till now. The incorporation of both of these properties of light in this strongly dissipative system is theoretically challenging. The large number of matter constituents does not allow for a treatment with numerically exact methods. On the other side, a rate equation approach is inherently semi-classical and relies on a classical distribution of photon and matter excitation, neglecting coherence effects. Additionally, as we will show, non-Markovianity will be necessary in various places. The central result of this thesis is an auxiliary particle representation of the driven-dissipative dye molecule solution in a thermal environment. It relies on mapping the molecule's discrete-level structure to auxiliary bosons with an additional operator constraint. This opens up the way to a rich variety of field theory methods, which are not applicable in the original representation due to the non-canonical commutation relations of the electronic operators. Within the field theory framework, the constraint can be implemented exactly, and photon fluctuation and coherence can be treated on the same footing. It allows the incorporation of Markovian and non-Markovian baths on general and flexible grounds. The drawback of Markovian baths is that they can not imprint a temperature onto the system. They can imprint occupation following thermal expectations if the coupling constants are chosen appropriately. However, they fail to imprint the crucial fluctuation-dissipation relation onto the system. This relation manifests in the spectra of correlation functions and is responsible for the Kennard-Stephanov relation between the molecule's absorption and emission spectra. Here, the two-time correlators are of particular interest, which the field theory method focuses on. The coherent photon field emerges with an intricate relation to the two-time correlator manifesting in the Hugenholtz-Pines relation, which we generalise to open systems.

The thesis is structured as follows.

In the first chapter, we introduce the experimental setup and a phenomenological explanation of the photon BEC. We will introduce the system's central Hamiltonian and show how the often employed master equation approach emerges. Here, we will encounter the central theme of this thesis, the phase coherence of light, and give the corresponding perspective on it from the master equation approach.

The second chapter is devoted to field theory methods in non-equilibrium many body systems. First, the Schwinger-Keldysh formalism will be introduced with a specific focus on bosonic open quantum systems. We will briefly outline how these systems can be treated numerically, solving for the two-time Green functions. Here, a central point are the Kadanoff-Baym (KB) equations involving self-energy kernels for which an adaptive time-stepper is developed. We will then go on exploring how the self-energies can be constructed in a conserving way. This leads us to the effective action formalism, where we will focus on the 2-particle irreducible effective action (2PI-EA). Within this formalism, we discuss relations between the usual Ward identities and the Ward identities obtained in the 2PI-EA, which will be necessary for later application to spontaneously broken symmetries.

The third chapter is devoted to the auxiliary particle theory. We introduce the mapping of the system to auxiliary particles, leading us to the necessity of imposing an operator constraint onto the dynamics. We show how this constraint can be implemented in a general non-equilibrium and open system setting. We discuss the formal consequences of a broken $U(1)$ symmetry in the photon sector and its influence on the equations of motion. Afterwards, a resummation technique inspired by Dynamical-Mean-Field-Theory (DMFT) is introduced to deal with large molecule reservoirs. We further discuss the Ward identities associated with the broken $U(1)$ symmetry in an open system setup and relate these to the limitation of the non-crossing approximation (NCA). The chapter is closed with comparisons to the cumulant expansion approach.

In the fourth chapter, we present results for a multi-mode cavity. We briefly recap all the processes included in the treatment. Afterwards, we discuss how the molecule spectra are obtained and contrast Markovian- and non-Markovian couplings to the solvent. It turns out that a non-Markovian coupling is necessary to implement the Kennard-Stephanov relation between absorption and emission spectra. We then turn to the discussion of the light in the cavity. First, we look at the photon dynamics in the normal state and show the thermalisation of the photon spectra. Here, two regimes are discussed. A pre-thermal stage shows the fluctuation-dissipation relation between the photon correlators but at an elevated temperature and a less dissipative thermal state, thermalising close to the temperature of the dye-reservoir.
We then turn to the condensed state. The condensate emerges energetically close below the fluctuation spectrum. Its energy is compared via Ward-identity, and the phases are analysed. The calculation necessarily includes anomalous photon propagators, which we will analyse afterwards. We close with a short discussion on the strong coupling regime.

Part I

Introduction to the photon BEC

Chapter 1

Fundamentals of the Photon BEC

The phenomenon of Bose-Einstein condensation (BEC) was for a long time believed to be reserved for massive particles. Already predicted in 1924-1925 by Einstein [9] applying the key insights of Bose on massive particles, it still took until 1995 [10] [11] to realise a BEC of massive bosons in an atomic gas. This triggered a rapid development such that quickly afterwards, various exotic atoms could be condensed, and even the BCS-BEC [12] crossover could be realised in 2005. Despite many fundamental concerns, in 2010 also, a BEC of photons could be realised by [2]. It is far from obvious that it is even possible to condense photons into a BEC state. In the case of massive bosons, the condensation is driven by a statistical enhancement due to the way how microstates are counted. It suppresses large spreads of the distribution of single-particle states. This leads to the famous Bose distribution, which in thermal equilibrium describes the particle number distribution by

$$b(\omega) = \frac{1}{e^{\beta(\omega-\mu)} - 1}\,, \tag{1.1}$$

where ω is the energy of the state and μ is the chemical potential. One of the key features of the distribution is the divergence for energies at μ. The reason why the chemical potential can be added in the first place is due to the conservation of the number of massive bosons. In this way, μ controls the total particle number given in a continuum limit by a density of states integral

$$N = N_0 + \int d\omega \rho(\omega) b(\omega) = N_0 + N_{ex}\,. \tag{1.2}$$

Here, N_{ex} is the number of particles above the ground state. In the continuum limit, the density of states at the ground state energy has zero measure. Therefore, if the ground state is not macroscopically degenerate, the occupation of the ground state N_0 needs to be added by hand. The formation of a BEC can be understood from here as follows. Increasing the chemical potential μ adds particles to the system, which distribute over the states of the system following the Bose distribution. But if the integral for the excited states N_{ex} is finite for $\mu = 0$, the occupation of these excited modes will saturate, and further increasing the particle number will occupy the ground state. Therefore, in the limit of large particle numbers, the ground state occupation will be of the order of the total particle number, which is then called a BEC. Note that this can also be achieved by tuning the temperature. It allows for a description in terms of either a critical particle number at a constant temperature or a critical temperature at a constant particle number. The requirement that $N_{ex}(\mu = 0)$ is finite is a condition on the density of states to vanish fast enough at the ground state energy. It also entails that the ground state is not macroscopically degenerate. The density of states of free particles in

dimensions $D > 2$ allows for a BEC to form. In trapped gasses [13], the density of states changes due to the trapping potential, e.g. for harmonically trapped gases also in $D = 2$, a BEC in the thermodynamics limit can be formed. In the resulting state, essentially all particles occupy the same single-particle wavefunction. This led Gross [14] and Pitaevskii [15] to the equations of motion of this single particle wavefunction, the Gross-Pitaevskii equation. As a key feature, it explicitly describes the BEC as a coherent wavefunction of the particle in the condensate. Photons are different in various regards from massive bosons. Most importantly, for the present case, their particle number is not conserved since they are gauge bosons of the electromagnetic force. The profound consequence of this is that no chemical potential can be added and the temperature determines the particle number. This leads to black body radiation [16] and a particle number scaling of $N \propto T^3$. Photons also do not directly interact with each other, unlike massive bosons. Therefore, the thermalisation process is vastly different. Where in the case of massive bosons collisions lead to thermalisation, it is emission and absorption processes with a thermal reservoir leading to a thermal distribution of light in the black body case. This process is not photon number conserving due to the conversion. These issues are intimately linked since the heat bath and the particle bath are the same. Disentangling these baths is the major challenge in achieving photon condensation.
This leads to three main requirements that need to be met to create a photon BEC: a thermalisation process that conserves photon number; a mechanism acting like a chemical potential, which allows for tuning the photon number independent of temperature; and, thirdly, a density of states allowing for the formation of a BEC. All these criteria could be attained by [2] in an optical microcavity filled with a fluorescent dye medium.

The experimental setup can be seen in Fig. 1.1. This system uses a microcavity with two curved mirrors to impose an effective harmonic potential onto the photon states. The longitudinal wavenumbers give a natural low-energy cut-off, on top of which the transversal modes are energetically equally spaced due to the harmonic potential. A dye solution is filled between the mirrors and kept at room temperature. It serves as a thermalising medium and a means through which the photons can be injected into the cavity modes. The dye is pumped via an external laser, which is blue detuned wrt. to the cavity modes and enters the cavity at a 45° angle. This prevents the cavity modes from being directly populated by the pump laser. Due to the strong reservoir coupling of the dye liquid, it thermalises rapidly so that the emitted photon spectrum is thermally distributed, as seen in Fig. 1.2. Upon reaching a critical pump strength and with this a critical particle number, the lowest transversal mode developed a peak, indicating the onset of BEC. In the following, we will detail how this setup meets the aforementioned requirements.

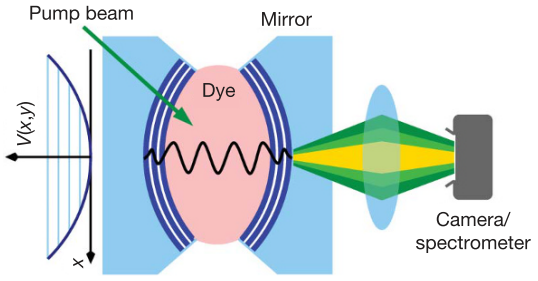

Figure 1.1: Scheme of the experimental setup. The trapping potential $V(x, y)$ for the two-dimensional photon gas imposed by the curved mirrors. [2]

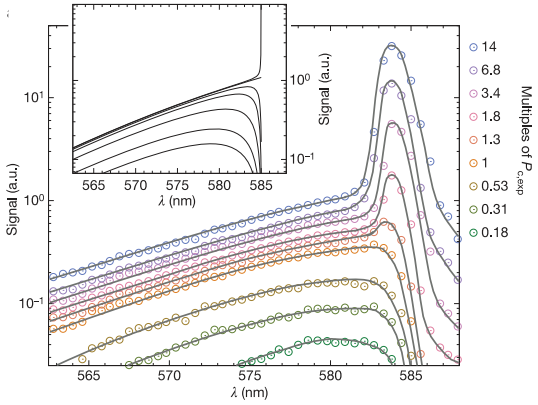

Figure 1.2: Spectral intensity distribution [2].

1.1 Thermalisation through the dye medium

The key ingredient for a number conserving thermalisation process are the dye molecules, in the present case mostly rhodamine 6G [2]. The dye is dissolved in a solvent, which is optically transparent at the cavity modes and minimises non-radiative losses [1], achieving a quantum efficiency of around 95%. The solution is kept at room temperature of $T \approx 300$ K. Even though tremendously complicated in the details, the physical picture of the dye molecules can be understood by the Franck-Condon principle, see Fig. 1.3. Here, we consider two electronic states, each having a vibrational substructure, which might be approximated by a harmonic oscillator around its respective minimum. By absorbing a photon, the electronic state changes abruptly from its ground state to its excited state. The process is so fast that the position of the heavy nuclei does not change, so in the new electron configuration, it is not in the equilibrium position of the excited state oscillator. Higher vibrational modes are excited by this transition, namely the one with the most spatial overlap to the initial vibration configuration. In a dense medium, this excited vibrational state relaxes quickly due to collisions to the new equilibrium position, so the lowest vibrational state [19]. The transition to the electronic ground state follows the same principle: the vibration configuration of the ground state with the most overlap with the vibration ground state of the excited electronic state. Here again, the equilibrium position changes and then relaxes back to the original ground state configuration. Transitions are most likely for wave functions of the initial and final states having a significant overlap at the atomic positions in the instant of absorption. This creates a symmetry between absorption and emission, where the initial and final vibrational states are interchanged. These processes result in an average conservation of the photon number but a net loss of photon energy between absorption and emission, the Stokes shift, giving rise to a characteristic shape of absorption and fluorescence spectra, e.g. for rhodamine 6G Fig. 1.4. This energy shift can be expressed by the sum rule of the frequency of the photon Ω, the

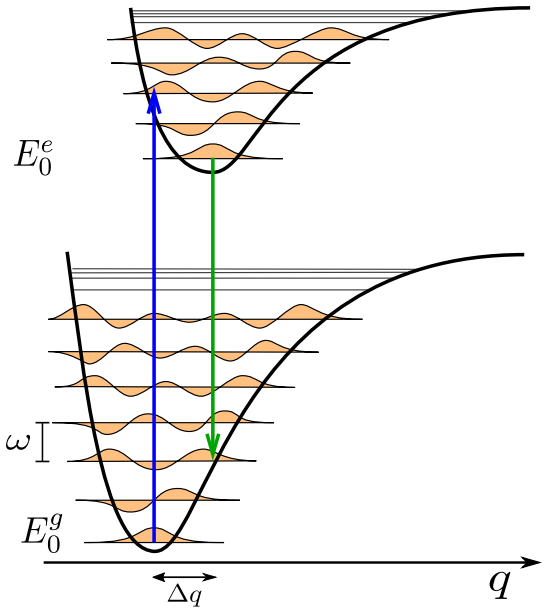

Figure 1.3: Franck–Condon principle energy diagram. The minima of the electronic potentials are shifted wrt. to each other. The rovibrational states involved in the absorption and emission are those that correspond to a minimal change in the nuclear coordinates and, therefore, most spatial overlap (adapted from [17]) .

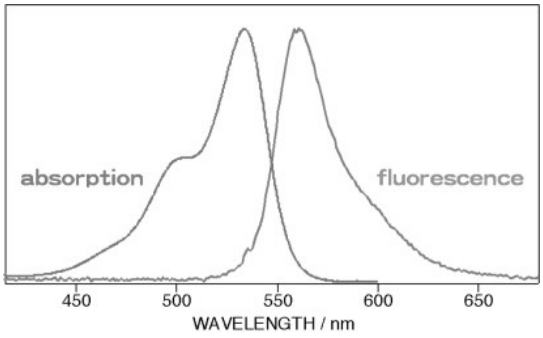

Figure 1.4: Absorption and fluorescence spectrum of rhodamin 6G [18].

frequency of the vibrations ω and the electronic level splitting Δ as

$$\Omega + n_g\omega = \Delta + n_e\omega\,.$$

If the relaxation of the vibrational state happens as fast as assumed, the thermal occupations of the phonons state in the respective electronic states $n_{e/g}$ must be related by $n_g/n_e = e^{\beta\delta}$, with the detuning $\delta = \Omega - \Delta$. In this case, the Kennard-Stepanov relation [1] for absorption and fluorescence spectra follows

$$\frac{B_{abs}(\delta)}{B_{em}(\delta)} = e^{\beta\delta}\,. \tag{1.3}$$

This relation usually holds around to the zero phonon line, at a detuning $\delta = 0$, but might be violated at larger detuning, strong coupling or when relaxation is not rapid enough to thermalise the vibrations in the excited state.

1.2 Particle number control

The control of the photon number inside the cavity can be understood from a rate equation approach, considering the molecules as effective two-level systems. Here molecules emit and absorb photons with a rate B_{em} and B_{abs} respectively in a process

$$\gamma + g \rightleftharpoons e$$

Additionally, the molecules are pumped by an external laser with a rate $\Gamma_\uparrow$. The pump laser is blue-detuned to the cavity modes, so it can not directly populate them. Processes which lead to a loss of molecule excitations are described by $\Gamma_\downarrow$. Either they decay non-radiatively or emit out of the cavity. The cavity modes themselves couple out of the cavity with a rate κ due to the finite reflectivity of the mirrors. This leads us to rate the equation for the number of excited molecules M_e and a single photon mode occupation n as

$$\partial_t M_e = \Gamma_\uparrow M_g - \Gamma_\downarrow M_e + B_{abs}M_g n - B_{em}M_e(n+1) \tag{1.4}$$

$$\partial_t n = -\kappa n + B_{em}M_e(n+1) - B_{abs}M_g n \tag{1.5}$$

In a steady state, we can compute the photon occupation as

$$n = \frac{1}{\frac{\kappa}{B_{em}M_e} + \frac{B_{abs}M_g}{B_{em}M_e} - 1}\,. \tag{1.6}$$

If we work in a regime where $B_{em}M_e \gg \kappa$, so the emission rate is far larger than the cavity loss, we might use the Kennard-Stepanov relation to define a chemical potential for the photon by

$$\frac{B_{abs}M_g}{B_{em}M_e} = e^{\beta(\delta-\mu)} \qquad \text{with} \quad \mu = -k_B T \log(M_g/M_e)\,. \tag{1.7}$$

The ratio of ground and excited state molecules can be obtained from the steady state as

$$\frac{M_g}{M_e} = \frac{\Gamma_\uparrow + B_{abs}n}{\Gamma_\downarrow + B_{em}(n+1)}\,. \tag{1.8}$$

With this, the chemical potential depends on the pump rate and the photon occupations inside the cavity. From here, we conclude that the photon occupation follows a Bose distribution with a chemical potential which can be tuned independently of the temperature via the pump rate.

$$n = \frac{1}{e^{\beta(\delta-\mu)} - 1}\,.$$

[1] For simplicity, we assume here the same vibration structure in the ground and excited state.

1.3 Density of states

The light is trapped in a cylindrical microcavity, which dispersion relation in the presence of the dye solution [20] is given by

$$\omega_k = \frac{c}{n}\sqrt{k_r^2 + k_z^2(r)}\,.$$

Here, the longitudinal wavenumber is given by $k_z(r) = \pi q/D(r)$ with $D(r)$ being the distance between the mirror as a function of the radial coordinate on the mirror. For a symmetric spherical cavity with curvature R it is given by $D(r) = D_0 - 2(R - \sqrt{R^2 - r^2})$. Experimentally, the curvature is far larger than the radial coordinate $R \gg r$ and therefore $D(r) \approx D_0 - r^2/R$. Additionally the mirror are rather far apart such that $D_0 \gg r^2/R$, so that we can use $k_z(r) \approx \frac{\pi q}{D_0}(1 + \frac{r^2}{RD_0})$. This allows us to write the dispersion relation in paraxial approximation as

$$\begin{aligned}\hbar\omega_k &= \hbar\frac{c}{n}k_z\sqrt{1 + \frac{k_r^2}{k_z^2}} \approx \hbar\frac{c}{n}k_z + \frac{1}{2}\frac{c\hbar}{n}k_r^2\frac{1}{k_z} \approx \hbar\frac{c}{n}\frac{\pi q}{D_0}(1 + \frac{r^2}{RD_0}) + \hbar\frac{1}{2}\frac{c}{n}k_r^2\frac{1}{\pi q}(D_0 - \frac{r^2}{R}) \\ &\approx \left(\frac{c}{n}\right)^2\frac{\hbar\pi qn}{cD_0} + \frac{1}{2}\frac{\hbar\pi qn}{cD_0}\frac{2c^2}{n^2RD_0}r^2 + \frac{1}{2}\left(\frac{\hbar\pi qn}{cD_0}\right)^{-1}\hbar^2k_r^2 \end{aligned} \tag{1.9}$$

We already suggestively ordered the expression so that we can define $m = \frac{\hbar\pi qn}{cD_0}$ and $\Omega = \sqrt{\frac{2c^2}{n^2RD_0}}$ to obtain

$$\hbar\omega_k = m\left(\frac{c}{n}\right)^2 + \frac{1}{2}m\Omega^2r^2 + \frac{\hbar^2k_r^2}{2m}\,. \tag{1.10}$$

It emerges that the dispersion is equivalent to a particle with mass m in a two-dimensional harmonic trap with frequency Ω. The energy spectrum can be written in terms of transversal quantum numbers $n_{x,y}$ as

$$\omega = \Omega(n_x + n_y + 1) + \omega_0\,. \tag{1.11}$$

The energies are linearly degenerate, and the density of states above the ground state energy in a continuum limit is given by $\rho(\omega) = \frac{1}{\hbar\Omega}\omega/\Omega$. It vanishes linearly for $\omega \to 0$, allowing the particle number integral to be finite. A simple estimate of the critical particle number can be given by

$$N_c \approx 2\int_0^\infty d\omega\rho(\omega)b(\omega) = 2\left(\frac{k_BT}{\hbar\Omega}\right)^2\frac{\pi^2}{6} \tag{1.12}$$

The factor of two comes from the two independent polarisations of the photon.

1.4 Phase coherence

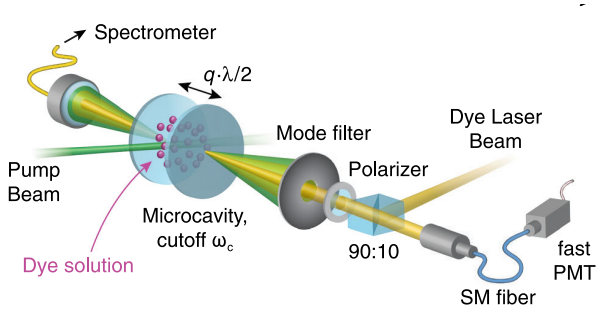

Figure 1.5: Overview of the experimental setup. From the emission out of the dye-filled micro-resonator, the condensate mode is filtered and, after a polariser, overlapped with the laser reference. The resulting beat signal is detected on a photomultiplier tube (PMT). Simultaneously, radiation transmitted through the second cavity mirror at the reverse side is used to record spectra of the photon gas. [8]

We have shown how a Bose distribution for the photon number spectrum arises from a phenomenological rate equation approach. When reaching the BEC regime, the system is expected to form a macroscopically occupied wavefunction in its ground states. This wavefunction has a spontaneously chosen random phase for each experimental realisation but should have a fixed phase in a single experimental run.

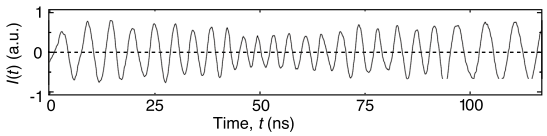

Figure 1.6: Temporal interference signals between photon condensate and reference laser in the canonical regime. (Adapted from [8]).

This has been experimentally investigated in [8]. The setup is shown in Fig. 1.5. The light from the cavity is spatially filtered to isolate the ground mode contribution and interfered with a reference laser. The signal is then detected with a photomultiplier tube. If the light coming from the cavity is coherent, beating signals should be observable. These beating signals have been observed in different regimes. In Fig. 1.6, the result in the canonical regime is shown. This regime is realised at larger detuning from the zero phonon line and is characterised by a larger photon number and a smaller number of excited molecules. This makes particle exchange small and reduces number fluctuation in the photon system. A steady beating signal could be observed, indicating that the ground mode is coherent.

This experiment shows that the light from the BEC has a classical electric field with a stable phase. From the canonical quantisation of light [21], one obtains the electric field operators[2] for a mode with wavefunction $\psi_k(x)$ as

$$\hat{E}_k(x,t) \propto \partial_t \left[\psi_k(x) a_k(t) + \psi_k^*(x) a_k^\dagger(t)\right] . \tag{1.13}$$

Therefore, if the observed light has a macroscopically well-defined electric field, it implies that $\langle \hat{E}(t) \rangle \neq 0$ and therefore also $\langle a_k(t) \rangle \neq 0$. This expectation value requires breaking the $U(1)$ symmetry of the photons. Its description will be the primary goal of this thesis.

[2]For simplicity, we drop the polarisation degree of freedom here.

1.5 Master equation approach

In this section, we will examine a widely used method to describe the system. Until now, most theory work on the photon BEC was done using a Markovian master equation approach. A few of the most relevant works in the present context are [22], [23], [24], [25]. Within this approach, the formation of a Bose distribution in the photon numbers could successfully be described, and various non-trivial phases and properties could be uncovered. Nevertheless, within this approach, the question of phase coherence demonstrated in [8] was not tackled before. Here, we want to review the essential steps in constructing the master equation and the treatment of the resulting equations of motion of the observables of interest. We especially want to see what this approach can tell us about the phase-coherent photon field.
We will start out with the Holstein-Tavis-Cummings model used in [23]

$$\mathcal{H} = \sum_k \delta_k a_k^\dagger a_k + \gamma \sum_{i,k} \left(a_k^\dagger \sigma_i^- + a_k \sigma_i^+ \right) + \sum_{i=1}^{M} \omega \left[b_i^\dagger b_i + s\sigma_i^z (b_i^\dagger + b_i) \right] . \tag{1.14}$$

We consider here a microcavity filled with M dye molecules. The energy difference between the photon modes and the 2-level splitting is the detuning δ_k. The molecules interact with the cavity modes via a Jaynes-Cummings interaction, which is the reason why we can write the energy of the two-level system and the photons just in terms of the detuning. The dye has various rovibrational modes. We assume we can treat them in the harmonic limit so that they can be modelled by a harmonic oscillator with operator b_i. Nevertheless, the minima of the electronic potentials from which we extract the oscillators in the electronic states are different. This is reflected in the last term. The oscillator part $\sigma_i^z(b_i^\dagger + b_i) \propto \sigma_i^z \hat{x}_i$ gives the displacement of the minima with a different sign between electronic ground and excited state. The displacement is parameterised by the Huang-Rhys factor s^2. It will lead to the characteristic shift between emission and absorption spectra. So, light is usually emitted at lower energies as it is absorbed. To proceed, we diagonalise the molecule part of the Hamiltonian via the Polaron transformation

$$U_i(s) = \exp\left(s\sigma_i^z (b_i^\dagger - b_i) \right) . \tag{1.15}$$

It is a shift of the oscillator minima to the origin. Consequently, the shift will appear in the interaction term with the photons, with an addition factor of two in the shift parameter reflecting that ground and excited state oscillators were separated symmetrically from the origin. This leads us, up to a constant, to the transformed Hamiltonian

$$\mathcal{H}' = \sum_k \delta_k a_k^\dagger a_k + \sum_i \omega b_i^\dagger b_i + \gamma \sum_{k,i} \left(D_i^\dagger(s) a_k^\dagger \sigma_i^- + D_i(s) a_k \sigma_i^+ \right) \tag{1.16}$$

$$\text{with} \qquad D_i(s) = \exp\left(2s(b_i^\dagger - b_i) \right) .$$

We assume that the phonons thermalise rapidly after absorption of a photon and emit from an equilibrium phonon distribution. To implement this approximation, we transform into an interaction picture wrt. the free photon and phonon part and obtain the von Neumann equation in the interaction picture as

$$\rho_I(t) = e^{iH_0 t} \rho e^{-iH_0 t} \quad \Rightarrow \quad i\partial_t \rho_I(t) = [V(t), \rho_I(t)] \tag{1.17}$$

where we used

$$V(t) = \gamma \sum_{k,i} \left(D_{i,c}^\dagger(t) a_k^\dagger(t) \sigma_i^-(t) + D_{i,c}(t) a_k(t) \sigma_i^+(t) \right) \quad \text{with} \quad D_{i,c}(t) = D_i(t) - \langle D_i \rangle_B . \tag{1.18}$$

To apply the Born approximation, we expand to the second order in V, obtaining

$$i\partial_t \rho_I(t) = [V(t), \rho_I(0)] - i\int_0^t dt'[V(t), [V(t'), \rho_I(t')]]\,. \tag{1.19}$$

The phonons are now treated as a bath in equilibrium, so the density matrices fractorise $\rho(t) = \rho_s(t) \otimes \rho_B$ and ρ_B is thermal. This can be done for each molecule individually. Therefore, we drop the molecule index for the moment. With this assumption, we can perform the partial trace of the phonon degrees of freedom, leading us to

$$i\partial_t \rho_s(t) = \mathrm{tr}_B\{[V(t), \rho(0)]\} - i\int_0^t dt' \mathrm{tr}_B\{[V(t), [V(t'), \rho(t')]]\} \tag{1.20}$$

The first-order vanishes, and the second-order contributions are generated by

$$\mathrm{tr}_B\{[V(t), [V(t'), \rho(t')]]\} = \gamma^2 \mathrm{tr}_B\{D_c^\dagger(t)a_k^\dagger(t)\sigma^-(t) + D_c(t)a_k(t)\sigma^+(t) \tag{1.21}$$

$$, [D_c^\dagger(t')a_{k'}^\dagger(t')\sigma^-(t') + D_c(t')a_{k'}(t')\sigma^+(t'), \rho(t')]]\} \tag{1.22}$$

This factors into three distinct contributions as

$$[D_c^\dagger(t)a_k^\dagger(t)\sigma^-(t), [D_c(t')a_{k'}(t')\sigma^+(t'), \rho(t')]] + [D_c(t)a_k(t)\sigma^+(t), [D_c^\dagger(t')a_{k'}^\dagger(t')\sigma^-(t'), \rho(t')]]$$
$$+[D_c^\dagger(t)a_k^\dagger(t)\sigma^-(t), [D_c^\dagger(t')a_{k'}^\dagger(t')\sigma^-(t'), \rho(t')]] + [D_c(t)a_k(t)\sigma^+(t), [D_c(t')a_{k'}(t')\sigma^+(t'), \rho(t')]]$$

The first line is responsible for the usual emission and absorption processes. The second line contains anomalous contributions, which are conjugate to each other. We go now through each of these terms separately and collect their contribution. For the first term, we find

$$a_k^\dagger(t)\sigma^-(t)a_{k'}(t')\sigma^+(t')\rho_s(t')\left\langle D_c^\dagger(t)D_c(t')\right\rangle_B - a_{k'}(t')\sigma^+(t')\rho_s(t')a_k^\dagger(t)\sigma^-(t)\left\langle D_c^\dagger(t)D_c(t')\right\rangle_B$$
$$-a_k^\dagger(t)\sigma^-(t)\rho_s(t')a_{k'}(t')\sigma^+(t')\left\langle D_c(t')D_c^\dagger(t)\right\rangle_B + \rho_s(t')a_{k'}(t')\sigma^+(t')a_k^\dagger(t)\sigma^-(t)\left\langle D_c(t')D_c^\dagger(t)\right\rangle_B$$

We now employ the Markov approximation to pull system operators acting at t' out of the remaining time integral. By this, we set the processes as instantaneous on system time scales. This has to be done by factoring fast time scales out of photons and electronic states. Here namely the detuning δ_k and electronic pump $\Gamma_\uparrow$ and loss processes $\Gamma_\downarrow$. Techniquely this is done as $a(t') = e^{-i\delta t'}a = e^{-i\delta(t'-t)}a(t)$ and $\sigma^\pm(t') = e^{-(\Gamma_\uparrow+\Gamma_\downarrow)/2|t-t'|}\sigma^\pm(t)$ [3]. After this transformation, all integrals can be extended to infinity due to scale separation to the phonon bath. The bath correlation function are only dependent on relative time $\tau = t - t'$ and we define them by $\mathcal{D}^>(t,t') = \left\langle D_c(t)D_c^\dagger(t')\right\rangle_B$ and $\mathcal{D}^<(t,t') = \left\langle D_c^\dagger(t')D_c(t)\right\rangle_B$ leading us to

$$\left[a_k^\dagger(t)\sigma^-(t)a_{k'}(t)\sigma^+(t)\rho_s(t) - a_{k'}(t)\sigma^+(t)\rho_s(t)a_k^\dagger(t)\sigma^-(t)\right]\int_0^\infty d\tau e^{-i\delta_{k'}\tau}e^{-\frac{\Gamma_\uparrow+\Gamma_\downarrow}{2}\tau}\mathcal{D}^<(-\tau)$$
$$+\left[\rho_s(t)a_{k'}(t)\sigma^+(t)a_k^\dagger(t)\sigma^-(t) - a_k^\dagger(t)\sigma^-(t)\rho_s(t)a_{k'}(t)\sigma^+(t)\right]\int_0^\infty d\tau e^{-i\delta_{k'}\tau}e^{-\frac{\Gamma_\uparrow+\Gamma_\downarrow}{2}\tau}\mathcal{D}^>(-\tau)$$

We now proceed with the other terms in the same approximation. The second term is given by

$$a_k(t)\sigma^+(t)a_{k'}^\dagger(t')\sigma^-(t')\rho_s(t')\left\langle D_c(t)D_c^\dagger(t')\right\rangle_B - a_{k'}^\dagger(t')\sigma^-(t')\rho_s(t')a_k(t)\sigma^+(t)\left\langle D_c(t)D_c^\dagger(t')\right]\rangle_B$$
$$-a_k(t)\sigma^+(t)\rho_s(t')a_{k'}^\dagger(t')\sigma^-(t')\left\langle D_c^\dagger(t')D_c(t)\right\rangle_B + \rho_s(t')a_{k'}^\dagger(t')\sigma^-(t')a_k(t)\sigma^+(t)\left\langle D_c^\dagger(t')D_c(t)\right\rangle_B$$

[3] The transformation for the Pauli matrices into an dissipative interaction picture is non-trivial and generally not possible [26], but will be justified by later comparison to another approach.

Applying the same approximations as before, we obtain

$$\left[a_k(t)\sigma^+(t)a^\dagger_{k'}(t)\sigma^-(t)\rho_s(t) - a^\dagger_{k'}(t)\sigma^-(t)\rho_s(t)a_k(t)\sigma^+(t)\right]\int_0^\infty d\tau e^{i\delta_{k'}\tau}e^{-\frac{\Gamma_\uparrow+\Gamma_\downarrow}{2}\tau}\mathcal{D}^>(\tau)$$
$$+\left[\rho_s(t)a^\dagger_{k'}(t)\sigma^-(t)a_k(t)\sigma^+(t) - a_k(t)\sigma^+(t)\rho_s(t)a^\dagger_{k'}(t)\sigma^-(t)\right]\int_0^\infty d\tau e^{i\delta_{k'}\tau}e^{-\frac{\Gamma_\uparrow+\Gamma_\downarrow}{2}\tau}\mathcal{D}^<(\tau)$$

The third term is given by

$$a^\dagger_k(t)\sigma^-(t)a^\dagger_{k'}(t')\sigma^-(t')\rho_s(t')\left\langle D^\dagger_c(t)D^\dagger_c(t')\right\rangle_B - a^\dagger_{k'}(t')\sigma^-(t')\rho_s(t')a^\dagger_k(t)\sigma^-(t)\left\langle D^\dagger_c(t)D^\dagger_c(t')\right\rangle_B$$
$$-a^\dagger_k(t)\sigma^-(t)\rho_s(t')a^\dagger_{k'}(t')\sigma^-(t')\left\langle D^\dagger_c(t')D^\dagger_c(t)\right\rangle_B + \rho_s(t')a^\dagger_{k'}(t')\sigma^-(t')a^\dagger_k(t)\sigma^-(t)\left\langle D^\dagger_c(t')D^\dagger_c(t)\right\rangle_B$$

Applying now the same approximations with $\mathcal{F}(t,t') = \left\langle D_c(t)D_c(t')\right\rangle_B$ we arrive at tremendously simplified expression since $(\sigma^\pm(t))^2 = 0$.

$$-a^\dagger_{k'}(t)\sigma^-(t)\rho_s(t)a^\dagger_k(t)\sigma^-(t)\int_0^\infty d\tau e^{i\delta_{k'}\tau}e^{-\frac{\Gamma_\uparrow+\Gamma_\downarrow}{2}\tau}F^*(-\tau)$$
$$-a^\dagger_k(t)\sigma^-(t)\rho_s(t')a^\dagger_{k'}(t)\sigma^-(t)\int_0^\infty d\tau e^{i\delta_{k'}\tau}e^{-\frac{\Gamma_\uparrow+\Gamma_\downarrow}{2}\tau}F^*(\tau)$$

The fourth term is given as

$$a_k(t)\sigma^+(t)a_{k'}(t')\sigma^+(t')\rho_s(t')\left\langle D_c(t)D_c(t')\right\rangle_B - a_{k'}(t')\sigma^+(t')\rho_s(t')a_k(t)\sigma^+(t)\left\langle D_c(t)D_c(t')\right\rangle_B$$
$$-a_k(t)\sigma^+(t)\rho_s(t')a_{k'}(t')\sigma^+(t')\left\langle D_c(t')D_c(t)\right\rangle_B + \rho_s(t')a_{k'}(t')\sigma^+(t')a_k(t)\sigma^+(t)\left\langle D_c(t')D_c(t)\right\rangle_B$$

After the same approximations, we are left with

$$-a_{k'}(t)\sigma^+(t)\rho_s(t)a_k(t)\sigma^+(t)\int_0^\infty d\tau e^{-i\delta_{k'}\tau}e^{-\frac{\Gamma_\uparrow+\Gamma_\downarrow}{2}\tau}\mathcal{F}(\tau)$$
$$-a_k(t)\sigma^+(t)\rho_s(t)a_{k'}(t)\sigma^+(t)\int_0^\infty d\tau e^{-i\delta_{k'}\tau}e^{-\frac{\Gamma_\uparrow+\Gamma_\downarrow}{2}\tau}\mathcal{F}(-\tau)$$

The explicit expressions for the correlators $\mathcal{D}$ and $\mathcal{F}$ can be found in the appendix. They depend on the specific phonon model used, but the expressions should cover many possible models. With this at hand we define now $K(\delta)$ and $P(\delta)$ as

$$K(\delta) = \gamma^2\int_0^\infty d\tau e^{-i\delta_{k'}\tau}e^{-\frac{\Gamma_\uparrow+\Gamma_\downarrow}{2}\tau}\mathcal{D}^>(\tau) = \gamma^2\int_0^\infty d\tau e^{-i\delta_{k'}\tau}e^{-\frac{\Gamma_\uparrow+\Gamma_\downarrow}{2}\tau}\mathcal{D}^<(-\tau) \tag{1.23}$$
$$P(\delta) = \gamma^2\int_0^\infty d\tau e^{-i\delta_{k'}\tau}e^{-\frac{\Gamma_\uparrow+\Gamma_\downarrow}{2}\tau}\mathcal{F}(\tau) = \gamma^2\int_0^\infty d\tau e^{-i\delta_{k'}\tau}e^{-\frac{\Gamma_\uparrow+\Gamma_\downarrow}{2}\tau}\mathcal{F}^*(-\tau) \tag{1.24}$$

We can now collect all contributions as

$$\left[a^\dagger_k(t)\sigma^-(t)a_{k'}(t)\sigma^+(t)\rho_s(t) - a_{k'}(t)\sigma^+(t)\rho_s(t)a^\dagger_k(t)\sigma^-(t)\right]K(\delta_{k'})$$
$$+\left[\rho_s(t)a^\dagger_{k'}(t)\sigma^-(t')a_k(t)\sigma^+(t) - a_k(t)\sigma^+(t)\rho_s(t)a^\dagger_{k'}(t)\sigma^-(t)\right]K^*(\delta_{k'})$$
$$+\left[\rho_s(t)a_{k'}(t)\sigma^+(t)a^\dagger_k(t)\sigma^-(t) - a^\dagger_k(t)\sigma^-(t)\rho_s(t)a_{k'}(t)\sigma^+(t)\right]K^*(-\delta_{k'})$$
$$+\left[a_k(t)\sigma^+(t)a^\dagger_{k'}(t)\sigma^-(t)\rho_s(t) - a^\dagger_{k'}(t)\sigma^-(t)\rho_s(t)a_k(t)\sigma^+(t)\right]K(-\delta_{k'})$$
$$-a^\dagger_{k'}(t)\sigma^-(t)\rho_s(t)a^\dagger_k(t)\sigma^-(t)(P(\delta_{k'}) + P^*(-\delta_{k'}))^* - a_{k'}(t)\sigma^+(t)\rho_s(t)a_k(t)\sigma^+(t)(P(\delta_{k'}) + P^*(-\delta_{k'}))$$

Splitting this in real and imaginary parts and assuming spatially orthogonal photon modes, we can drop $k \neq k'$ terms and obtain

$$\begin{aligned}
&\left[a_k^\dagger(t)\sigma^-(t)a_k(t)\sigma^+(t)\rho_s(t) + \rho_s(t)a_k^\dagger(t)\sigma^-(t')a_k(t)\sigma^+(t) - 2a_k(t)\sigma^+(t)\rho_s(t)a_k^\dagger(t)\sigma^-(t)\right] \mathrm{Re}K(\delta_k) \\
&+\left[\rho_s(t)a_k(t)\sigma^+(t)a_k^\dagger(t)\sigma^-(t) + a_k(t)\sigma^+(t)a_k^\dagger(t)\sigma^-(t)\rho_s(t) - 2a_k^\dagger(t)\sigma^-(t)\rho_s(t)a_k(t)\sigma^+(t)\right] \mathrm{Re}K(-\delta_k) \\
&+i\left[a_k^\dagger(t)a_k(t)P_g\rho_s(t) - \rho_s(t)a_k^\dagger(t)a_k(t)P_g(t)\right] \mathrm{Im}K(\delta_k) \\
&+i\left[a_k(t)a_k^\dagger(t)P_e\rho_s(t) - \rho_s(t)P_e a_k(t)a_k^\dagger(t)\right] \mathrm{Im}K(-\delta_k) \\
&-a_k(t)\sigma^+(t)\rho_s(t)a_k(t)\sigma^+(t)(P(\delta_k) + P^*(-\delta_k)) - a_k^\dagger(t)\sigma^-(t)\rho_s(t)a_k^\dagger(t)\sigma^-(t)(P(\delta_k) + P^*(-\delta_k))^*
\end{aligned}$$

The first two lines give us the emission and absorption processes in Lindblad form, and the third and fourth lines are contributions to the Hamiltonian, the Lamb-shift. The fifth line has not been mentioned in the literature until now and only contributes in the coherent photon phase.
The third and fourth lines might be written as

$$\begin{aligned}
&i\left[a_k^\dagger(t)a_k(t)P_g\rho_s(t) - \rho_s(t)a_k^\dagger(t)a_k(t)P_g(t)\right] \mathrm{Im}K(\delta_k) \\
&+i\left[a_k(t)a_k^\dagger(t)P_e\rho_s(t) - \rho_s(t)P_e a_k(t)a_k^\dagger(t)\right] \mathrm{Im}K(-\delta_k) \\
=&i\left[a_k^\dagger(t)a_k(t)P_g\rho_s(t) - \rho_s(t)a_k^\dagger(t)a_k(t)P_g(t)\right] (\mathrm{Im}K(\delta_k) - \mathrm{Im}K(-\delta_k)) \\
&+i\left[a^\dagger(t)_k(t)a_k(t)\rho_s(t) - \rho_s(t)a^\dagger(t)_k a_k(t)\right] \mathrm{Im}K(-\delta_k) + i\left[P_e\rho_s(t) - \rho_s(t)P_e\right] \mathrm{Im}K(-\delta_k)
\end{aligned}$$

The last two terms contribute to a Hamiltonian term $\Delta H = \mathrm{Im}K(-\delta_k)P_e + \mathrm{Im}K(-\delta_k)a^\dagger a$. We can gauge these contributions and have as the sole Hamiltonian part

$$\delta H = \mathrm{Im}(K(\delta_k) - K(-\delta_k))a_k^\dagger a_k P_g$$

We can now transform back into the Schrödiger picture and restore the molecule index to obtain the Lindblad master equation.

$$\partial_t\rho(t) = -i[\tilde{H},\rho] + \sum_k \frac{\kappa}{2}\mathcal{L}[a_k] + \sum_i\left[\frac{\Gamma_\uparrow}{2}\mathcal{L}[\sigma_i^+] + \frac{\Gamma_\downarrow}{2}\mathcal{L}[\sigma_i^-] + \frac{\gamma_\phi}{2}\mathcal{L}[\sigma_i^z]\right] \tag{1.25}$$

$$+\sum_{k,i}\left[\frac{B_{em}(\delta_k)}{2}\mathcal{L}[a_k^\dagger\sigma_i^-] + \frac{B_{abs}(\delta_k)}{2}\mathcal{L}[a_k\sigma_i^+]\right] \tag{1.26}$$

$$+\sum_{k,i}\left[\alpha(\delta_k)a_k\sigma_i^+\rho a_k\sigma_i^+ + \alpha^*(\delta_k)a_k^\dagger\sigma_i^-\rho a_k^\dagger\sigma_i^-\right] \tag{1.27}$$

$$\text{with}\quad \tilde{H} = \sum_k(\delta_k + \eta_k P_g)a_k^\dagger a_k + \sum_{i,k}\gamma_\beta(a_k^\dagger\sigma_i^- + a_k\sigma_i^+) \quad\text{and}\quad \mathcal{L}[X] = 2X\rho X^\dagger - \{X^\dagger X,\rho\}$$

The coupling constants are given by $\eta_k = \mathrm{Im}K(\delta_k) - \mathrm{Im}(K(-\delta_k))$, $\gamma_\beta = \gamma\langle D\rangle_B$, $B_{em} = 2\mathrm{Re}(K(\delta_k))$, $B_{abs} = 2\mathrm{Re}(K(-\delta_k))$ and $\alpha(\delta_k) = P(\delta_k) + P^*(-\delta_k)$. An example of emission and absorption spectra obtained using $K(\delta)$ can be seen in Fig. 1.7 taken from [24]. Furthermore, κ is the cavity loss, and γ_ϕ is the dephasing of the molecules due to collisions.
The master equation obtained in [22] contains the Lindblad emission and absorption parts and was extended by the renormalisation of the coherent coupling in [24]. The last term, coupling via α, was not shown before but does not alter any of the results obtained by these authors

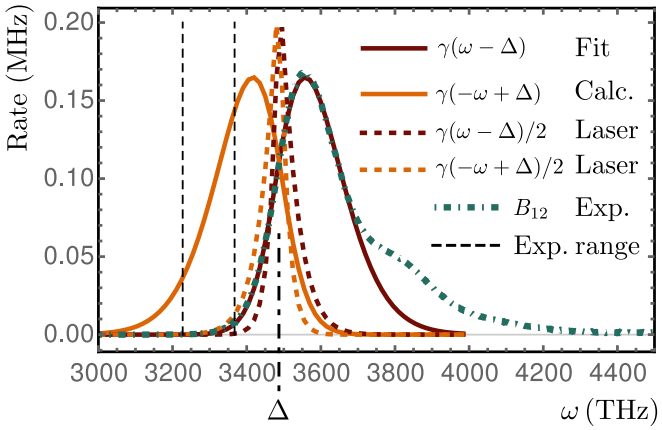

Figure 1.7: Absorption and emission spectra obtained by [24] using $K(\delta)$ from eq. (11.5) with a super Ohmic phonon density of states.

since it only couples to $U(1)$ variant averages, which were not analysed before.
We can use this master equation to obtain the Markovian equation of motion for averages. For this, we use the fact that the molecules are uncorrelated and, therefore, averages of operators on different molecules factorise. Using this, we treat every molecule in the same way and drop the index, introducing the factor M for the molecule number. We aim here to describe the coherent and incoherent parts of the photons. This requires breaking the $U(1)$ symmetry of the photons, which has been discarded in the studies until now. The argument for this is that the phase will be randomly selected in each experimental run and average to zero when averages are performed over many experimental realisations. Here, we take a different perspective and focus on one specific phase to see if the system supports a state with a finite coherent field.

Technically, the equations of motion for the observables are generated from

$$\partial_t \langle A(t)\rangle = \mathrm{tr}\left[(\partial_t \rho(t))A\right] . \tag{1.28}$$

This usually generates a large set of averages on the rhs. for which also equations of motion must be obtained. However, the so-generated set of equations does not close, and truncations must be applied. A cumulant expansion of the expectation values can achieve this [27]. Technically the averages are decomposed in cumulants as $\langle AB\rangle = \langle AB\rangle_c + \langle A\rangle\langle B\rangle$ and $\langle ABC\rangle = \langle ABC\rangle_c + \langle AB\rangle_c\langle C\rangle + \langle AC\rangle_c\langle B\rangle + \langle BC\rangle_c\langle A\rangle + \langle A\rangle\langle B\rangle\langle C\rangle$. The higher-order cumulants are then dropped at some point to close the set of equations.

We will simplify our setup to get some insight into the mechanisms involved. We focus on a single photon mode and drop the Lamp-shift as also the term proportional to α. None of the conclusions drawn hereafter are altered by including them.

It is worthwhile to first look back again at the phenomenological rate equation we used before. These can be obtained from the master equation by only considering the averages $n = \langle a^\dagger a\rangle$ and $M_e = \langle \sigma^+\sigma^-\rangle$.

$$\partial_t n = -\kappa n + B_e M_e(n+1) - B_a(M - M_e)n \tag{1.29}$$
$$\partial_t M_e = \Gamma_\uparrow M - (\Gamma_\uparrow + \Gamma_\downarrow)M_e - B_e M_e(n+1) + B_a(M - M_e)n\,. \tag{1.30}$$

Let us compute the steady state. We express the excited state molecule number through the

photon number by

$$M_e = \frac{\Gamma_\uparrow M - \kappa n}{\Gamma_\uparrow + \Gamma_\downarrow} = \bar{\Gamma_\uparrow} M - \bar{\kappa} n \quad \text{with} \quad \bar{\Gamma_\uparrow} = \frac{\Gamma_\uparrow}{\Gamma_\uparrow + \Gamma_\downarrow} \qquad \bar{\kappa} = \frac{\kappa}{\Gamma_\uparrow + \Gamma_\downarrow} \,. \tag{1.31}$$

This leads us to a quadratic equation for the photon number as

$$cn^2 - bn - a = 0 \Rightarrow n = \frac{b}{2c} + \sqrt{(b/2c)^2 + a/c} = n_a + \sqrt{n_a^2 + n_b^2} \tag{1.32}$$

$$a = B_e \bar{\Gamma_\uparrow} M \quad , \quad b = -\kappa + B_e \bar{\Gamma_\uparrow} M - B_e \bar{\kappa} - B_a M + \bar{\Gamma_\uparrow} M B_a \quad , \quad c = \bar{\kappa}(B_e + B_a) \tag{1.33}$$

$$n_a = \frac{\Gamma_\uparrow (B_e M - \kappa) - \Gamma_\downarrow (B_a M + \kappa) - \kappa B_e}{2\kappa (B_e + B_a)} \quad , \quad n_b^2 = \frac{B_e \Gamma_\uparrow M}{\kappa (B_e + B_a)} \tag{1.34}$$

At large molecule numbers, the photon number has two distinct regimes, which differ in the sign of n_a. For large negative n_a and small κ, one obtains

$$n = n_a + |n_a| \sqrt{1 + n_b^2/n_a^2} \approx \frac{n_b^2}{2|n_a|} \approx \Gamma_\uparrow \frac{B_e}{|\Gamma_\uparrow B_e - \Gamma_\downarrow B_a|} \tag{1.35}$$

which does not scale with the molecule number. For large positive n_a, one obtains

$$n \approx 2n_a \approx M \frac{\Gamma_\uparrow}{\kappa} \frac{B_e}{B_e + B_a} \,. \tag{1.36}$$

In this regime, the photon number scales with the molecule number, leading to a sharp rise in the photon number when the pump rate is increased. This is at the root of the behaviour uncovered in the more sophisticated multi-mode setup in [22].

Let us now include the phase coherent photon field. Just adding its equations of motion additional to (1.29) and (1.30) will lead to an equation of motion of $\langle a \rangle$, which is similar to the whole photon number but misses spontaneous emission. Therefore, in the longtime limit, $\langle a \rangle$ will vanish, and no steady state with a finite value can be obtained. The minimal set of averages, which allows for a finite coherent part in the steady state, can be achieved by including $\langle \sigma^- \rangle$. With $\langle a \rangle = \varphi$, $\langle a^\dagger a \rangle_c = n_c$ and $\langle \sigma^- \rangle = \chi$ the equations of motion obtained from the master equation are

$$\partial_t n_c = B_e M_e + \left[-\kappa + B_e M_e - B_a (M - M_e) \right] n_c \tag{1.37}$$

$$\partial_t \varphi = -i\delta\varphi - i\gamma_\beta M \chi + \frac{1}{2} \left[-\kappa + B_e M_e - B_a (M - M_e) \right] \varphi \tag{1.38}$$

$$\partial_t \chi = -i\gamma_\beta \varphi (M - 2M_e) - \left[(\Gamma_\uparrow + \Gamma_\downarrow) + B_a n_c + B_e (n_c + 1) + (B_e + B_a) |\varphi|^2 \right] \chi/2 \tag{1.39}$$

$$\begin{aligned} \partial_t M_e = &-i\gamma_\beta M \left[\varphi \chi^* - \varphi^* \chi \right] + \left[B_a (M - M_e) - B_e M_e \right] |\varphi|^2 \\ &+ \Gamma_\uparrow M - (\Gamma_\uparrow + \Gamma_\downarrow) M_e + B_a (M - M_e) n_c - B_e M_e (n_c + 1) \end{aligned} \tag{1.40}$$

We look now for a steady-state solution for the densities $|\Psi|^2$ and $|\chi|^2$.
One quickly arrives, using (1.37) at

$$\frac{B_e M_e}{M n_c} |\varphi|^2 (2M_e - M) = \left[(\Gamma_\uparrow + \Gamma_\downarrow) + B_a n_c + B_e (n_c + 1) + (B_e + B_a) |\varphi|^2 \right] |\chi|^2 \tag{1.41}$$

The rhs. is positive. Therefore, a condition for a finite phase coherent part is $(2M_e - M) > 0$. This condition is not altered when all second-order cumulants and the term proportional to α are included. This is the usual population inversion criterium obtained in lasers. If population

inversion is not possible, the transition in the phenomenological rate equations still exists. Therefore, the transition found here is likely a laser transition, not a BEC transition. However, the experiments operate far from population inversion.

Another odd property is that the density of phase-coherent photons is explicitly dependent on the square of the detuning, so it does not contain information about the sign. This hints at a possible reason why the rate equations lead to odd results for phase-coherent averages. In performing the Markov approximation, one assumes that the bath is unstructured on all energy scales of the system. This reduces the complicated molecule dynamics to Markovian two-level dynamics. Therefore, energetically, the photons see a single two-level system with a fixed energy. Nevertheless, the vibrational bath is structured and has states at large detuning, which the photons interact with. This leads to a scenario closer to a multi-level system.

In the rest of this thesis, we will develop a formalism to explain the observed phase coherence. We incorporate the phonon dynamics in a non-Markovian way, keeping as many spectral and memory effects as possible. For this, we will need various field theoretical tools, which we will introduce in the following chapter.

Part II

Quantum Many-Body Systems out of Equilibrium

Chapter 2

Non-equilibrium Quantum Field Theory

2.1 Schwinger-Keldysh formalism

A natural approach to non-equilibrium physics is the Schwinger-Keldysh formalism, which is most easily implemented in the path integral formalism. It allows us to treat general systems as open and driven quantum systems. We follow here essentially [28] and [29][1]. The key ideas can most easily be motivated by considering how a quantum average of a time-dependent operator is computed. For the moment, let us consider a Hamiltonian system prepared in an arbitrary initial state $\rho(t_0)$. The time-dependent average of an operator A is then given by

$$\langle A(t)\rangle = \mathrm{tr}(U(t_0,t)\,A\,U(t,t_0)\rho(t_0)) \tag{2.1}$$

Reading the expression from right to left, the initial state is time evolved from t_0 to the time t at which the operator A is applied, and then time evolved back to the initial time t_0. The forward- and backward-time evolution appearing here is the crucial idea, which should also be reflected in the time-slicing procedure used to derive a path integral.

We will be interested in bosonic many-body systems and specialise to this case here. They can be described by canonically commuting creation $b^\dagger$ and annihilation operators b. The path integral representation is then set up using coherent states as a basis defined by their eigenvalue equations

$$b\,|\phi\rangle = \phi\,|\phi\rangle \quad , \quad \langle\phi|\,b^\dagger = \phi^*\,\langle\phi|\,. \tag{2.2}$$

These states form an overcomplete basis, and their explicit (unnormalised) form and overlap are

$$|\phi\rangle = e^{\phi b^\dagger}\,|0\rangle \quad , \quad \langle\phi|\phi'\rangle = e^{\phi^*\phi'}\,. \tag{2.3}$$

From this follows the resolution of unity as

$$\mathbb{1} = \int d\phi^* d\phi e^{-|\phi|^2}\,|\phi\rangle\,\langle\phi|\,. \tag{2.4}$$

In the later chapters, we will construct a moment-generating functional whose basis is laid here by considering the time-dependent partition function

$$Z[t] = \mathrm{tr}(U(t_0,t)U(t,t_0)\rho(t_0))\,. \tag{2.5}$$

[1]The reader might also be interested in [30] and [31].

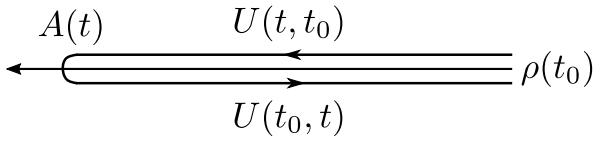

Figure 2.1: Illustration of the time evolution of eq. (2.1)

At this stage, the definition does not look too helpful since $U(t_0,t)U(t,t_0) = \mathbb{1}$ and the density matrix is normalised, giving us $Z = 1$. Nevertheless, constructing the time-sliced version of this expression will allow us to generalise it to a more useful object. To this end, let us consider a system with dynamics governed by a normal-ordered, time-independent Hamiltonian leading to matrix elements and time evolution operator

$$\langle\phi|\, H(b^\dagger, b)\, |\phi'\rangle = H(\phi^*, \phi')\, \langle\phi|\phi'\rangle \quad , \quad U(t,t') = e^{-iH(t-t')/\hbar}\,. \tag{2.6}$$

The time evolution operator has the group property $U(t,t') = U(t,\bar{t})U(\bar{t},t')$ and therefore

$$U(t,t') = \prod_{n=1}^{N} e^{-iH\Delta t_n/\hbar} \qquad \text{with} \quad \sum_{n=1}^{N} \Delta t_n = t - t'\,. \tag{2.7}$$

In principle, the Δt_n's can be chosen non-equidistantly, but we will specialise to the equidistant case $\Delta t_n = \Delta t$. The time-slicing procedure is now done by using this decomposition and inserting resolutions of unity in the coherent state basis with $t > t_0$ as

$$\begin{aligned}
U(t,t_0) &= e^{-iH\Delta t/\hbar} e^{-iH\Delta t/\hbar} e^{-iH\Delta t/\hbar} \ldots e^{-iH\Delta t/\hbar} && (2.8)\\
&= \int d^2\phi_N e^{-|\phi_N|^2}\, |\phi_N\rangle\, \langle\phi_N|\, e^{-iH\Delta t/\hbar} \int d^2\phi_{N-1} e^{-|\phi_{N-1}|^2}\, |\phi_{N-1}\rangle\, \langle\phi_{N-1}|\, e^{-iH\Delta t/\hbar} \ldots . && (2.9)\\
&= \Big[\prod_{n=1}^{N} \int d_n^2\phi_n e^{-|\phi_n|^2}\Big]\, |\phi_N\rangle\, \langle\phi_N|\, e^{-iH\Delta t/\hbar}\, |\phi_{N-1}\rangle\, \langle\phi_{N-1}|\, e^{-iH\Delta t/\hbar}\, |\phi_{N-2}\rangle\, \langle\phi_{N-2}|\, \ldots && (2.10)
\end{aligned}$$

The remaining matrix elements can be computed in the limit of $N \to \infty$, $\Delta t \to 0$ with $N\Delta t = t - t_0$ by expanding the exponential to first order and later re-exponentiation as

$$\begin{aligned}
\langle\phi_n|\, e^{-iH\Delta t/\hbar}\, |\phi_{n-1}\rangle &\approx \langle\phi_n|\, 1 - iH(b^\dagger, b)\Delta t/\hbar\, |\phi_{n-1}\rangle && (2.11)\\
&= \langle\phi_n|\phi_{n-1}\rangle\, (1 - iH(\phi_n^*, \phi_{n-1})\Delta t/\hbar) && (2.12)\\
&\approx \langle\phi_n|\phi_{n-1}\rangle\, e^{-iH(\phi_n^*,\phi_{n-1})\Delta t/\hbar} && (2.13)\\
&= e^{\phi_n^*\phi_{n-1}} e^{-iH(\phi_n^*,\phi_{n-1})\Delta t/\hbar}\,. && (2.14)
\end{aligned}$$

Collecting all these contributions, we obtain

$$\begin{aligned}
U(t,t_0) &= \int \left[\prod_{n=2}^{N} d^2\phi_n e^{-|\phi_n|^2} e^{\phi_n^*\phi_{n-1}} e^{-iH(\phi_n^*,\phi_{n-1})\Delta t/\hbar}\right] e^{-|\phi_1|^2}\, |\phi_N\rangle\, \langle\phi_1|\, d^2\phi_1 && (2.15)\\
&= \int \left[\prod_{n=2}^{N} d^2\phi_n \exp\left(i\Delta t/\hbar \left\{i\hbar\phi_n^* \frac{\phi_n - \phi_{n-1}}{\Delta t} - H(\phi_n^*, \phi_{n-1})\right\}\right)\right] e^{-|\phi_1|^2}\, |\phi_N\rangle\, \langle\phi_1|\, d^2\phi_1 && (2.16)
\end{aligned}$$

The backward part of the time evolution can be done analogously, noting that the time interval Δt must be chosen with a different orientation, leading to an additional minus sign in front of

the Hamiltonian and a derivative which points in the negative time direction. This means in the following expression, increasing n gives decreasing physical times, leading us to

$$U(t_0,t) = \int \left[\prod_{n=N+2}^{2N} d^2\phi_n \exp\left(-i\Delta t/\hbar \left\{ -i\hbar\phi_n^* \frac{\phi_n - \phi_{n-1}}{\Delta t} - H(\phi_n^*, \phi_{n-1}) \right\} \right) \right] \tag{2.17}$$

$$e^{-|\phi_{N+1}|^2} |\phi_{2N}\rangle \langle\phi_{N+1}| \, d^2\phi_{N+1} \tag{2.18}$$

Combining these expressions with the definition, $\delta t_n = \pm\Delta t$ being $+$ if n is on the forward time evolution and $-$ if it is on the backward time evolution, we find

$$Z = \int \left[\prod_{n=1}^{2N} d^2\phi_n \right] \exp\left\{ i \sum_{n=2}^{2N} \delta t_n/\hbar \left[i\hbar\phi_n^* \frac{\phi_n - \phi_{n-1}}{\delta t_n} - H(\phi_n^*, \phi_{n-1}) \right] \right\} e^{-|\phi_1|^2} \langle\phi_1| \, \rho(t_0) \, |\phi_{2N}\rangle$$

We will usually work with the continuum limit of this expression, but it is worthwhile to note the structure of the discrete time-sliced version.

The initial state is encoded in the matrix element at the end of the expression. For a Gaussian initial state, $\rho(t_0) = \rho_0^{b^\dagger b}$, it can be expressed as $\langle\phi_1| \, \rho(t_0) \, |\phi_{2N}\rangle = e^{\phi_1^* \rho_0 \phi_{2N}}$. For a quadratic Hamiltonian, this leads to a matrix form of the action, which is nearly bi-diagonal, except for the matrix element encoding the initial state. This is crucial in the matrix inverse, directly related to the correlation functions.

We will only be concerned with Gaussian initial states and only briefly comment on more complicated initial conditions. In principle they can be encoded, but lead to various complications. The most used non-Gaussian state is the thermal state of an interacting system. Here, the initial state can be added to the Keldysh contour as a piece from $\tau = i\beta \to \tau = 0$. This requires the implementation of the Kubo-Martin-Schwinger (KMS) boundary conditions when determining correlation functions. Already, this approach covers a large class of initial states since the Hamiltonian on the imaginary time branch can be chosen independently from the time evolution.[2] General initial states can encoded in the n-PI EA formalism [32] [33]. However, the computational cost to solve the eom. following this approach is too high to be useful at the moment.

In the continuum limit, the initial conditions are not written explicitly but must be remembered when eom. are solved. From here on out, we will take $\hbar = 1$, until further noted. The partition function on the time contour then reads

$$Z = \int \mathcal{D}\phi \exp\left\{ i \int_c dt \left[\phi^*(t) i\partial_t \phi(t) - H(\phi^*, \phi) \right] \right\} = \int \mathcal{D}\phi e^{iS} \tag{2.19}$$

The action S is now formulated along the Keldysh contour but should be decomposed into the usual physical time for practical calculations. This is done by a characteristic doubling of the degrees of freedom $\phi(t)$ in non-equilibrium. We introduce a field $\phi_+(t)$ on the forward contour and $\phi_-(t)$ on the backward contour. Decomposing the contour integral and taking care of the orientation of the contour, we may write

$$\int dt_c \left[\phi^*(t) i\partial_t \phi(t) - H(\phi^*, \phi) \right] \tag{2.20}$$

$$= \int_{t_0}^{\infty} dt \left\{ \left[\phi_+^*(t) i\partial_t \phi_+(t) - H(\phi_+^*, \phi_+) \right] - \left[\phi_-^*(t) i\partial_t \phi_-(t) - H(\phi_-^*, \phi_-) \right] \right\} . \tag{2.21}$$

[2] Note, that in these cases also the adiabatic theorem needs to be used to apply Wick's theorem [30].

It will in the following be useful to define the "free" part of the action as the quadratic part of the action and collect it in $g_c^{-1}(t,t')$, writing it on the contour as

$$S_0 = \int_c dtdt' \phi^*(t) g_c^{-1}(t,t') \phi(t') = \int dtdt' \phi_+^*(t) g_{+,+}^{-1}(t,t') \phi_+(t') + \int dtdt' \phi_-^*(t) g_{-,-}^{-1}(t,t') \phi_-(t') - \int dtdt' \phi_+^*(t) g_{+,-}^{-1}(t,t') \phi_-(t') - \int dtdt' \phi_-^*(t) g_{-,+}^{-1}(t,t') \phi_+(t') \quad (2.22)$$

Note that in the definition of $g_c^{-1}(t,t')$ often contour-delta functions are used, which are defined by contour-theta functions as $\delta_c(t,t') = \partial_t \Theta_c(t,t')$. In decomposing the contour- into real-line integrals and attaching contour indices to the time arguments, one arrives at an additional minus sign at the backward contour, namely

$$\Theta_c(t,t') = \begin{cases} \Theta(t-t') & \text{if} \quad t,t' \in + \\ 1 & \text{if} \quad t \in -\,,\, t' \in + \\ 0 & \text{if} \quad t \in +\,,\, t' \in - \\ \Theta(t'-t) & \text{if} \quad t,t' \in - \end{cases} \quad \Rightarrow \quad \delta_c(t,t') = \delta(t,t') \left[\delta_{t,+}\delta_{t',+} - \delta_{t,-}\delta_{t',-} \right] \quad (2.23)$$

The functions $g_c(t,t')$ are the non-interacting 2-time correlators of the system namely

$$g_c(t,t') = -i \left\langle T_c(\phi(t)\phi^*(t')) \right\rangle_0 . \quad (2.24)$$

Here T_c is the contour ordering symbol, and the subscript zero at the average denotes that the corresponding action is taken to be Gaussian. It emphasises the need to keep in mind that initial conditions are implicit in the continuum representation and must be applied when solving for the free Green function via the equations of motion

$$\int_c dt' g_c^{-1}(t_1,t') g_c(t',t_2) = \delta_c(t_1,t_2) . \quad (2.25)$$

We will briefly give some definitions here that will be helpful later. The different components of $g_c(t,t')$ on the contour are called

$$g_{+,+}(t,t') = -i \left\langle T(\phi_+(t)\phi_+^*(t')) \right\rangle = g^T(t,t') \quad \text{time-ordered Green function} \quad (2.26)$$

$$g_{-,-}(t,t') = -i \left\langle \tilde{T}(\phi_-(t)\phi_-^*(t')) \right\rangle = g^{\tilde{T}}(t,t') \quad \text{anti-time-ordered Green function} \quad (2.27)$$

$$g_{+,-}(t,t') = -i \left\langle \phi_-^*(t')\phi_+(t) \right\rangle = g^<(t,t') \quad \text{lesser Green function} \quad (2.28)$$

$$g_{-,+}(t,t') = -i \left\langle \phi_-(t)\phi_+^*(t') \right\rangle = g^>(t,t') \quad \text{greater Green function} \quad (2.29)$$

The time- and anti-time ordered Green functions can be decomposed as

$$g^T(t,t') = \theta(t-t')g^>(t,t') + \theta(t'-t)g^<(t,t') \quad (2.30)$$

$$g^{\tilde{T}}(t,t') = \theta(t'-t)g^>(t,t') + \theta(t-t')g^<(t,t') \quad (2.31)$$

This notation, connecting the contour index with the label, will also be used later for the full Green functions G. In this thesis, we will decompose all these Green functions into greater and lesser functions. To give some intuition about these functions, let us consider an equilibrium system. For fermions, the lesser function gives the particle contributions and is proportional to the Fermi function $f(\omega)$. The greater function, on the other hand, is proportional to $1 - f(\omega)$ due to the anti-commutation relation of fermion operators. It is usually interpreted as the hole contributions. For bosons, it is more intuitive to take a different perspective and think about

these correlators as a probe of the systems properties. A lesser function gives information if we can remove a particle from the system. Therefore, for bosons, as in the fermionic case, it contains information on particle occupation and is proportional to the Bose function $b(\omega)$. The greater function tells us if we can add a particle to the system. In the fermionic case, it checks if a hole is present. For bosons, it is proportional to $1 + b(\omega)$. One can add particles to a bosonic system via spontaneous and stimulated emission.

All these components can be collected in a 2×2 structure in $g_c(t, t')$. But one can choose different basis representations, giving different fundamental Green functions. Nevertheless, following from the 2×2 structure, only two can be truly independent. The choice depends on the problem at hand. A popular choice is the basis of retarded-/advanced- and Keldysh Green functions. Here retarded and advanced are related by conjugation and interchange of time arguments. This basis can directly be implemented on the level of fields by transforming to a "classical-quantum" basis (c, q) defined by the average and difference of the $(+, -)$ basis[3]

$$\phi_c(t) = (\phi_+(t) + \phi_-(t))/\sqrt{2} \quad , \quad \phi_q(t) = (\phi_+(t) - \phi_-(t))/\sqrt{2}\,. \tag{2.32}$$

Another basis choice is then spectral function A and the occupation function ρ, [4] being in the boson case, averages of the commutator and anti-commutator, of the fields at different times. Even though it might be the most physically intuitive representation to the best of the author's knowledge, there is no transformation of the fields leading to this decomposition due to the requirement of implementing time-ordering theta functions. For reasons becoming clearer in later chapters, a representation in terms of greater and lesser functions will be the most suitable for the case at hand.

2.2 Lindbladians in path integral representation

One of the primary methods to incorporate open quantum system dynamics is the Lindblad formalism. The Lindblad form of the Master equation is intimately related to the structure of the Schwinger-Keldysh contour. In [34], the path integral formulation belonging to a master equation of the density matrix is derived. We will take a different route, considering the Hamiltonian of the system and bath as fundamental and show how the Lindblad form emerges in the action. This approach allows for easier generalise to more complicated bath situations as shown in [35].
As a starting point, we take the same setup as in the usual derivation of the Lindblad formalism. Consider the full Hamiltonian of system and bath with operators b linearly coupled to some system operator A as

$$H = H_s + H_B + \gamma(A^\dagger b + h.c.)\,. \tag{2.33}$$

For simplicity, we will take the bath Hamiltonian to be quadratic [5]. The action follows with the field representation of the system operators as

$$S = S_s + \int_c dt dt' b^\dagger(t) g_c^{-1}(t, t') b(t') + \gamma \int dt (A_+^\dagger(t) b_+(t) - A_-^\dagger(t) b_-(t) + h.c.)\,. \tag{2.34}$$

[3] This transformation is not so straightforward for fermions, see [28].
[4] Note that the letters for these two functions vary in the literature, e.g. [32] reverses the definitions.
[5] For more complicated bath, see methods used in [35].

We can complete the square using the inverse of g_c^{-1} leaving us with

$$S = S_s + \int_c dtdt' d\tau d\tau' \left(b^\dagger(t)\delta_c(t,\tau) + \gamma A^\dagger(t) g_c(t,\tau) \right) g_c^{-1}(\tau,\tau') \left(\delta_c(\tau',t')b(t') + \gamma g_c(\tau',t')A(t') \right) - \gamma^2 \int_c dtdt' A^\dagger(t) g_c(t,t') A(t') \,. \tag{2.35}$$

We assumed that the initial state factorises in a product of the system and bath density matrices. This allows us to obtain the free bath correlators only considering the bath state and dynamics. With this assumption, the integral over the bath fields can be performed by a shift that does not change the path integral measure. This leaves us with the last term and leads to the dissipative action

$$S = S_s - \gamma^2 \int dtdt' A_+^\dagger(t) g_{+,+}(t,t') A_+(t') - \gamma^2 \int dtdt' A_-^\dagger(t) g_{-,-}(t,t') A_-(t') \tag{2.36}$$

$$+ \gamma^2 \int dtdt' A_+^\dagger(t) g_{+,-}(t,t') A_-(t') + \gamma^2 \int dtdt' A_-^\dagger(t) g_{-,+}(t,t') A_+(t') \,. \tag{2.37}$$

We now perform the Markov approximation. To this end, we consider the symmetry properties of greater and lesser functions

$$g^>(t,t') = -i \left\langle b(t) b^\dagger(t') \right\rangle \qquad (g^>(t,t'))^\dagger = -g^>(t',t) \tag{2.38}$$

$$g^<(t,t') = -i \left\langle b^\dagger(t') b(t) \right\rangle \qquad (g^<(t,t'))^\dagger = -g^<(t',t) \tag{2.39}$$

They are anti-hermitian and in a steady state, as in equilibrium, only depending on relative time. Until now, we did not consider the mode structure of the bath, but it can easily be restored. For bosonic modes with energy ω_k in equilibrium, these functions are

$$g_k^<(t,t') = -ie^{-i\omega_k(t-t')} n_b(\omega_k) \quad , \quad g_k^>(t,t') = -ie^{-i\omega_k(t-t')}(n_b(\omega_k)+1) \,. \tag{2.40}$$

In the expression before, we should now sum over all the bath modes. We assume that the bandwidth of the bath is large so the time integrals only have little support in relative time wrt. to the time scales of the system. It allows us to assume both system operators at equal time and the remaining integrals are of the type

$$\int_{-\infty}^{\infty} dt g^<(t) = \int_0^\infty dt g^<(t) + \int_{-\infty}^0 dt g^<(t) \tag{2.41}$$

$$= \int_0^\infty dt \left[g^<(t) - (g^<)^*(t) \right] = 2i \mathrm{Im} \int_0^\infty dt g^<(t) \,. \tag{2.42}$$

To obtain the Lindblad form, one assumes an empty bath, meaning $n_b(\omega_k) = 0$. This sets the lesser function to zero, and in the greater function, only the density of states contributes, which will be absorbed in the coupling constant later. The integrals for the $(+,+)$ and $(-,-)$ components can be computed as

$$\int dtdt' A_+^\dagger(t) g_{+,+}(t,t') A_+(t') \approx \int_{-\infty}^\infty dt A_+^\dagger(t) A_+(t) \int_{-\infty}^\infty dt' g_{+,+}(t,t') \tag{2.43}$$

$$= \int_{-\infty}^\infty dt A_+^\dagger(t) A_+(t) \int_0^\infty dt' g^>(t') \tag{2.44}$$

$$\int dtdt' A_-^\dagger(t) g_{-,-}(t,t') A_-(t') \approx \int_{-\infty}^\infty dt A_-^\dagger(t) A_-(t) \int_{-\infty}^\infty dt' g_{-,-}(t,t') \tag{2.45}$$

$$= \int_{-\infty}^\infty dt A_+^\dagger(t) A_+(t) \int_{-\infty}^0 dt' g^>(t') \,. \tag{2.46}$$

The remaining integrals can be complex and are related by

$$\int_0^\infty dt g^>(t) = -\int_0^\infty dt (g^>(-t))^* = -\int_{-\infty}^0 dt (g^>(t))^* = -\left[\int_{-\infty}^0 dt g^>(t)\right]^* := \kappa\,. \tag{2.47}$$

Collecting all the terms we obtain

$$\begin{aligned} S =& S_s - \gamma^2\kappa \int dt A_+^\dagger(t)A_+(t) + \kappa^*\gamma^2 \int dt A_-^\dagger(t)A_-(t) + 2i\mathrm{Im}(\kappa)\gamma^2 \int dt A_-^\dagger(t)A_+(t) && (2.48)\\ =& S_s - \chi/2 \int dt A_+^\dagger(t)A_+(t) + \chi^*/2 \int dt A_-^\dagger(t)A_-(t) + i\mathrm{Im}(\chi) \int dt A_-^\dagger(t)A_+(t) && (2.49)\end{aligned}$$

If the system operators are linear in the fields, the real part of χ can be absorbed into the free part of the Hamiltonian as a Lamb shift. For other cases, the bath density of states can be chosen symmetrically such that χ is purely imaginary, leading to the standard form of

$$S = S_s + i\Gamma/2 \int dt A_+^\dagger(t)A_+(t) + i\Gamma/2 \int dt A_-^\dagger(t)A_-(t) - i\Gamma \int dt dt' A_-^\dagger(t)A_+(t)\,. \tag{2.50}$$

The general structure of the Lindblad equation is here directly reflected. The first two terms represent the anti-commutator. Therefore, the doubling of the degrees of freedom can be seen in the master equation as the application of operators from the left or the right of the density matrix. Further discussion of the operator perspective on the doubling of dof. can be found in [36].

We will mostly be interested in the case where the system exchanges particles with the bath. Here, we want to see how this influences the free propagators of the system. For this, it is sufficient to consider a single non-interacting bosonic mode with action

$$S_0 = \int dt \left[\phi_+^*(t)(i\partial_t - \epsilon)\phi_+(t) - \phi_-^*(t)(i\partial_t - \epsilon)\phi_-(t)\right]\,. \tag{2.51}$$

We now include dissipation by a particle pump and a loss. The system operators in (2.33) are then $A_{loss} = \phi$ and $A_{pump} = \phi^*$ leading us to

$$\begin{aligned} S_0 =& \int dt \left[\phi_+^*(t)(i\partial_t - \epsilon + i/2(\kappa_\uparrow + \kappa_\downarrow))\phi_+(t) - \phi_-^*(t)(i\partial_t - \epsilon - i/2(\kappa_\uparrow + \kappa_\downarrow))\phi_-(t)\right]\\ &- \int dt \left[i\kappa_\uparrow \phi_+^*(t)\phi_-(t) + i\kappa_\downarrow \phi_-^*(t)\phi_+(t)\right] \end{aligned} \tag{2.52}$$

In the following chapters, we will deal with the phenomenon of condensation, which emerges here due to the spontaneous breaking of a $U(1)$ symmetry. In foresight thereof, we extend the application of $g^{-1}(t,t')$ also to give us the time evolution of anomalous (explicitly symmetry breaking) averages. To this end, we need to specify a matrix structure for the operators contained in g, which we choose in the usual Nambu/Beliaev form as [37]

$$\mathcal{P}^c(t,t') = -i\begin{pmatrix} \langle T_c(a(t)a^\dagger(t'))\rangle & \langle T_c(a(t)a(t'))\rangle \\ \langle T_c(a^\dagger(t)a^\dagger(t'))\rangle & \langle T_c(a^\dagger(t)a(t'))\rangle \end{pmatrix} := \begin{pmatrix} P^c(t,t') & f^c(t,t') \\ \bar{f}^c(t,t') & P^c(t',t) \end{pmatrix} \tag{2.53}$$

This structure ensures the symmetry under hermitian conjugation namely $\mathcal{P}^{\gtrless}(t,t') = -(\mathcal{P}^{\gtrless}(t',t))^\dagger$. Similar relations hold for time- and anti-time ordered Green functions. The inverse propagators acting from the left can directly be obtained from the action. Here, one needs to take

into account that the time derivative acting on the conjugate field gets a minus from partial integration, leading us to

$$g^{-1}_{+,+} = \begin{pmatrix} i\partial_t - \epsilon + i/2(\kappa_\uparrow + \kappa_\downarrow) & 0 \\ 0 & -i\partial_t - \epsilon + i/2(\kappa_\uparrow + \kappa_\downarrow) \end{pmatrix} \tag{2.54}$$

$$g^{-1}_{-,-} = \begin{pmatrix} -(i\partial_t - \epsilon - i/2(\kappa_\uparrow + \kappa_\downarrow)) & 0 \\ 0 & -(-i\partial_t - \epsilon - i/2(\kappa_\uparrow + \kappa_\downarrow)) \end{pmatrix} \tag{2.55}$$

$$g^{-1}_{-,+} = \begin{pmatrix} i\kappa_\downarrow & 0 \\ 0 & i\kappa_\uparrow \end{pmatrix} \quad , \quad g^{-1}_{+,-} = \begin{pmatrix} i\kappa_\uparrow & 0 \\ 0 & i\kappa_\downarrow \end{pmatrix} . \tag{2.56}$$

Note here a subtlety when applying these operators from the right; the rhs. of the eom. is a contour delta function. Therefore, the free inverse propagators acting from the right are minus the hermitian conjugated acting from the left. This essentially reflects that the derivative is acting on the conjugate operator. Let us now carry on and calculate the eom. of the greater and lesser components.

$$\begin{aligned} g^{-1}_{-,+}\mathcal{P}_{+,+} - g^{-1}_{-,-}\mathcal{P}_{-,+} = &\begin{pmatrix} i\partial_t - \epsilon - i/2(\kappa_\uparrow + \kappa_\downarrow) & 0 \\ 0 & -i\partial_t - \epsilon - i/2(\kappa_\uparrow + \kappa_\downarrow) \end{pmatrix} \begin{pmatrix} P^>(t,t') & f(t',t) \\ \bar{f}(t,t') & P^<(t',t) \end{pmatrix} \\ &+ \begin{pmatrix} i\kappa_\downarrow & 0 \\ 0 & i\kappa_\uparrow \end{pmatrix} \begin{pmatrix} P^T(t,t') & f^T(t',t) \\ \bar{f}^T(t,t') & P^T(t',t) \end{pmatrix} \end{aligned} \tag{2.57}$$

$$\begin{aligned} g^{-1}_{+,+}\mathcal{P}_{+,-} - g^{-1}_{+,-}\mathcal{P}_{-,-} = &\begin{pmatrix} i\partial_t - \epsilon + i/2(\kappa_\uparrow + \kappa_\downarrow) & 0 \\ 0 & -i\partial_t - \epsilon + i/2(\kappa_\uparrow + \kappa_\downarrow) \end{pmatrix} \begin{pmatrix} P^<(t,t') & f(t,t') \\ \bar{f}(t',t) & P^>(t',t) \end{pmatrix} \\ &- \begin{pmatrix} i\kappa_\uparrow & 0 \\ 0 & i\kappa_\downarrow \end{pmatrix} \begin{pmatrix} P^{\tilde{T}}(t,t') & f^{\tilde{T}}(t',t) \\ \bar{f}^{\tilde{T}}(t,t') & P^{\tilde{T}}(t',t) \end{pmatrix} \end{aligned} \tag{2.58}$$

For the normal greater/lesser functions in the presence of dissipation, we find

$$i\partial_t P^>(t,t') = (\epsilon + i/2(\kappa_\uparrow + \kappa_\downarrow))P^>(t,t') - i\kappa_\downarrow P^T(t,t') \tag{2.59}$$

$$i\partial_t P^<(t,t') = (\epsilon - i/2(\kappa_\uparrow + \kappa_\downarrow))P^<(t,t') + i\kappa_\uparrow P^{\tilde{T}}(t,t') . \tag{2.60}$$

In the end, we will need to time evolve these equations. Therefore, we separate the time derivative and multiply with σ_z to switch the sign in the lower component, leading us to

$$\begin{aligned} \begin{pmatrix} i\partial_t & 0 \\ 0 & i\partial_t \end{pmatrix} \begin{pmatrix} P^<(t,t') & f(t',t) \\ \bar{f}(t,t') & P^>(t',t) \end{pmatrix} = &\begin{pmatrix} \epsilon - i/2(\kappa_\uparrow + \kappa_\downarrow) & 0 \\ 0 & -\epsilon + i/2(\kappa_\uparrow + \kappa_\downarrow) \end{pmatrix} \begin{pmatrix} P^<(t,t') & f(t',t) \\ \bar{f}(t,t') & P^>(t',t) \end{pmatrix} \\ &+ \begin{pmatrix} i\kappa_\uparrow & 0 \\ 0 & -i\kappa_\downarrow \end{pmatrix} \begin{pmatrix} P^{\tilde{T}}(t,t') & f^{\tilde{T}}(t',t) \\ \bar{f}^{\tilde{T}}(t,t') & P^{\tilde{T}}(t',t) \end{pmatrix} \end{aligned} \tag{2.61}$$

$$\begin{aligned} \begin{pmatrix} i\partial_t & 0 \\ 0 & i\partial_t \end{pmatrix} \begin{pmatrix} P^>(t,t') & f(t',t) \\ \bar{f}(t,t') & P^<(t',t) \end{pmatrix} = &\begin{pmatrix} \epsilon + i/2(\kappa_\uparrow + \kappa_\downarrow) & 0 \\ 0 & -\epsilon - i/2(\kappa_\uparrow + \kappa_\downarrow) \end{pmatrix} \begin{pmatrix} P^>(t,t') & f(t',t) \\ \bar{f}(t,t') & P^<(t',t) \end{pmatrix} \\ &- \begin{pmatrix} i\kappa_\downarrow & 0 \\ 0 & -i\kappa_\uparrow \end{pmatrix} \begin{pmatrix} P^T(t,t') & f^T(t',t) \\ \bar{f}^T(t,t') & P^T(t',t) \end{pmatrix} \end{aligned} \tag{2.62}$$

We will also consider the one-point field $\langle\phi(t)\rangle = \varphi(t)$. As a one-time function, it must be the same on both branches of the Keldysh contour. It will describe the phase coherent part of the light field. The eom. are obtained as

$$\begin{aligned} g^{-1}_{+,+}\varphi^+(t) - g^{-1}_{+-}\varphi^-(t) &= (i\partial_t - \epsilon + \frac{i}{2}(\kappa_\uparrow + \kappa_\downarrow))\varphi(t) - i\kappa_\uparrow\varphi(t) \\ \Rightarrow i\partial_t\varphi(t) &= \left[\epsilon + \frac{i}{2}(\kappa_\uparrow - \kappa_\downarrow)\right]\varphi(t) \end{aligned} \tag{2.63}$$

2.3 Influence of interaction in non-equilibrium

Until now, the discussion has been limited to non-interacting systems. In interacting systems, the rhs. of the equations of motion have additional self-energy terms. How these emerge will be discussed in the next chapter. Here, we only want to give the general structure of these equations for future reference. The rhs. are given in terms of a contour integral of a self-energy Σ with a Green function G. After the contour is decomposed, and time- and anti-time order Green functions are written in terms of greater and lesser functions one finds

$$\begin{aligned} \int_c d\bar{t}\,\Sigma(t^-,\bar{t})G(\bar{t},t^+) = &\int_{t_0}^{t'} d\bar{t}\Sigma^>(t,\bar{t})G^<(\bar{t},t') - \int_{t_0}^{t} d\bar{t}\Sigma^<(t,\bar{t})G^>(\bar{t},t') \\ &+ \int_{t_0}^{t} d\bar{t}\Sigma^>(t,\bar{t})G^>(\bar{t},t') - \int_{t_0}^{t'} d\bar{t}\Sigma^>(t,\bar{t})G^>(\bar{t},t') \end{aligned} \tag{2.64}$$

$$\begin{aligned} \int_c d\bar{t}\,\Sigma(t^+,\bar{t})G(\bar{t},t^-) = &\int_{t_0}^{t} d\bar{t}\Sigma^>(t,\bar{t})G^<(\bar{t},t') - \int_{t_0}^{t'} d\bar{t}\Sigma^<(t,\bar{t})G^>(\bar{t},t') \\ &+ \int_{t_0}^{t'} d\bar{t}\Sigma^<(t,\bar{t})G^<(\bar{t},t') - \int_{t_0}^{t} d\bar{t}\Sigma^<(t,\bar{t})G^<(\bar{t},t')\,. \end{aligned} \tag{2.65}$$

The eom. for the two-time Green functions are called the Kadanoff-Baym (KB) equation. They represent the main challenge in solving interacting non-equilibrium problems.

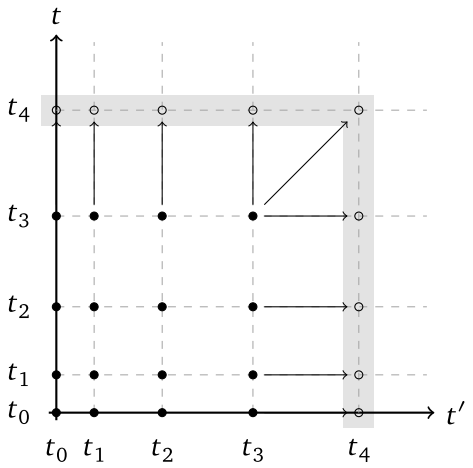

Figure 2.2: Time-stepping procedure [38]

2.4 Numerical solution of Kadanoff-Baym equations

The general non-equilibrium set-up leads us to an initial values problem, whose main difficulty is solving the two-time Kadanoff-Baym equations given by non-linear Volterra integro-differntial equations (VIDE). In a unified notation for the self-energy parts they may be written as

$$i\partial_t G(t,t') = h_0(t)G(t,t') + \int_{\gamma'} \mathrm{d}\bar{t}\, \Sigma(t,\bar{t})G(\bar{t},t') \ , \tag{2.66}$$

here the integral boundaries are $\gamma' = [t_0, t]$ or $\gamma' = [t_0, t']$ due to causality, as already shown when employing the decomposition in greater and lesser Green functions. Note here that the usual quadratic part $h_0(t)$ is time dependent as we will need later. The equations of motion in t' can be obtained from eq. (2.66) by employing the symmetries of the Green function under conjugation. For complex fields, the equations of motion in t' are the adjoint of the equations of motion in t. In [38], we developed a variable order and variable step size Adams (predictor-corrector) method, which we will outline here only briefly and refer for more details to the paper and references therein. The package is written in Julia and can be found on Github or as package import KadanoffBaym.jl. Specific details of the symmetry and dissipative properties of the KB equation for the system considered will be discussed in later chapters.

We take the Cartesian product of a non-equidistant one-dimensional grid

$$\mathcal{T} := \{t_0 < t_1 < ... < t_i < ... < t_N\} \tag{2.67}$$

with itself, to obtain a symmetric mesh $\mathcal{T} \times \mathcal{T} = \left\{(t,t') \,|\, t \in \mathcal{T}, t' \in \mathcal{T}\right\}$ for the two-time plane. The time-stepping procedure can be visualised as fan-like stepping in the symmetric two-time mesh, as depicted in Fig. 2.2. Due to the symmetry of the Green functions, only one of the half-planes $t \geq t'$ or $t' \geq t$ must be computed. The other can be inferred by reflection. The KB equation can now be understood as a system of vector-valued differential equations

$$\begin{aligned}
i\partial_{t_i}\mathbf{G}^v(t_i) &= h_0(t_i)\mathbf{G}^v(t_i) + (\mathbf{\Sigma}\circ\mathbf{G})^v(t_i) \quad \text{(vertical step)} \\
-i\partial_{t_i}\mathbf{G}^h(t_i) &= \mathbf{G}^h(t_i)h_0(t_i)^\dagger + (\mathbf{G}\circ\mathbf{\Sigma})^h(t_i) \quad \text{(horizontal step)} \\
i\partial_{t_i}\mathbf{G}^d(t_i) &= h_0(t_i)\mathbf{G}^d(t_i) - \mathbf{G}^d(t_i)h_0(t_i)^\dagger + (\mathbf{\Sigma}\circ\mathbf{G} - \mathbf{G}\circ\mathbf{\Sigma})^d(t_i) \quad \text{(diagonal step)} \ ,
\end{aligned} \tag{2.68}$$

where

$$\begin{aligned}\mathbf{G}^v(t_i) &= \big[G(t_i,t_0), G(t_i,t_1), ..., G(t_i,t_i)\big] \ , \\ \mathbf{G}^h(t_i) &= \big[G(t_0,t_i), G(t_1,t_i), ..., G(t_i,t_i)\big] \ , \\ \mathbf{G}^d(t_i) &= \big[G(t_i,t_i)\big] \ ,\end{aligned} \tag{2.69}$$

and $\circ$ denotes the element-wise Volterra integration

$$(\mathbf{A}\circ\mathbf{B})^v(t_i) = \left[\int_{\gamma'} \mathrm{d}\bar{t}\, A(t_i,\bar{t})B(\bar{t},t_0), \int_{\gamma'} \mathrm{d}\bar{t}\, A(t_i,\bar{t})B(\bar{t},t_1), ..., \int_{\gamma'} \mathrm{d}\bar{t}\, A(t_i,\bar{t})B(\bar{t},t_i)\right] \ . \tag{2.70}$$

As the dimension of the KB equations grows with each time-step, also the size of $\mathbf{G}^v(t)$ and $\mathbf{G}^d(t)$ grows by one. This requires a continued resizing of the equations and is one reason why such equations are not straightforwardly compatible with the extensive amount of available ODE solvers. The new equations added have a self-energy kernel over past points. This can is visualised in Fig. 2.2 for a diagonal step. The self-energy integrals involve an integration over the points in the shaded region. This emphasises why we build a non-equidistant but symmetrical time mesh. For a general non-symmetric mesh, the points for these integrals must be interpolated, and the reflection symmetry of the Green functions can not be directly used, introducing another layer of complexity. In terms of the system of vector-values differential equations eq. (2.68), the KB integration procedure can be solved as an effective one-time ODE problem.

Following the structure of eq. (2.68), we consider a univariate non-linear VIDE

$$y'(t) = F[t,y(t)] + \int_{t_0}^{t} \mathrm{d}s\, K[t,s,y(s)] \ , \tag{2.71}$$

which can be seen as a system of two equations, where one is an ordinary differential equation and the other a Volterra integral equation with initial conditions $y(t_0) = y_0$ as

$$y'(t) = F[t,y(t)] + z(t) \quad , \quad z(t) = \int_{t_0}^{t} \mathrm{d}s\, K[t,s,y(s)] \, . \tag{2.72}$$

We use a variable order and variable step size Adams (predictor-corrector) method. It provides a good trade-off between cost (two function evaluations per step) and overall accuracy, even when the number of equations is very large. We first integrate eq. (2.72) from t_n to t_{n+1} to obtain

$$y(t_{n+1}) = y(t_n) + \int_{t_n}^{t_{n+1}} \mathrm{d}s\, \big\{F[s,y(s)] + z(s)\big\} \ . \tag{2.73}$$

The integrals are then evaluated with interpolating quadrature formulas. The main computational bottleneck is in the computation of $z(t)$, which can be evaluated with a direct quadrature method as

$$z(t_n) = \int_{t_0}^{t} \mathrm{d}s\, K\left[t_n,s,y(s)\right] = \sum_{\ell=0}^{n-1} \int_{t_\ell}^{t_{\ell+1}} \mathrm{d}s\, K\left[t_n,s,y(s)\right] \ . \tag{2.74}$$

The variable Adams method [39] is a predictor-corrector scheme where the integrand of eq. (2.73) is approximated by a Newton polynomial of previously computed points, and a prediction

y^*_{n+1} for the solution of $y(t_{n+1})$ is obtained with an explicit method with a $(k-1)$-th order polynomial as

$$y^*_{n+1} = y_n + \int_{t_n}^{t_{n+1}} \mathrm{d}s \sum_{j=0}^{k-1} \left[\prod_{i=0}^{j-1} (s - t_{n-i}) \right] \delta^j \left\{ F\left[t_n, y(t_n)\right] + z(t_n) \right\} \ . \tag{2.75}$$

The divided differences are defined recursively as

$$\begin{aligned} \delta^0 F\left[t_\ell, y(t_\ell)\right] &= F\left[t_\ell, y(t_\ell)\right] \ , \\ \delta^j F\left[t_\ell, y(t_\ell)\right] &= \frac{\delta^{j-1} F\left[t_\ell, y(t_\ell)\right] - \delta^{j-1} F\left[t_{\ell-1}, y(t_{\ell-1})\right]}{t_\ell - t_{\ell-j}} \ . \end{aligned} \tag{2.76}$$

The prediction for $y(t_{n+1})$ is corrected via an implicit method, where the k-th order interpolation polynomial of the integrand depends on the predicted value y^*_{n+1}:

$$y_{n+1} = y^*_{n+1} + \int_{t_n}^{t_{n+1}} \mathrm{d}s \left[\prod_{i=0}^{k-1} (s - t_{n-i}) \right] \delta^k \left\{ F[t_{n+1}, y(t_{n+1})] + z(t_{n+1}) \right\} \ . \tag{2.77}$$

The integrals in eq. (2.74) can be evaluated in the same predictor-corrector manner:

$$\begin{aligned} z^*_n &= \sum_{\ell=0}^{n-1} \int_{t_\ell}^{t_{\ell+1}} \mathrm{d}s \sum_{j=0}^{k-1} \left[\prod_{i=0}^{j-1} (s - t_{\ell-i}) \right] \delta^j K_n\left[t_\ell, y(t_\ell)\right] \ , \\ z_n &= z^*_n + \sum_{\ell=0}^{n-1} \int_{t_\ell}^{t_{\ell+1}} \mathrm{d}s \left[\prod_{i=0}^{k-1} (s - t_{\ell-i}) \right] \delta^k K_n\left[t_{\ell+1}, y(t_{\ell+1})\right] \ , \end{aligned} \tag{2.78}$$

with divided differences defined as

$$\begin{aligned} \delta^0 K_n\left[t_\ell, y(t_\ell)\right] &= K\left[t_n, t_\ell, y(t_\ell)\right] \ , \\ \delta^j K_n\left[t_\ell, y(t_\ell)\right] &= \frac{\delta^{j-1} K_n\left[t_\ell, y(t_\ell)\right] - \delta^{j-1} K_n\left[t_{\ell-1}, y(t_{\ell-1})\right]}{t_\ell - t_{\ell-j}} \ . \end{aligned} \tag{2.79}$$

The predictor-corrector equations (2.75) and (2.77) can be solved by recurrence formulas [39], making the evaluation of the integrals and j-th derivatives more efficient. An estimate of the local truncation error can be obtained by $\tilde{y}_{n+1} - y_{n+1}$, where $\tilde{y}_{n+1}$ is the result of the implicit step using a $(k+1)$-th order formula. A measure of this error satisfying specific tolerances is obtained via

$$le_k(n+1) := \frac{\tilde{y}_{n+1} - y_{n+1}}{\texttt{atol} + \texttt{rtol} \cdot \max\left(|y_n|, |y_{n+1}|\right)} \ , \tag{2.80}$$

for which the integration step is accepted if

$$\left\| le_k(n+1) \right\| \leq 1 \ , \quad \text{with} \quad \|x\| = \left(\frac{1}{n} \sum_i^n |x_i|^2 \right)^{\frac{1}{2}} \ . \tag{2.81}$$

The local error is then used to adjust both the step size $h_n := (t_{n+1} - t_n)$ and the order k, such that the next time step is chosen as the largest possible step that still satisfies the local error

being $\lesssim 1$. For more details, see [38] and [39] III.5 and III.7. Given this acceptance criterion, the roles of the tolerances `rtol` and `atol` in (2.80) can be better understood considering them separately under the infinity-norm. In this scenario, $-\log_{10}$ `rtol` controls the minimum number of correct digits between time steps, while `atol` is a threshold for the magnitude of the elements of y for which the minimum number of correct digits is guaranteed.

Since publication, native support for one-time functions and improved methods determining the integration weights using the Vandermonde matrix [40] has been implemented.

2.4.1 Spectra

Understanding the information contained in two-time Green functions can be tricky and most of the insight can be gained by analysing spectra in the steady state. For this, the Green functions must first be rotated to Wigner coordinates defined by $T = (t + t')/2$ and $\tau = t - t'$. In the particular case of our non-equidistant grid, the data of the Green functions must first be interpolated into an equidistant time grid. Afterwards, we can map the Green functions to Wigner coordinates via

$$G(t, t') = G(T + \tau/2, T - \tau/2)\,. \tag{2.82}$$

To obtain the spectra, it is Fourier transformed wrt. to relative time τ, leaving us with $G(T, \omega)$, which is then on the equidistant time and frequency grid. The package has native functions implemented for this procedure. In a steady state $G(T, \omega)$ can be interpreted as spectra of the respective Green functions. Note that during the time evolution, when the steady has not yet been reached, the interpretation as spectra does not strictly hold. Nevertheless, the obtained signal can still give valuable insight into the dynamics. One should also be careful with spectra extracted close to the end of the time evolution. Here, the data for the Fourier transform is only in a small time domain; therefore, various artefacts are bound to appear. This is especially pronounced for sharp peaks in the frequency spectrum, which require long time intervals to be resolved.

2.4.2 Memory truncation

In many systems of interest, the self-energies and Green functions have a finite memory, which means they decay away from the equal-time diagonal $t = t'$. Usually, the self-energies decay faster than the Green functions. An example often encountered is small self-energy contributions so that the Green function has a plane-wave-like structure in the two-time plane with a small exponential decay in relative time due to interactions. In this case, the self-energy is closely confined to the equal time diagonal $t = t'$, but the Green function has long time scales. The photon Green functions we will consider behave in this way. Therefore, if we can assume that the self-energies are decayed on a scale t_Σ away from the equal time diagonal, we can approximate the integrals in the KB equations (2.65) and (2.64) as

$$\int_0^t d\bar{t}\,\Sigma(t,\bar{t})G(\bar{t},t') \approx \theta(t_\Sigma - t)\int_0^t d\bar{t}\Sigma(t,\bar{t})G(\bar{t},t') + \theta(t - t_\Sigma)\int_{t-t_\Sigma}^t d\bar{t}\Sigma(t,\bar{t})G(\bar{t},t') \tag{2.83}$$

The second integral up to t' can cross the equal time diagonal and is different in the case $t > t'$ or $t' > t$. In the two cases, we can approximate the integrals as

$$\begin{aligned}
\int_0^{t'} d\bar{t}\,\Sigma(t,\bar{t})G(\bar{t},t') \approx \theta(t-t')\Bigg[&\theta(t_\Sigma - t)\int_0^{t'}\Sigma(t,\bar{t})G(\bar{t},t') + \theta(t-t_\Sigma)\theta(t'+t_\Sigma - t)\int_{t-t_\Sigma}^{t'}\Sigma(t,\bar{t})G(\bar{t},t')\Bigg] \\
&+ \theta(t'-t)\Big[\theta(t_\Sigma - t)\Big\{\theta((t_\Sigma + t) - t')\int_0^{t'} d\bar{t}\,\Sigma(t,\bar{t})G(\bar{t},t') \\
&\qquad + \theta(t' - (t_\Sigma + t))\int_0^{t+t_\Sigma} d\bar{t}\,\Sigma(t,\bar{t})G(\bar{t},t')\Big\} \\
&+ \theta(t-t_\Sigma)\Big\{\theta((t_\Sigma + t) - t')\int_{t-t_\Sigma}^{t'} d\bar{t}\,\Sigma(t,\bar{t})G(\bar{t},t') \\
&\qquad + \theta(t' - (t_\Sigma + t))\int_{t-t_\Sigma}^{t+t_\Sigma} d\bar{t}\,\Sigma(t,\bar{t})G(\bar{t},t')\Big\}\Big]
\end{aligned} \tag{2.84}$$

Chapter 3

2-Particle Irreducible Effective Action

Non-equilibrium dynamics pose a challenging problem in the formulation of consistent approximation schemes. The equation of motion will necessarily have strong non-linearities to capture relaxation dynamics, but here, care has to be taken to preserve conservation law during time evolution [41]. This chapter will introduce a functional method to formulate such problems and approximation schemes. The method goes back to [42] [43] [44] and has a rich history with many contributions from various perspectives [45] [46]. We will follow here closer in the spirit of [47]. First, we will show the main train of thought and techniques on the 1-particle irreducible (1-PI) effective action (EA). The approach can be generalised to a 2-PI EA, which is better suited for perturbative approaches and allows for the generation of conserving equations of motion for 2-time propagators. After introducing the 2-PI EA we will discuss properties of approximations and their effect on Ward identities. This chapter will be rather technical; for a broader overview of the technique, see [33] [32] [29]; for a more technical introduction, see [48].

3.1 1-PI Effective action

We will start with the 1-PI formulation following [31]. For clarity's sake, we focus on a scalar theory, but the generalisation to a complex theory is straightforward. We first define a generating functional with an external source J and restoring $\hbar$ as

$$Z[J] = \int \mathcal{D}\phi e^{\frac{i}{\hbar}[S[\phi]+J\phi]} \,. \tag{3.1}$$

The first step is to shift the integration variable $\phi \to \phi + \phi_0$. This does not change the domain of the integral, nor introduces a Jacobian factor leading us to

$$Z[J] = e^{\frac{i}{\hbar}[S[\phi_0]+J\phi_0]} \int \mathcal{D}\phi e^{\frac{i}{\hbar}[S[\phi+\phi_0]-S[\phi_0]+J\phi]} = e^{\frac{i}{\hbar}[S[\phi_0]+J\phi_0]} Z_1[J] \,. \tag{3.2}$$

The cumulant generating functional or the generator of connected Green functions is then

$$W[J] = -i\hbar \log(Z[J]) = S[\phi_0] + J\phi_0 + W_1 \quad \text{with} \quad W_1 = -i\hbar \log(Z_1[J]) \,. \tag{3.3}$$

Till now, ϕ_0 was arbitrary, but we will fix it now to be the full one point average $\phi_0 = \langle\phi\rangle = \frac{\delta W}{\delta J} = \varphi$. This will determine the external field $J[\varphi]$ as a function of φ through the equation

$$\varphi = \frac{\delta W}{\delta J} = \left[\frac{\delta S}{\delta \varphi} + J + \frac{\delta W_1}{\delta \varphi}\right] \frac{\delta \varphi}{\delta J} + \varphi \Rightarrow \left[\frac{\delta S}{\delta \varphi} + J + \frac{\delta W_1}{\delta \varphi}\right] \frac{\delta \varphi}{\delta J} = 0 \,. \tag{3.4}$$

The factor $\frac{\delta\varphi}{\delta J}$ generates the connected 2-point Green function and is therefore generally non-zero. We will show that shortly. Therefore the equation determining J as a function of φ is

$$J = -\left[\frac{\delta S}{\delta\varphi} + \frac{\delta W_1}{\delta\varphi}\right] . \tag{3.5}$$

We will now introduce the 1-PI effective action $\Gamma_1[\varphi]$ as the Legendre (-Fenchel) transformation of the $W[J]$, which is therefore a functional of $\frac{\delta W}{\delta J} = \varphi$

$$\Gamma_1[\varphi] = W[J] - J\frac{\delta W}{\delta J} = W[J] - J\varphi = S[\varphi] + W_1[\varphi] \quad \text{with} \quad J = -\frac{\delta\Gamma_1}{\delta\varphi} \tag{3.6}$$

where in the last equality, it is implied that all dependencies of J in W_1 must be re-expressed in terms of eq. (3.5), which leads us explicitly to

$$W_1 = -i\hbar\log\left(\int\mathcal{D}\phi\exp\left\{\frac{i}{\hbar}\left[S[\phi+\varphi] - S[\varphi] - \phi\left[\frac{\delta S[\varphi]}{\delta\varphi} + \frac{\delta W_1[\varphi]}{\delta\varphi}\right]\right]\right\}\right) \tag{3.7}$$

$$= -i\hbar\log\left(\int\mathcal{D}\phi\exp\left\{\frac{i}{\hbar}\left[S[\phi+\varphi] - S[\varphi] - \phi\frac{\delta\Gamma_1[\varphi]}{\delta\varphi}\right]\right\}\right) . \tag{3.8}$$

The connected 2-point Green function will in the following only be called G and is given by

$$\frac{\delta^2 W}{\delta J^2} = \frac{i}{\hbar}\left[\langle\phi^2\rangle - \langle\phi\rangle^2\right] = -G^{(2)} = -G\,. \tag{3.9}$$

Another useful relation can be shown from the properties of the Legendre transform, namely

$$\delta_{i,j} = \frac{\delta\phi_i}{\delta\phi_j} = \int dz\frac{\delta\phi_i}{\delta J_z}\frac{\delta J_z}{\delta\phi_j} = \int dz\frac{\delta^2 W}{\delta J_z\delta J_i}\frac{-\delta^2\Gamma_1}{\delta\phi_z\phi_j} = \int dz\frac{\delta^2\Gamma_1}{\delta\phi_j\phi_z}G_{z,i}\,. \tag{3.10}$$

This means that $\frac{\delta^2\Gamma}{\delta^2\phi} = G^{-1}$, so the 1-PI EA generates the inverse 2-point Green function as its Hessian matrix.

We start evaluating W_1 and show that the theory governed by this functional has some pleasant properties, namely that the one-point averages vanish. This can already be anticipated from the choice of $\phi_0 = \varphi$, but we will explicitly show it here. Therefore let us consider the derivative of W_1 wrt. to φ governed by the action $\tilde{S} = S[\phi+\varphi] - S[\varphi] - \phi\left[\frac{\delta S[\varphi]}{\delta\varphi} + \frac{\delta W_1[\varphi]}{\delta\varphi}\right]$

$$\frac{\delta W_1}{\delta\varphi} = \frac{1}{Z_1}\int\mathcal{D}\phi e^{\frac{i}{\hbar}\tilde{S}}\left[\frac{\delta S[\phi+\varphi]}{\delta\varphi} - \frac{\delta S[\varphi]}{\delta\varphi} - \phi\frac{\delta^2}{\delta\varphi^2}\left[S[\varphi] + W_1[\varphi]\right]\right] . \tag{3.11}$$

The first term can be rewritten in terms of

$$\int\mathcal{D}\phi e^{\frac{i}{\hbar}\tilde{S}}\frac{\delta S[\phi+\varphi]}{\delta\varphi} = -i\hbar\int\mathcal{D}\phi\frac{\delta}{\delta\phi}e^{\frac{i}{\hbar}\tilde{S}} + \int\mathcal{D}\phi e^{\frac{i}{\hbar}\tilde{S}}\frac{\delta}{\delta\varphi}\left[S[\varphi] + W_1[\varphi]\right] . \tag{3.12}$$

The first term is a total derivative, vanishing when integrated so that we can write

$$\frac{\delta W_1}{\delta\varphi} = \frac{1}{Z_1}\int\mathcal{D}\phi e^{\frac{i}{\hbar}\tilde{S}}\left[\frac{\delta}{\delta\varphi}\left[S[\varphi] + W_1[\varphi]\right] - \frac{\delta S[\varphi]}{\delta\varphi} - \phi\frac{\delta^2}{\delta\varphi^2}\left[S[\varphi] + W_1[\varphi]\right]\right] \tag{3.13}$$

$$= \frac{1}{Z_1}\int\mathcal{D}\phi e^{\frac{i}{\hbar}\tilde{S}}\left[\frac{\delta W_1}{\delta\varphi} - \phi\frac{\delta^2}{\delta\varphi^2}\left[S[\varphi] + W_1[\varphi]\right]\right] \tag{3.14}$$

$$= \frac{\delta W_1}{\delta\varphi} - \frac{\delta^2}{\delta\varphi^2}\left[S[\varphi] + W_1[\varphi]\right]\int\frac{\mathcal{D}\phi}{Z_1}e^{\frac{i}{\hbar}\tilde{S}}\phi\,. \tag{3.15}$$

For the equation to hold, the second term must vanish. We note that $\frac{\delta^2}{\delta\varphi^2}\left[S[\varphi]+W_1[\varphi]\right]=\frac{\delta^2\Gamma_1}{\delta\phi^2}$, which is by the construction of the Legendre transform the inverse Green function. The relation must hold for all J. So, we obtain the result that the first moment of the probability distribution given by action $\tilde{S}$ must vanish.
With this, we have shown that W_1 contains all 1-PI connected vacuum diagrams from the theory generated by $\tilde{S}$. To obtain these diagrams, the action $\tilde{S}[\phi]$ can be expanded around small ϕ dropping terms until the first order to obtain a theory governed by a new free propagator given by the second derivative of the action and interaction given by all higher derivatives

$$S_0[\phi]=\frac{1}{2}\frac{\delta^2 S[\varphi]}{\delta\varphi^2}\phi^2 \qquad , \qquad S_I=\sum_{n=3}^{\infty}\frac{1}{n!}\frac{\delta^n S[\varphi]}{\delta\varphi^n}\phi^n\,. \tag{3.16}$$

From now on, we will always define the free propagator as $G_0^{-1}=\frac{\delta^2 S[\varphi]}{\delta\varphi^2}$. To obtain a more explicit form for the 1-PI EA we normalise the integral inside the logarithm of W_1 with $\det(G_0)$ to obtain proper averages so we can write

$$\Gamma_1[\varphi]=S[\varphi]+\frac{i\hbar}{2}\mathrm{tr}\ln(G_0^{-1})-i\hbar\ln\left\langle e^{\frac{i}{\hbar}S_I}\right\rangle_{S_0}+const\,. \tag{3.17}$$

This result can be understood as follows. In a perturbative expansion, Z contains all vacuum diagrams and therefore W contains all connected vacuum diagrams. The Legendre transformation factors out all diagrams, which are 1-particle reducible. All 1-PI diagrams are now written in terms of free propagators G_0. Expectation values are obtained by first decomposing them into cumulants as derivatives of W. The cumulants can then be calculated using the Hessian of the Legendre transforms, which must be the minus inverse of each other. This defines the full two-point Green function from the 1PI EA, namely

$$\delta_{i,j}=\int dz\frac{\delta^2\Gamma_1}{\delta\phi_j\phi_z}G_{z,i}\,. \tag{3.18}$$

This allows us to derive various exact relations between expectation values. We will return to the explicit procedure later and contrast it to the 2-PI EA case.
The 1-PI EA is constructed with a free propagator G_0 and, therefore, lacks strong non-linearities necessary for various physical processes such as thermalisation. In the following, we will introduce the 2-PI EA, which better suits perturbative approaches capturing essential non-linearities.

3.2 2-PI Effective action

The 2-PI formulation is constructed along similar lines but has the advantage that the resulting equations of motion are in terms of full 1- and 2-point Green functions. The arguments are nevertheless more complicated and involved. Therefore, we will tackle this problem from different perspectives. First, we set up the general ideas and expression. From there, we can prove that the remaining diagrammatic part is 1-PI in the sense we discussed before and only contains full 2-point Green function lines. Afterwards, the explicit expression from [47] will be discussed. With this ansatz, an explicit expression for the diagrammatic part can be found, showing that it contains only 2-PI diagrams. This allows us to perform explicit perturbative expansions. The starting point is a moment-generating functional, including a 2-point source R. We stick here again to a scalar theory. The moment- and cumulants generating functionals are then

$$Z[J,R] = \int \mathcal{D}\phi e^{\frac{i}{\hbar}\left[S[\phi]+J\phi+\frac{1}{2}\phi R\phi\right]} = e^{\frac{i}{\hbar}W[J,R]}\,. \tag{3.19}$$

We perform the same trick as in the 1-PI case and shift $\phi \to \phi + \phi_0$

$$Z[J,R] = e^{\frac{i}{\hbar}\left[S[\phi_0]+J\phi_o+\frac{1}{2}\phi_0 R\phi_0\right]} \int \mathcal{D}\phi e^{\frac{i}{\hbar}\left[S[\phi+\phi_0]-S[\phi_0]+(J+R\phi_0)\phi+\frac{1}{2}\phi R\phi\right]} \tag{3.20}$$

$$= e^{\frac{i}{\hbar}\left[S[\phi_0]+J\phi_0+\frac{1}{2}\phi_0 R\phi_0\right]} Z_1[J,R]\,. \tag{3.21}$$

The cumulant generating function may then be written as

$$W[J,R] = S[\phi_0] + J\phi_o + \frac{1}{2}\phi_0 R\phi_0 + W_1 \quad \text{with} \quad W_1 = -i\hbar\log(Z_1[J,R])\,. \tag{3.22}$$

We again fix ϕ_0 to be the full 1-point average φ and obtain the 2-PI EA as

$$\Gamma[G,\varphi] = W - \frac{\delta W}{\delta J}J - \frac{\delta W}{\delta R}R = W - \varphi J - \frac{1}{2}R\left[i\hbar G + \varphi^2\right] \tag{3.23}$$

$$= S[\varphi] + J\varphi + \frac{1}{2}\varphi^2 R + W_1 - \varphi J - \frac{1}{2}R\left[i\hbar G + \varphi^2\right] \tag{3.24}$$

$$= S[\varphi] + W_1 - \frac{i\hbar}{2}RG\,. \tag{3.25}$$

We used here the connection of derivatives wrt. to J and R of $W[J,R]$ to the correlation functions, namely

$$\frac{\delta W}{\delta J} = \langle\phi\rangle = \varphi \tag{3.26}$$

$$\frac{\delta^2 W}{\delta J^2} = \frac{i}{\hbar}\left[\langle\phi^2\rangle - \langle\phi\rangle^2\right] = -G \tag{3.27}$$

$$\frac{\delta W}{\delta R} = \frac{1}{2}\langle\phi^2\rangle = \frac{1}{2}\left[\varphi^2 + i\hbar G\right]\,. \tag{3.28}$$

The first derivatives of the 2-PI EA give the connection to the source fields as

$$\frac{\delta\Gamma}{\delta\varphi} = \frac{\delta W}{\delta\varphi} - J - \varphi\frac{\delta J}{\delta\varphi} - \varphi R - \frac{\delta W}{\delta R}\frac{\delta R}{\delta\varphi} \tag{3.29}$$

$$= \frac{\delta W}{\delta J}\frac{\delta J}{\delta\varphi} + \frac{\delta W}{\delta R}\frac{\delta R}{\delta\varphi} - J - \varphi\frac{\delta J}{\delta\varphi} - \varphi R - \frac{\delta W}{\delta R}\frac{\delta R}{\delta\varphi} = -J - \varphi R \tag{3.30}$$

$$\frac{\delta\Gamma}{\delta G} = \frac{\delta W}{\delta G} - \varphi\frac{\delta J}{\delta G} - \frac{i\hbar}{2}R - \frac{\delta W}{\delta R}\frac{\delta R}{\delta G} \tag{3.31}$$

$$= \frac{\delta W}{\delta R}\frac{\delta R}{\delta G} + \frac{\delta W}{\delta J}\frac{\delta J}{\delta G} - \varphi\frac{\delta J}{\delta G} - \frac{i\hbar}{2}R - \frac{\delta W}{\delta R}\frac{\delta R}{\delta G} = -\frac{i\hbar}{2}R\,. \tag{3.32}$$

From here, we obtain the key feature and the reason why this formulation is called the effective action. At the physical point, where J and R vanish, the theory of interest, also the derivatives of $\Gamma[\varphi, G]$ vanish

$$\frac{\delta\Gamma}{\delta\varphi}\Big|_{J,R=0} = 0 \qquad , \qquad \frac{\delta\Gamma}{\delta G}\Big|_{J,R=0} = 0\,. \tag{3.33}$$

This leads to a variational principle for quantum field theories.
We now follow the ideas of the analysis in the 1-PI case and analyse the theory given by W_1. Taking the derivative wrt. to φ leads us to

$$\frac{\delta W_1}{\delta\varphi} = \frac{1}{Z_1}\int \mathcal{D}\phi e^{\frac{i}{\hbar}\tilde{S}}\left[\frac{\delta S[\phi+\varphi]}{\delta\varphi} - \frac{\delta S[\varphi]}{\delta\varphi} - \phi\frac{\delta^2\Gamma}{\delta\varphi^2} + \frac{1}{2}\phi^2\frac{\delta R}{\delta\varphi}\right] \tag{3.34}$$

$$= \frac{1}{Z_1}\int \mathcal{D}\phi e^{\frac{i}{\hbar}\tilde{S}}\left[\frac{\delta S[\phi+\varphi]}{\delta\varphi} - \frac{\delta S[\varphi]}{\delta\varphi} - \phi\frac{\delta^2\Gamma}{\delta\varphi^2} + \frac{i}{\hbar}\phi^2\frac{\delta^2\Gamma}{\delta\varphi\delta G}\right]. \tag{3.35}$$

We can write the first term, dropping boundary terms again as

$$-i\hbar\int \mathcal{D}\phi\frac{\delta}{\delta\phi}e^{\frac{i}{\hbar}\tilde{S}} = \int \mathcal{D}\phi e^{\frac{i}{\hbar}\tilde{S}}\left[\frac{\delta S[\phi+\varphi]}{\delta\varphi} - \frac{\delta\Gamma}{\delta\varphi} + 2\frac{i}{\hbar}\phi\frac{\delta\Gamma}{\delta G}\right] = 0 \tag{3.36}$$

$$\Rightarrow \int \mathcal{D}\phi e^{\frac{i}{\hbar}\tilde{S}}\frac{\delta S[\phi+\varphi]}{\delta\varphi} = \int \mathcal{D}\phi e^{\frac{i}{\hbar}\tilde{S}}\left[\frac{\delta\Gamma}{\delta\varphi} - 2\frac{i}{\hbar}\phi\frac{\delta\Gamma}{\delta G}\right]. \tag{3.37}$$

Using this result, we can rewrite the expression as

$$\frac{\delta W_1}{\delta\varphi} = \frac{1}{Z_1}\int \mathcal{D}\phi e^{\frac{i}{\hbar}\tilde{S}}\left[\frac{\delta\Gamma}{\delta\varphi} - 2\frac{i}{\hbar}\phi\frac{\delta\Gamma}{\delta G} - \frac{\delta S[\varphi]}{\delta\varphi} - \phi\frac{\delta^2\Gamma}{\delta\varphi^2} + \frac{i}{\hbar}\phi^2\frac{\delta^2\Gamma}{\delta\varphi\delta G}\right] \tag{3.38}$$

$$= \frac{1}{Z_1}\int \mathcal{D}\phi e^{\frac{i}{\hbar}\tilde{S}}\left[\frac{\delta W_1}{\delta\varphi} - \frac{i\hbar}{2}\frac{\delta R}{\delta\varphi}G - \phi\frac{\delta^2\Gamma}{\delta\varphi^2} + \frac{i}{\hbar}\phi^2\frac{\delta^2\Gamma}{\delta\varphi\delta G} - 2\frac{i}{\hbar}\phi\frac{\delta\Gamma}{\delta G}\right] \tag{3.39}$$

$$= \frac{1}{Z_1}\int \mathcal{D}\phi e^{\frac{i}{\hbar}\tilde{S}}\left[\frac{\delta W_1}{\delta\varphi} + \frac{\delta^2\Gamma}{\delta G\delta\varphi}G - \phi\frac{\delta^2\Gamma}{\delta\varphi^2} + \frac{i}{\hbar}\phi^2\frac{\delta^2\Gamma}{\delta\varphi\delta G} - 2\frac{i}{\hbar}\phi\frac{\delta\Gamma}{\delta G}\right] \tag{3.40}$$

$$= \frac{\delta W_1}{\delta\varphi} + \frac{1}{Z_1}\frac{\delta^2\Gamma}{\delta\varphi\delta G}\int \mathcal{D}\phi e^{\frac{i}{\hbar}\tilde{S}}\left[G + \frac{i}{\hbar}\phi^2\right] - \frac{1}{Z_1}\left[\frac{\delta^2\Gamma}{\delta\varphi^2} + 2\frac{i}{\hbar}\frac{\delta\Gamma}{\delta G}\right]\int \mathcal{D}\phi e^{\frac{i}{\hbar}\tilde{S}}\phi\,. \tag{3.41}$$

Both terms in front of the integrals are non-zero due to the invertibility of the Legendre transform from the convexity of W already assumed. Therefore we obtain $\langle\phi\rangle_{\tilde{S}} = 0$ and $\langle\phi^2\rangle_{\tilde{S}} = i\hbar G$, so all diagrams contained in W_1 are 1-PI and written in terms of full propagators G.
We can further isolate all 2-PI diagrams. Here, we follow the approach of [47], which uses a clever ansatz for the effective action, which we will justify later, namely

$$\Gamma[\varphi, G] = S[\varphi] + \frac{i\hbar}{2}\mathrm{tr}\log G^{-1} + \frac{i\hbar}{2}\mathrm{tr}G_0^{-1}G + \Gamma^2[\varphi, G] + const\,. \tag{3.42}$$

Here, Γ^2 is the remaining diagrammatic part containing only 2-PI vacuum diagrams. We will call this form the CJT form of the 2PI EA. Taking the derivative, we obtain the equations of motion and define the self-energy by analogy with Dyson's equation as $\Sigma = \frac{2i}{\hbar}\frac{\delta\Gamma^2}{\delta G}$.

$$\frac{\delta\Gamma}{\delta G} = -\frac{i\hbar}{2}G^{-1} + \frac{i\hbar}{2}G_0^{-1} + \frac{\delta\Gamma^2}{\delta G} = \frac{-i\hbar}{2}R \quad \Rightarrow \quad \left[G^{-1} = G_0^{-1} - \Sigma\right]_{J=R=0} \tag{3.43}$$

$$\frac{\delta\Gamma}{\delta\varphi} = \frac{\delta S}{\delta\varphi} + \frac{i\hbar}{2}\frac{\delta G_0^{-1}}{\delta\varphi}G + \frac{\delta\Gamma^2}{\delta\varphi} = -J - \varphi R\,. \tag{3.44}$$

In the case of complex fields, one must be more careful at this point and remember that the Green functions are two index objects of complex fields. This means the derivatives must be performed keeping the appropriate order of indices as

$$\left.\begin{aligned}\frac{\delta}{\delta G_{i,j}}\sum_k \log(G^{-1})_{k,k} &= \sum_{k,p} G^{-1}_{k,p}\frac{\delta G_{p,k}}{\delta G_{i,j}} = G^{-1}_{j,i}\\ \frac{\delta}{\delta G_{i,j}}\sum_{k,p}(G_0^{-1})_{k,p}G_{p,k} &= (G_0^{-1})_{j,i}\end{aligned}\right\} \Rightarrow \Sigma_{i,j} = \frac{2i}{\hbar}\frac{\delta\Gamma^2}{\delta G_{j,i}}\,. \tag{3.45}$$

Note that if Γ^2 contains only 2-PI vacuum diagrams, then Σ contains 1-PI diagrams with external indices. The sources can now be represented as

$$R = G^{-1} - G_0^{-1} + \frac{2i}{\hbar}\frac{\delta\Gamma^2}{\delta G} = G^{-1} - G_0^{-1} + \Sigma \tag{3.46}$$

$$J = -\frac{\delta\Gamma}{\delta\varphi} + \Big[G^{-1} - G_0^{-1} + \Sigma\Big]\,\varphi\,. \tag{3.47}$$

This allows us to obtain the 2-PI EA more explicitly using its integral representation.

$$\begin{aligned}
e^{\frac{i}{\hbar}\Gamma} &= \int d\phi \exp\frac{i}{\hbar}\left[S[\phi] + J(\phi-\varphi) + \frac{1}{2}R(\phi^2-\varphi^2-i\hbar G)\right]\\
&= e^{\frac{i}{\hbar}S[\varphi]}\int d\phi \exp\frac{i}{\hbar}\left[S[\phi+\varphi] - S[\varphi] + (J+\varphi R)\phi + \frac{1}{2}R(\phi^2 - i\hbar G)\right]\\
&= e^{\frac{i}{\hbar}S[\varphi]}\int d\phi \exp\frac{i}{\hbar}\left[S[\phi+\varphi] - S[\varphi] - \frac{\delta\Gamma}{\delta\varphi}\phi + \frac{1}{2}(G^{-1} - G_0^{-1} + \Sigma)(\phi^2 - i\hbar G)\right]\\
&= e^{\frac{i}{\hbar}\left[S[\varphi] + \frac{i\hbar}{2}G_0^{-1}G - \frac{i\hbar}{2}\mathrm{tr}1\right]}\int d\phi \exp\frac{i}{\hbar}\left[S[\phi+\varphi] - S[\varphi] - \frac{\delta\Gamma}{\delta\varphi}\phi + \frac{1}{2}\phi^2(G^{-1} - G_0^{-1}) + \frac{1}{2}\Sigma(\phi^2 - i\hbar G)\right]\\
&= e^{\frac{i}{\hbar}\left[S[\varphi] + \frac{i\hbar}{2}G_0^{-1}G - \frac{i\hbar}{2}\mathrm{tr}1\right]}\int d\phi \exp\frac{i}{\hbar}\left[\frac{1}{2}\phi G^{-1}\phi + S_I[\phi,\varphi] + \frac{1}{2}\Sigma(\phi^2 - i\hbar G) + \phi\left(\frac{\delta S}{\delta\varphi} - \frac{\delta\Gamma}{\delta\varphi}\right)\right]
\end{aligned}$$

where we have defined the effective interaction as $S_I = \sum_{n=3}\frac{1}{n!}\frac{\delta^n S[\varphi]}{\delta\varphi^n}\phi^n$. We now pull the remaining integral into the exponent and normalise the integral by its Gaussian part, obtaining $\mathrm{tr}(\log(G))$. In this way, we find for $\Gamma[\varphi, G]$ and the diagrammatic part Γ^2 the expressions

$$\Gamma[\varphi,G] = S[\varphi] + \frac{i\hbar}{2}G_0^{-1}G - \frac{i\hbar}{2}\mathrm{tr}1 + \frac{i\hbar}{2}\mathrm{tr}\ln(G^{-1}) + \Gamma^2 \tag{3.48}$$

$$\Gamma^2 = -i\hbar\ln\Big[\int\frac{d\phi}{\sqrt{\det(G)}}\exp\frac{i}{\hbar}\Big[\frac{1}{2}\phi G^{-1}\phi + S_I[\phi,\varphi] + \frac{1}{2}\Sigma(\phi^2 - i\hbar G) + \phi\left(\frac{\delta S}{\delta\varphi} - \frac{\delta\Gamma}{\delta\varphi}\right)\Big]\Big]\,. \tag{3.49}$$

We can equate this with what we have found before from the CJT ansatz.

$$\begin{aligned}
\Gamma[\varphi,G] &= S[\varphi] + \frac{i\hbar}{2}\mathrm{tr}\log G^{-1} + \frac{i\hbar}{2}\mathrm{tr}G_0^{-1}G + \Gamma^2[\varphi,G] + const &(3.50)\\
&= S[\varphi] + W_1 - \frac{i\hbar}{2}\mathrm{tr}(RG)\\
&\Rightarrow \Gamma_2 = W_1 - \frac{i\hbar}{2}\mathrm{tr}(R + G_0^{-1})G + \frac{i\hbar}{2}\mathrm{tr}\log G + const &(3.51)
\end{aligned}$$

We now analyse Γ^2 diagrammatically at the saddle point, so when the equations of motion hold and the sources vanish. For this, we factor G_0 in its free contribution, coming from the quadratic part of the action g_0 and the interacting part V_I to find

$$\Gamma^2[\varphi, G] = W_1 - \frac{i\hbar}{2}\mathrm{tr}G_0^{-1}G + \frac{i\hbar}{2}\mathrm{tr}\log(1 + (\Sigma - \frac{\delta^2 V_I}{\delta\varphi^2})G) + const\,. \tag{3.52}$$

Expanding the logarithm in powers of the self-energy we obtain

$$\Gamma^2[\varphi, G] = W_1 - \frac{i\hbar}{2}\mathrm{tr}G_0^{-1}G - \frac{i\hbar}{2}\sum_{n=1}\frac{1}{n}\left[(\frac{\delta^2 V_I}{\delta\varphi^2} - \Sigma)G\right]^n + const\,. \tag{3.53}$$

The third term generates all 2-PR diagrams assuming that Σ contains only 1-PI diagrams in a loop $\mathrm{tr}(G\Sigma G\Sigma) + ...$[1]. Here, for bosons, the additional factor $\frac{\delta^2 V_I}{\delta\varphi^2}$ appears, which removes condensate insertions in propagators. These are already included by the definition of G_0^{-1}. This shows that the assumption that $\Sigma \propto \frac{\delta\Gamma^2}{\delta G}$ contains only 1-PI diagrams is consistent with the form of Γ^2. Therefore Γ^2 must only contain 2-PI diagrams, with lines given by full Green functions and vertices given by $S_I = \sum_{n=3}\frac{1}{n!}\frac{\delta^n S[\varphi]}{\delta\varphi^n}\phi^n$.

3.2.1 Explicit expansion

We want to show here how explicit approximations can be obtained. We focus on the $\hbar$ expansion, but also expansion in terms of coupling constants [31] or $1/N$ [49] are obtainable from the expression of Γ^2. The reason for the focus on the $\hbar$ expansion is that it measures quantum fluctuations. This can be seen directly from the path integral by the weighting factor $1/\hbar$ in front of the action, measuring deviation from the classical path. Therefore, one can often obtain good results even in strong coupling regimes if a well-defined mean field exists and fluctuations around it are small. We now focus on the path integral inside of the logarithm. Note here that this already has a factor of $\hbar$ in front. Let us first scale the integral variable explicitly with $\hbar$ as $\phi \to \sqrt{\hbar}\phi$ leading us to

$$\int \frac{d\phi}{\sqrt{\det(G)}}\exp i\left[\frac{1}{2}\phi G^{-1}\phi + \tilde{S}_I + \frac{i}{\hbar}\frac{\delta\Gamma^2}{\delta G}(\phi^2 - iG) - \sqrt{\hbar}\phi\left(\frac{1}{2}\frac{\delta^3 S}{\delta\varphi^3}G + \frac{1}{\hbar}\frac{\delta\Gamma^2}{\delta\varphi}\right)\right] \tag{3.54}$$

with $\tilde{S}_I = \sum_{n=3}\frac{\hbar^{n/2-1}}{n!}\frac{\delta^n S}{\delta\varphi^n}\phi^n$. The first term of the $\hbar$ expansion starts at the second order since we already factored out the first order via the logarithm. Therefore we can expand $\Gamma^2 = \sum_{n=2}\hbar^n\Gamma_n^2$. To be explicit, we focus now on a theory, which only contains terms up to ϕ^4 in its interaction. Let us start collecting the orders of $\hbar$ in the action up to order $\hbar^2$

$$\frac{1}{2}\phi G^{-1}\phi + \sqrt{\hbar}\left[\frac{1}{3!}\frac{\delta^3 S}{\varphi^3}\phi^3 - \phi\frac{1}{2}\frac{\delta^3 S}{\delta\varphi^3}G\right] + \hbar\left[\frac{1}{4!}\frac{\delta^4 S}{\delta\varphi^4}\phi^4 + \frac{\delta\Gamma_2^2}{\delta G}(i\phi^2 + G)\right] + \mathcal{O}(\hbar^{3/2})\,. \tag{3.55}$$

We now expand the exponential around a Gaussian with second moment G in powers of $\hbar$. Note that we do not need to expand around a shifted Gaussian since we have already shown

[1] Some reader might wonder where diagrams are contained, which are not apparent loops, like ladder diagrams, which are reducible by cutting two lines at the same rung. All these diagrams can be obtained by self-energy insertions into Green function lines. The ladder diagrams, for example, are produced via self-energy insertions of NCA-type diagrams.

that the theory has a vanishing central moment. A direct expansion leads us to

$$\int \frac{d\phi}{\sqrt{\det G}} e^{\frac{i}{2}\phi G^{-1}\phi} \left[1 + i\sqrt{\hbar}\left[\frac{1}{3!}\frac{\delta^3 S}{\varphi^3}\phi^3 - \phi\frac{1}{2}\frac{\delta^3 S}{\delta\varphi^3}G\right] + \frac{\hbar}{2}i^2\left[\frac{1}{3!}\frac{\delta^3 S}{\varphi^3}\phi^3 - \phi\frac{1}{2}\frac{\delta^3 S}{\delta\varphi^3}G\right]^2 \right. \tag{3.56}$$

$$\left. + i\frac{\hbar}{4!}\frac{\delta^4 S}{\delta\varphi^4}\phi^4 + i\hbar\frac{\delta\Gamma_2^2}{\delta G}(i\phi^2 + G) + \mathcal{O}(\hbar^{3/2})\right] . \tag{3.57}$$

Now, we have to remember that the integral is inside a logarithm; therefore, all disconnected parts are factored, so we only need to consider the connected part. The $\sqrt{\hbar}$ order drops out since we average wrt. to a symmetric Gaussian. In order $\hbar$, we find first the Hartree-Fock diagrams, which are connected and 2-PI. The last term in the second line vanishes since the propagator of the shifted theory is the full Green function. The last term in the first line generates the non-crossing [2] approximation (NCA) and also needs to cancel the dumbbell diagram, namely

$$\left[\frac{1}{3!}\frac{\delta^3 S}{\varphi^3}\phi^3\right]^2 + \left[\frac{1}{2}\phi\frac{\delta^3 S}{\delta\varphi^3}G\right]^2 - 2\left[\frac{1}{3!}\frac{\delta^3 S}{\varphi^3}\phi^3\frac{1}{2}\phi\frac{\delta^3 S}{\delta\varphi^3}G\right] . \tag{3.58}$$

Let us explicitly show the cancellation using the diagrammatic representation of the three terms.

$$\left[\frac{1}{3!}\frac{\delta^3 S}{\varphi^3}\phi^3\right]^2 = \frac{1}{3!^2}\left[3 * 2 *$$  $$+ 3 * 3 *$$ 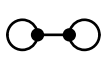 $$\right] \tag{3.59}$$

$$\left[\frac{1}{2}\phi\frac{\delta^3 S}{\delta\varphi^3}G\right]^2 = \frac{1}{4} *$$  $$\tag{3.60}$$

$$2\left[\frac{1}{3!}\frac{\delta^3 S}{\varphi^3}\phi^3\frac{1}{2}\phi\frac{\delta^3 S}{\delta\varphi^3}G\right] = \frac{1}{3!}3 *$$  $$\tag{3.61}$$

Collecting all the terms, the dumbbell diagram cancels, and we only obtain the NCA diagram

$$\frac{1}{2!}$$  $$+ \frac{1}{4}$$  $$+ \frac{1}{4}$$  $$- \frac{1}{2}$$  $$= \frac{1}{2!}$$  $$. \tag{3.62}$$

The first contributions are of order $\hbar^2$ as anticipated and are the NCA diagram and HF given by

$$\Gamma_2^2 = \hbar^2\left[\frac{1}{2}\frac{\delta^3 S}{\delta\varphi^3}G^3\frac{\delta^3 S}{\delta\varphi^3} - \frac{1}{8}\frac{\delta^4 S}{\delta\varphi^4}G^2\right] \tag{3.63}$$

Higher order contributions are now obtained iteratively since the next order will depend on Γ_2^2, which is needed to cancel various 2-PR contributions.

[2] Often called the sunset diagram.

3.3 Approximations of 2-PI EA

The 2-PI EA is tremendously helpful in developing conserving approximations for a theory. Nevertheless, various caveats should be kept in mind when interpreting results. Here, we want to investigate a few of these issues. To clarify the point, let us first look at how expectation values are computed in an approximation of the 1PI EA Γ_1. As an example, let us take a four-point average. The idea is to decompose the expectation value into its cumulants and then compute the cumulants using the 1PI EA. To this end, one obtains

$$\begin{aligned}
\langle\phi_i\phi_j\phi_k\phi_l\rangle = \quad & \tfrac{\delta W}{\delta J_i}\tfrac{\delta W}{\delta J_j}\tfrac{\delta W}{\delta J_k}\tfrac{\delta W}{\delta J_l} \\
& -\hbar^2\left(\tfrac{\delta^2 W}{\delta J_i\delta J_j}\tfrac{\delta^2 W}{\delta J_k\delta J_l} + 2\,\text{permutations}\right) \\
& -i\hbar^2\left(\tfrac{\delta W}{\delta J_i}\tfrac{\delta W}{\delta J_j}\tfrac{\delta^2 W}{\delta J_k\delta J_l} + 5\,\text{permutations}\right) \\
& -\hbar^2\left(\tfrac{\delta^3 W}{\delta J_i\delta J_j\delta J_k}\tfrac{\delta W}{\delta J_l} + 3\,\text{permutations}\right) \\
& +i\hbar^3\tfrac{\delta^4 W}{\delta J_i\delta J_j\delta J_k\delta J_l}
\end{aligned}$$

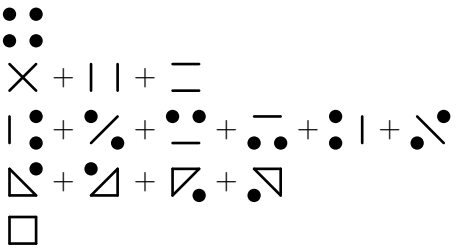

Here, we have introduced an intuitive graphical notation to clarify permutations. Each corner is one of the indices (i, j, k, l) connected to various cumulants. The first four lines separate all processes, which have some independent parts, and the last line gives the non-separable part of the average. From now on, we will need to keep track of internal indices, which need to be summed up. We use a sum convention that over every index, which is a number, is summed and integrated appropriately, and every letter is an external index.
The cumulants are obtained from the approximation of the 1PI EA using recursion as follows. We know that the second derivative of the 1PI EA is the inverse 2-point Green function

$$\frac{\delta^2\Gamma_1}{\delta\varphi_i\delta\varphi_1}G_{1,j} = \delta_{i,j} \Leftrightarrow G_{i,j} = \left[\frac{\delta^2\Gamma_1}{\delta\varphi\delta\varphi}\right]^{-1}_{i,j} = -\frac{\delta^2 W}{\delta J_i\delta J_j}\,. \tag{3.64}$$

We can now obtain the next cumulant by chain rule as

$$\frac{\delta^3 W}{\delta J_i\delta J_j\delta J_k} = -\frac{\delta}{\delta J_k}\left[\frac{\delta^2\Gamma_1}{\delta\varphi\delta\varphi}\right]^{-1}_{i,j} \tag{3.65}$$

$$= -\frac{\delta\varphi_1}{\delta J_k}\frac{\delta}{\delta\varphi_1}\left[\frac{\delta^2\Gamma_1}{\delta\varphi\delta\varphi}\right]^{-1}_{i,j} = \frac{\delta\varphi_1}{\delta J_k}\left[\frac{\delta^2\Gamma_1}{\delta\varphi\delta\varphi}\right]^{-1}_{i,2}\frac{\delta^3\Gamma_1}{\delta\varphi_1\delta\varphi_2\delta\varphi_3}\left[\frac{\delta^2\Gamma_1}{\delta\varphi\delta\varphi}\right]^{-1}_{3,j} \tag{3.66}$$

$$= -G_{k,1}G_{i,2}G_{j,3}\frac{\delta^3\Gamma_1}{\delta\varphi_1\delta\varphi_2\delta\varphi_3} = \tag{3.67}$$

The diagrams represent the three derivatives of Γ and attach three Green functions to the external legs. The fourth cumulant can be computed using the same method, leading us to

$$\frac{\delta^4 W}{\delta J_i\delta J_j\delta J_k\delta J_l} = -\frac{\delta G_{k,1}}{\delta J_l}G_{i,2}G_{j,3}\frac{\delta^3\Gamma_1}{\delta\varphi_1\delta\varphi_2\delta\varphi_3} - \frac{\delta G_{i,2}}{\delta J_l}G_{k,1}G_{j,3}\frac{\delta^3\Gamma_1}{\delta\varphi_1\delta\varphi_2\delta\varphi_3} \tag{3.68}$$

$$-\frac{\delta G_{j,3}}{\delta J_l}G_{i,2}G_{k,1}\frac{\delta^3\Gamma_1}{\delta\varphi_1\delta\varphi_2\delta\varphi_3} - G_{k,1}G_{i,2}G_{j,3}\frac{\delta}{\delta J_l}\frac{\delta^3\Gamma_1}{\delta\varphi_1\delta\varphi_2\delta\varphi_3} \tag{3.69}$$

$$= G_{k,1}G_{l,2}\frac{\delta^3\Gamma_1}{\delta\varphi_1\delta\varphi_2\delta\varphi_3}G_{3,4}\frac{\delta^3\Gamma_1}{\delta\varphi_4\delta\varphi_5\delta\varphi_6}G_{5,i}G_{6,j} + (2\,\text{permutations}) \tag{3.70}$$

$$+ G_{k,1}G_{i,2}G_{j,3}G_{l,4}\frac{\delta^3\Gamma_1}{\delta\varphi_1\delta\varphi_2\delta\varphi_3\delta\varphi_4} \tag{3.71}$$

$$= 3\ \text{permutations of} \tag{3.72}$$

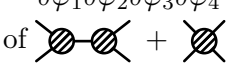

Note here that all derivatives of W are taken wrt. J and of Γ with φ. Each of these derivatives commutes, and therefore, the averages will always have the correct symmetry imposed by the action. From this property, one can derive the exact Ward identities, which we will show later. The case of the 2-PI EA is different in that here derivatives wrt. to the second source R produce expectation values that can be decomposed in derivatives wrt. J. This already occurs for quadratic averages and, more importantly, for cubic averages as

$$\frac{\delta W}{\delta R_{x,y}} = \frac{1}{2}\left[\frac{\delta W}{\delta J_x}\frac{\delta W}{\delta J_y} - i\hbar\frac{\delta^2 W}{\delta J_x \delta J_y}\right] \tag{3.73}$$

$$\frac{\delta^2 W}{\delta R_{x,y}\delta J_z} = \frac{1}{2}\left[\frac{\delta^2 W}{\delta J_x \delta J_z}\frac{\delta W}{\delta J_y} + \frac{\delta^2 W}{\delta J_y \delta J_z}\frac{\delta W}{\delta J_x}\right] - \frac{i\hbar}{2}\frac{\delta^3 W}{\delta J_x \delta J_y \delta J_z}\,. \tag{3.74}$$

The set of relations generated by this procedure strictly holds only if no approximations are employed [50] [51] [52] [53]. Applying approximation might lead to a violation of these identities between different correlation functions following the exact structure of the theory. We will start now to derive exact relations from the 2-PI EA for the self-energy and show where such problems can arise. As a starting point, we use that the 2-PI EA is constructed via a Legendre transformation. Therefore, the Hessian matrices of W and Γ must be inverse, such that the transformation is involutive. We first represent the sources J and R in term of derivatives of Γ as

$$\frac{\delta\Gamma}{\delta\varphi_i} - \frac{2}{i\hbar}\frac{\delta\Gamma}{\delta G_{i,1}}\varphi_1 = -J_i \quad \text{and} \quad \frac{2}{i\hbar}\frac{\delta\Gamma}{\delta G_{i,j}} = -R_{i,j}\,. \tag{3.75}$$

The two relevant relations between the second derivatives in the present case can then be constructed as

$$\delta_{i,j} = \frac{\delta J_i}{\delta J_j} = -\left[\frac{\delta\varphi_1}{\delta J_j}\frac{\delta}{\delta\varphi_1} + \frac{\delta G_{1,2}}{\delta J_j}\frac{\delta}{\delta G_{1,2}}\right]\left[\frac{\delta\Gamma}{\delta\varphi_i} - \frac{2}{i\hbar}\frac{\delta\Gamma}{\delta G_{i,3}}\varphi_3\right] \tag{3.76}$$

$$= -\frac{\delta^2 W}{\delta J_j \delta J_1}\left[\frac{\delta^2\Gamma}{\delta\varphi_1\delta\varphi_i} - \frac{2}{i\hbar}\frac{\delta^2\Gamma}{\delta G_{i,3}\delta\varphi_1}\varphi_3 - \frac{2}{i\hbar}\frac{\delta\Gamma}{\delta G_{1,i}}\right] \tag{3.77}$$

$$+ \frac{\delta^3 W}{\delta J_j \delta J_1 \delta J_2}\left[\frac{\delta^2\Gamma}{\delta G_{1,2}\delta\varphi_i} - \frac{2}{i\hbar}\frac{\delta^2\Gamma}{\delta G_{1,2}\delta G_{i,3}}\varphi_3\right] \tag{3.78}$$

$$0 = \frac{\delta R_{k,l}}{\delta J_i} = -\frac{2}{i\hbar}\left[\frac{\delta\varphi_1}{\delta J_i}\frac{\delta}{\delta\varphi_1} + \frac{\delta G_{1,2}}{\delta J_i}\frac{\delta}{\delta G_{1,2}}\right]\frac{\delta\Gamma}{\delta G_{k,l}} \tag{3.79}$$

$$= -\frac{2}{i\hbar}\left[\frac{\delta^2 W}{\delta J_i \delta J_1}\frac{\delta^2\Gamma}{\delta\varphi_1\delta G_{k,l}} - \frac{\delta^3 W}{\delta J_i \delta J_1 \delta J_2}\frac{\delta^2\Gamma}{\delta G_{1,2}\delta G_{k,l}}\right] \tag{3.80}$$

The second relation can be used to cancel the explicit dependence of φ in the first relation to obtain

$$\delta_{i,j} = G_{j,1}\left[\frac{\delta^2\Gamma}{\delta\varphi_1\delta\varphi_i} - \frac{2}{i\hbar}\frac{\delta\Gamma}{\delta G_{1,i}}\right] + \frac{\delta^3 W}{\delta J_j \delta J_1 \delta J_2}\frac{\delta^2\Gamma}{\delta G_{1,2}\delta\varphi_i}\,. \tag{3.81}$$

To relate this expression to the self-energies we now use the CJT form of the 2-PI EA and take the required derivatives, leading us to

$$\Gamma[\varphi, G] = S[\varphi] + \frac{i\hbar}{2}\mathrm{tr}\log G^{-1} + \frac{i\hbar}{2}\mathrm{tr}G_0^{-1}G + \Gamma^2[\varphi, G] + const \tag{3.82}$$

$$\frac{\delta\Gamma}{\delta G_{x,y}} = -\frac{i\hbar}{2}G^{-1}_{x,y} + \frac{i\hbar}{2}(G_0^{-1})_{x,y} + \frac{\delta\Gamma^2}{\delta G_{x,y}} \tag{3.83}$$

$$\frac{\delta^2\Gamma}{\delta\varphi_x\delta\varphi_y} = \frac{\delta^2 S}{\delta\varphi_x\delta\varphi_y} + \frac{i\hbar}{2}\left(\frac{\delta^4 S}{\delta\varphi_x\delta\varphi_y\delta\varphi_1\delta\varphi_2}G_{2,1}\right) + \frac{\delta^2\Gamma^2}{\delta\varphi_x\delta\varphi_y} \tag{3.84}$$

$$\frac{\delta^2\Gamma}{\delta\varphi_x\delta G_{a,b}} = \frac{i\hbar}{2}\frac{\delta^3 S}{\delta\varphi_x\delta\varphi_a\delta\varphi_b} + \frac{\delta^2\Gamma^2}{\delta\varphi_x\delta G_{a,b}} \tag{3.85}$$

$$\frac{\delta^2\Gamma}{\delta G_{a,b}\delta G_{x,y}} = \frac{i\hbar}{2}G^{-1}_{a,x}G^{-1}_{b,y} + \frac{\delta^2\Gamma^2}{\delta G_{a,b}\delta G_{x,y}}\,. \tag{3.86}$$

At the physical point where the sources vanish, we obtain through these relations

$$\delta_{i,j} = G_{i,1}\left[\frac{\delta^2 S}{\delta\varphi_1\delta\varphi_j} + \frac{i\hbar}{2}\left(\frac{\delta^4 S}{\delta\varphi_1\delta\varphi_j\delta\varphi_2\delta\varphi_3}G_{2,3}\right) + \frac{\delta^2\Gamma^2}{\delta\varphi_1\delta\varphi_j}\right] \tag{3.87}$$

$$+ \frac{\delta^3 W}{\delta J_i\delta J_1\delta J_2}\left[\frac{i\hbar}{2}\frac{\delta^3 S}{\delta\varphi_1\delta\varphi_2\delta\varphi_j} + \frac{\delta^2\Gamma^2}{\delta\varphi_j\delta G_{1,2}}\right]. \tag{3.88}$$

By comparison with the Dyson equation, we can identify the self-energy part of the equation as

$$-G_{i,1}\Sigma_{1,j} = G_{i,1}\left[\frac{i\hbar}{2}\left(\frac{\delta^4 S}{\delta\varphi_1\delta\varphi_j\delta\varphi_2\delta\varphi_3}G_{2,3}\right) + \frac{\delta^2\Gamma^2}{\delta\varphi_1\delta\varphi_j}\right] \tag{3.89}$$

$$+ \frac{\delta^3 W}{\delta J_i\delta J_1\delta J_2}\left[\frac{i\hbar}{2}\frac{\delta^3 S}{\delta\varphi_1\delta\varphi_2\delta\varphi_j} + \frac{\delta^2\Gamma^2}{\delta\varphi_j\delta G_{1,2}}\right]. \tag{3.90}$$

In this thesis, we will only be interested in cubic interaction, which reduces the expression to

$$G_{i,1}\Sigma_{1,j} = -\frac{i\hbar}{2}\frac{\delta^3 W}{\delta J_i\delta J_1\delta J_2}\frac{\delta^3 S}{\delta\varphi_1\delta\varphi_2\delta\varphi_j} = -\frac{\delta^3 W}{\delta J_i\delta J_1\delta J_2}\frac{\delta^2\Gamma}{\delta G_{1,2}\delta\varphi_j}\,. \tag{3.91}$$

This gives us a direct connection between the self-energy contributions in the KB eq, and certain expectation values related to the interaction. We can further establish a consistency equation for the self-energy. For this, we take another look at the second Hessian equation to obtain

$$G_{i,1}\frac{\delta^2\Gamma}{\delta\varphi_1\delta G_{k,l}} = -\frac{\delta^3 W}{\delta J_i\delta J_1\delta J_2}\frac{\delta^2\Gamma}{\delta G_{1,2}\delta G_{k,l}}\,. \tag{3.92}$$

We now use that we can construct the inverse of $\frac{\delta^2\Gamma}{\delta G^2}$ via a Bethe-Salpeter equation to obtain

$$G_{i,1}\frac{\delta^2\Gamma}{\delta\varphi_1\delta G_{2,3}}\left[\frac{\delta^2\Gamma}{\delta G^2}\right]^{-1}_{2,3,4,5}\frac{\delta^2\Gamma}{\delta G_{4,5}\delta\varphi_j} = -\frac{\delta^3 W}{\delta J_i\delta J_1\delta J_2}\frac{\delta^2\Gamma}{\delta G_{1,2}\delta\varphi_j}\,. \tag{3.93}$$

Compared with our previous result for a cubic interaction, this leads us to an equality for the self-energy

$$\frac{i\hbar}{2}\frac{\delta^3 S}{\delta\varphi_i\delta\varphi_1\delta\varphi_2}\left[G^{-1}G^{-1}+\frac{\delta\Sigma}{\delta G}\right]^{-1}_{1,2,3,4}\frac{\delta^3 S}{\delta\varphi_3\delta\varphi_4\delta\varphi_j}=\Sigma_{i,j}\,. \tag{3.94}$$

One might note that most conserving self-energy approximations do not fulfil this relation. In [50] [51] [52], it was shown that (3.94) is crucial to preserve the proper connections between correlation functions of different order due to symmetry. They proposed a way to restore this symmetry again by using (3.94) to supplement the missing diagrammatic channels. This means one first chooses an approximation for Γ^2 and extracts the self-energies accordingly. The insertion in the lhs. of (3.94) will usually lead to an infinite class of distinct diagrams defining the self-energy which should be used. The solution of this system will usually now also involve the solutions of a Bethe-Salpether equation, which determines the new self-energy approximation. This approach is tremendously hard to implement. Therefore, one might wonder what we are losing if (3.94) is not implemented.

3.4 Ward-Takahashi identities

Later on, we will investigate systems with spontaneously broken symmetry (SSB). In this case, the action and the path integral measure, following from there also the effective action, are invariant under continuous transformations. However, the solutions of the equations of motion generated do not necessarily have the full symmetry but pick a specific subgroup. An example is the Heisenberg model in $d = 3$, in which the Hamiltonian is invariant under rotations. Nevertheless, in the thermodynamic limit at low temperatures, a magnetisation with a specific direction, which is spontaneously chosen, can form. The symmetry of the model nevertheless restricts the dynamics in the SSB phase. These restrictions are most clearly stated in the Ward-Takahashi identities, which are most easily derived from the 1-PI formalism. In this section, we focus on the problem that the effective actions are rarely known exactly and need to be approximated and truncated, leading to non-equivalence of different N-PI effective actions [32]. However, we will see different effective actions lead to different Ward identities, which are only equivalent when evaluated exactly. We will limit ourselves here to only the first-order Ward-identities. Let us begin by considering the 1-PI EA $\Gamma_1[\Phi]$, with n scalar fields Φ, which is invariant under a continuous transformation $O = e^{aT}$, where T is the generator of the transformation. Since the effective action is invariant under all transformations of this kind, we can look at an infinitesimal transformation and see how the correlation functions behave. First, we expand to linear order in the parameter a and obtain

$$\begin{aligned}\Gamma_1[\Phi]=\Gamma_1[O\Phi]=\Gamma_1[(1+aT+..)\Phi]&=\Gamma_1[\Phi]+\frac{\partial\Gamma_1}{\partial a}a+...=\Gamma_1[\Phi]+\frac{\delta\Gamma_1[\Phi]}{\delta\Phi}\frac{\partial aT\Phi}{\partial a}a+...\\&=\Gamma_1[\Phi]+a\left[\frac{\delta\Gamma_1[\Phi]}{\delta\Phi_1}T_{1,2}\Phi_2\right]+...\\&\Rightarrow\frac{\delta\Gamma_1[\Phi]}{\delta\Phi_1}T_{1,2}\Phi_2=0\,.\end{aligned} \tag{3.95}$$

Since the relation must hold for all a, every coefficient in the power series must vanish. Note here that this is not just a constraint on Γ_1 on the physical solution but on the whole functional.

Therefore, we can differentiate again wrt. to Φ_x and obtain

$$0 = \frac{\delta^2\Gamma_1[\Phi]}{\delta\Phi_x\delta\Phi_1}T_{1,2}\Phi_2 + \frac{\delta\Gamma_1[\Phi]}{\delta\Phi_1}T_{1,x}\,. \tag{3.96}$$

At the physical point, the second term vanishes, and we obtain for the physical solutions that

$$0 = \frac{\delta^2\Gamma_1[\Phi]}{\delta\Phi_x\delta\Phi_1}T_{1,2}\Phi_2 = G^{-1}_{x,1}T_{1,2}\Phi_2\,.. \tag{3.97}$$

Let us now consider a bosonic theory with a $U(1)$ symmetry, which we can easily obtain by choosing $\Phi_a = \phi$ and $\Phi_b = \phi^*$. The Ward identity leads us then to

$$\int dt' \left[G^{-1}_{\phi,\phi}(t,t')\phi(t') - G^{-1}_{\phi,\phi^*}(t,t')\phi^*(t')\right] = 0 \tag{3.98}$$

$$= \int dt' \left[-\Sigma_{\phi,\phi}(t,t')\phi(t') - \left(\delta_{t,t'}(i\partial_t - h_0) - \Sigma_{\phi,\phi^*}(t,t')\right)\phi^*(t')\right] \tag{3.99}$$

To understand the implications, let us consider that the system reached a steady state, which implies $\Phi(t) = \Phi_0$ [3] and the self-energies only depend on relative time so that they can be represented in frequency space. With this, we obtain the Hugenholtz-Pines relation

$$[h_0 - \Sigma_{\phi,\phi}(\omega = 0) + \Sigma_{\phi,\phi^*}(\omega = 0)]\Phi_0 = 0 \tag{3.100}$$

which relates the normal and anomalous self-energies to the chemical potential and ground state energy contained in h_0. This enforces the pole position of the Green function so that it is not invertible at the frequency $\omega = 0$. This fact can be most easily understood in equilibrium, where the distribution function is the Bose function with a pole at $\omega = 0$. The spectral function must change sign and at least linearly vanish at this point so that the fluctuating particle number spectrum remains finite and positive. It is an essential consequence of the stable, macroscopically occupied single-particle wavefunction ϕ.
Taking higher order derivatives of (3.96) leads to further connections between response functions, whose dynamics are all restricted by symmetry.

The case of the 2-PI EA is more complicated. Here also, the Green functions need to be transformed, meaning that we now obtain after infinitesimal transformation

$$\Gamma[\Phi, G] = \Gamma[O\Phi, O^\dagger GO] = \Gamma[(1+aT)\Phi, (1+aT)G(1+aT)] = \Gamma[(1+aT)\Phi, G + a(GT+TG) + ...]$$
$$= \Gamma[\Phi, G] + a\left[\frac{\delta\Gamma}{\delta\Phi_1}T_{1,2}\Phi_2 + \frac{\delta\Gamma}{\delta G_{1,2}}\left[G_{1,3}T_{3,2} + T_{1,3}G_{3,2}\right]\right] \tag{3.101}$$

Therefore, generally, the 2-PI Ward-ID is different from the 1-PI Ward-ID, namely generated by

$$\frac{\delta\Gamma}{\delta\Phi_1}T_{1,2}\Phi_2 + \frac{\delta\Gamma}{\delta G_{1,2}}\left[G_{1,3}T_{3,2} + T_{1,3}G_{3,2}\right] = 0\,. \tag{3.102}$$

Explicitly, we again take the Φ_x derivative using here that this must hold for all Φ and G being independent and then restricting to the saddle point, leading us to

$$\frac{\delta^2\Gamma}{\delta\Phi_x\delta\Phi_1}T_{1,2}\Phi_2 + \frac{\delta^2\Gamma}{\delta\Phi_x\delta G_{1,2}}\left[G_{1,3}T_{3,2} + T_{1,3}G_{3,2}\right] = 0\,. \tag{3.103}$$

[3] Generally, a time evolution with a phase factor involving the ground state energy is possible, which in the translational invariant, weakly interacting Bose gas is chosen to be zero. We will come back to this point when we analyse the system of interest.

At this point, one might be tempted to declare the second term as the culprit of this changed Ward-identity. But in the 2-PI EA case, $\delta^2\Gamma/\delta\Phi^2$ also has a different meaning from the full inverse Green function. Therefore, the result should better be interpreted as a condition onto the two-point Green function to fulfil

$$\frac{\delta^2\Gamma}{\delta\Phi_x\delta\Phi_1}T_{1,2}\Phi_2 + \frac{\delta^2\Gamma}{\delta\Phi_x\delta G_{1,2}}\left[G_{1,3}T_{3,2} + T_{1,3}G_{3,2}\right] \overset{!}{=} G^{-1}_{x,1}T_{1,2}\Phi_2 \tag{3.104}$$

Let us again specialise in the case of a cubic theory, where we can use the identities obtained in the previous section. This allows us to write

$$(G_0^{-1})_{x,1}T_{1,2}\Phi_2 + \frac{\delta^2\Gamma}{\delta\Phi_x\delta G_{1,2}}\left[G_{1,3}T_{3,2} + T_{1,3}G_{3,2}\right] \overset{!}{=} ((G_0^{-1})_{x,1} - \Sigma_{x,1})T_{1,2}\Phi_2 \tag{3.105}$$

We can find another identity from (3.102) by taking a derivative wrt. to the Green function to obtain

$$\frac{\delta^2\Gamma}{\delta G_{x,y}\delta\Phi_1}T_{1,2}\Phi_2 + \frac{\delta^2\Gamma}{\delta G_{x,y}\delta G_{1,2}}\left[G_{1,3}T_{3,2} + T_{1,3}G_{3,2}\right] + \left[T_{y,1}\frac{\delta\Gamma}{\delta G_{1,x}} + \frac{\delta\Gamma}{\delta G_{y,1}}T_{1,x}\right] = 0\,. \tag{3.106}$$

The last bracket will vanish at the saddle point, and we can manipulate the first two terms to obtain

$$-\frac{\delta^2\Gamma}{\delta\varphi_x\delta G_{1,2}}\left[\frac{\delta^2\Gamma}{\delta G^2}\right]^{-1}_{1,2,3,4}\frac{\delta^2\Gamma}{\delta G_{3,4}\delta\varphi_5}T_{5,6}\varphi_6 = \frac{\delta^2\Gamma}{\delta\varphi_x\delta G_{1,2}}\left[G_{1,3}T_{3,2} + T_{1,3}G_{3,2}\right] \tag{3.107}$$

The left-hand side contains the expression for the self-energy found before. This means the Ward identity will only be fulfilled if the self-energy fulfils eq. (3.94). The interpretation in non-equilibrium is that the condensate energy should be at the pole position of the Green functions following eq. (3.97). If the self-energy does not follow (3.94), the condensate's energy is no longer constrained to this position.
An approach to remedy this problem was proposed in [54]. Here, one discards the equation of motion of the condensate generated by the stationarity condition of the 2-PI EA in favour of eq. (3.97). This will force the condensate to the pole of the Green function determined by the approximation of Γ^2. This approach, nevertheless, can lead to a loss of solutions in some cases [55].
One should note that dissipation in the form of particle loss and gain will not alter any of the arguments given above. The $U(1)$ symmetry, usually used to argue particle number conservation, is still present on the path integral level but can now not be decoupled in the $(+)$ and $(-)$ branch of Keldysh contours independently. From this follows a continuity equation rather than a conservation law [34]. But the Ward identities are formally the same as in eq. (3.97). Here, the free propagator contains additional dissipative contributions, which must then be taken into account.

Part III

Auxiliary-Particle Theory

Chapter 4

Auxiliary-Particles Representation

We now turn to the auxiliary particle representation of the Hamiltonian. The approach was first followed in [56–58]. This method is generally applicable if the system can be mapped to an effective single impurity model and has been applied to strongly correlated electron systems for a long time [59]. The mapping to a single impurity model can be archived by various methods. In the present case, we will employ ideas from Dynamical-Mean-Field Theory (DMFT). The underlying insight is that if the photon self-energy is a local quantity, then a local mean field can capture the effect on the molecule. In the present case, the molecule solution is dilute in the sense that the dye molecules are uncorrelated. Therefore, the photon self-energies generated by the photon-molecule interactions are purely local, and we can treat the molecules as single impurity systems coupled to a dynamical photon bath. For this reason, we drop the molecule and photon mode indices at the present stage and focus on the single impurity problem. How large molecule reservoirs and multiple photon modes are treated will be discussed later. The Hamiltonian in the rotating frame of the molecule was already introduced and reads:

$$\mathcal{H} = \delta a^\dagger a + \Big(\omega b^\dagger b + s\omega\sigma^z(b^\dagger + b)\Big) + \gamma(a^\dagger\sigma^- + a\sigma^+) \tag{4.1}$$

The aim is to treat the problem with field theoretical methods. Pauli matrices have the property that they do not commute canonically, which means that the commutator of two Pauli matrices again produces a Pauli matrix. This leads to various problems when working with them, among others, Wick's theorem does not hold. One of the methods to circumvent this is to introduce auxiliary bosons, which explicitly address the basis states with a set of bosonic operators. The key idea for the problem at hand is to enlarge the basis such that all physically different states are represented by their own bosonic single-particle state. It allows us to introduce auxiliary particles and create the original states from a vacuum as

$$|e,n\rangle = d^\dagger_{e,n}\,|vac\rangle \qquad |g,n\rangle = d^\dagger_{g,n}\,|vac\rangle\ . \tag{4.2}$$

Note that this approach is completely independent of the specifics of the molecule model used. This is one reason why this method is tremendously flexible regarding which systems can be treated.

To construct the operator in the new basis, we start by considering the action of the physical operators b and $\sigma^\pm$ on this new bosonic Hilbert space. The creation and annihilation operator for the phonons can then be decomposed in bilinear terms, which destroys a particle in a state with n - phonons and creates a state with $n+1$, or $n-1$, phonons giving an appropriate matrix element. These operators preserve the electronic state $\sigma \in \{e,g\}$ and can be written as

$$b^\dagger = \sum_{n,\sigma} \sqrt{n+1}\, d^\dagger_{\sigma,n+1} d_{\sigma,n} \qquad b = \sum_{\sigma,n} \sqrt{n+1}\, d^\dagger_{\sigma,n} d_{\sigma,n+1}\,. \tag{4.3}$$

The auxiliary bosons have the usual commutation relation: $[d_{\sigma,n}, d^\dagger_{\sigma',m}] = \delta_{m,n}\delta_{\sigma,\sigma'}$. The original operators act now as effective hopping between states with different phonon numbers. However, we need to preserve the commutation relation between the original operators, which leads us to:

$$\begin{aligned}
[b, b^\dagger] &= \sum_{m,\sigma,n,\sigma'} \sqrt{(n+1)(m+1)}[d^\dagger_{\sigma,n} d_{\sigma,n+1}, d^\dagger_{\sigma',m+1} d_{\sigma',m}] \\
&= \sum_{m,n,\sigma} \sqrt{(n+1)(m+1)}\left(d^\dagger_{\sigma,n}[d_{\sigma,n+1}, d^\dagger_{\sigma,m+1} d_{\sigma,m}] + [d^\dagger_{\sigma,n}, d^\dagger_{\sigma,m+1} d_{\sigma,m}] d_{\sigma,n+1} \right) \\
&= \sum_{\sigma,m,n} \sqrt{(n+1)(m+1)}\Big(d^\dagger_{\sigma,n}(d^\dagger_{\sigma,m+1}[d_{\sigma,n+1}, d_{\sigma,m}] \\
&\quad + \underbrace{[d_{\sigma,n+1}, d^\dagger_{\sigma,m+1}]}_{\delta_{n+1,m+1}} d_{\sigma,m}) + (d^\dagger_{\sigma,m+1} \underbrace{[d^\dagger_{\sigma,n}, d_{\sigma,m}]}_{-\delta_{m,n}} + [d^\dagger_{\sigma,n}, d^\dagger_{\sigma,m+1}] d_{\sigma,m}) d_{\sigma,n+1} \Big) \\
&= \sum_{\sigma,m,n} \sqrt{(n+1)(m+1)}(d^\dagger_{\sigma,n} d_{\sigma,m} \delta_{m+1,n+1} - d^\dagger_{\sigma,m+1} d_{\sigma,n+1} \delta_{m,n}) \\
&= \sum_\sigma \left(d^\dagger_{\sigma,0} d_{\sigma,0} + \sum_{n=1} d^\dagger_{\sigma,n} d_{\sigma,n}(n+1-n) \right) = \sum_{\sigma,n=0} d^\dagger_{\sigma,n} d_{\sigma,n} := \hat{Q} = \mathbb{1}\,. \qquad (4.4)
\end{aligned}$$

This equation gives us an operator constraint we have to impose on the Hilbert space to be the physical subspace. We will call this operator constraint $\hat{Q}$. It tells us that only one of the states we introduced can be occupied to have a faithful representation of our original system. So, a product state must have a definite electronic state and phonon number. Still, superpositions of states in this subspace are physical.

We now calculate the other relevant terms for the Hamiltonian:

$$\begin{aligned}
b^\dagger b &= \sum_{m,n,\sigma,\sigma'} \sqrt{(n+1)(m+1)} d^\dagger_{\sigma,n+1} d_{\sigma,n} d^\dagger_{\sigma',m} d_{\sigma',m+1} \\
&= \sum_{\sigma,\sigma',m,n} \sqrt{(n+1)(m+1)} d^\dagger_{\sigma,n+1} d^\dagger_{\sigma',m} d_{\sigma,n} d_{\sigma',m+1} + \sum_{\sigma,m,n} \sqrt{(n+1)(m+1)} d^\dagger_{\sigma,n+1} d_{\sigma,m+1} \delta_{m,n} \\
&= \sum_{\sigma,m=0} m\, d^\dagger_{\sigma,m} d_{\sigma,m} + \sum_{\sigma,\sigma',m,n} \sqrt{(n+1)(m+1)} d^\dagger_{\sigma,n+1} d^\dagger_{\sigma',m} d_{\sigma,n} d_{\sigma',m+1} \qquad (4.5)
\end{aligned}$$

The last term is a normal ordered product of two creation and two annihilation operators. This term vanishes in the physical space, where $\hat{Q} = \mathbb{1}$ since the physical system is constrained to a total auxiliary particle number of one. Therefore, two destruction operators annihilate this subspace. Terms of this kind can be dropped. The Pauli matrices in this basis are given by:

$$\sigma^+ = \sum_n d^\dagger_{e,n} d_{g,n} \quad ; \quad \sigma^- = \sum_n d^\dagger_{g,n} d_{e,n} \quad ; \quad \sigma^z = \sum_n (d^\dagger_{e,n} d_{e,n} - d^\dagger_{g,n} d_{g,n})\,. \qquad (4.6)$$

The commutation relations lead again to the same constraint $\hat{Q}$. In this basis, we find the Hamiltonian in the constraint subspace as:

$$\begin{aligned}
\mathcal{H} =& \delta a^\dagger a + \sum_n \omega n d^\dagger_{e,n} d_{e,n} + \sum_n \omega n d^\dagger_{g,n} d_{g,n} \\
&- \sum_n s\omega\sqrt{n+1}\,(d^\dagger_{g,n+1} d_{g,n} + d^\dagger_{g,n} d_{g,n+1}) + \sum_n s\omega\sqrt{n+1}\,(d^\dagger_{e,n+1} d_{e,n} + d^\dagger_{e,n} d_{e,n+1}) \\
&+ \gamma \sum_n (a^\dagger d^\dagger_{g,n} d_{e,n} + a d^\dagger_{e,n} d_{g,n}) \qquad (4.7)
\end{aligned}$$

Even though, for some applications, collecting all quantum numbers in subscripts is pretty useful and will be employed for certain derivations later, it is often more transparent to make the electronic quantum number explicit by $d_{g,n} = g_n$ and $d_{e,n} = e_n$. It will later on make the naming of 2-time Green functions more intuitive. The Hamiltonian reads now

$$\begin{aligned}\mathcal{H} =&\delta a^\dagger a + \sum_n \omega n e_n^\dagger e_n + \sum_n \omega n g_n^\dagger g_n + \sum_n s\omega\sqrt{n+1}\,(e_{n+1}^\dagger e_n - g_{n+1}^\dagger g_n + h.c.)\\ &+ \gamma \sum_n (a^\dagger g_n^\dagger e_n + a e_n^\dagger g_n)\,. \end{aligned} \tag{4.8}$$

The molecule part of the Hamiltonian, which is not interacting with physical particles, is still bilinear. This is a characteristic of the auxiliary particle method and allows for diagonalisation of the free molecule part by the analogon of the polaron transformation. As in the original theory, this will lead to a photon interaction strength $\gamma_{n,m}$, which explicitly mixes different phonon states n and m. The coefficients are given by Frank-Condon integrals, as shown in the appendix. This representation can be useful in derivations of rate equations, where the molecule part is taken as stationary equilibrium distributions. However, it does not lead to meaningful simplifications for dynamical calculations, which we are primarily interested in.

4.1 Auxiliary particle projection

We now discuss how the auxiliary particle constraint $Q = \mathbb{1}$ can generally be implemented exactly in a field theoretical Green function approach. This procedure is model-independent, and we call the auxiliary particle creation and annihilation operators just $d^\dagger$ and d. We will call the operator, which we did not represent as auxiliary particles, the physical particle operators. In the problem at hand it would be the photons.

The first observation is that every auxiliary particle Hamiltonian commutes with the constraint $[H, Q] = 0$. This follows from the fact that every operator represented by the auxiliary particles must commute independently with the constraint. Therefore, if the initial conditions can be projected to the correct Hilbert space, the density matrix will stay in the correct subspace during the time evolution. Historically, this has been archived in equilibrium via a chemical potential [59]. Here, we take an equivalent route but focus on the fugacity, which more intuitively generalises to non-equilibrium situations.
Let us consider an operator $\hat{A}$, which we represented through auxiliary particle operators. We want to compute the average of this operator in the physical Hilbert space. This operator will always annihilate the vacuum of the auxiliary particle theory. Furthermore, we can always choose the density matrix of the auxiliary particle system to factorise in the different particle number sectors Q. We will label these particle number sectors by attaching a factor ζ^Q to the density matrix $\rho \to \rho\zeta^Q$. The traces in the averages can then be taken separately in the different Q number sectors. For reasons which will become clear in a second, we will divide the grand canonical average $\langle A\rangle$ by the average of the constraint $\langle Q\rangle$ and separate the different $Q-$sectors explicitly as

$$\frac{\langle A\rangle}{\langle Q\rangle} = \frac{\mathrm{tr}(\rho\zeta^Q A)}{\mathrm{tr}(\rho\zeta^Q Q)} = \frac{\mathrm{tr}_{Q=0}(\rho\zeta^0 A) + \mathrm{tr}_{Q=1}(\rho\zeta^1 A) + \mathrm{tr}_{Q=2}(\rho\zeta^2 A) + ...}{\mathrm{tr}_{Q=0}(\rho\zeta^0 0) + \mathrm{tr}_{Q=1}(\rho\zeta^1 1) + \mathrm{tr}_{Q=2}(\rho\zeta^2 2) + ...} \tag{4.9}$$

$$= \frac{\mathrm{tr}_{Q=1}(\rho A) + \zeta\,\mathrm{tr}_{Q=2}(\rho A) + ...}{\mathrm{tr}_{Q=1}(\rho) + 2\zeta\,\mathrm{tr}_{Q=2}(\rho) + ...} \tag{4.10}$$

From this expression, we can obtain the average over the desired subspace $Q = 1$ by taking the limit of $\zeta \to 0$ as

$$\langle A\rangle_c = \frac{\mathrm{tr}_{Q=1}(\rho A)}{\mathrm{tr}_{Q=1}(\rho)} = \lim_{\zeta\to 0}\frac{\langle A\rangle}{\langle Q\rangle}\,. \tag{4.11}$$

This means we can do computations in a grand canonical setting with a density matrix $\rho\zeta^Q$, where Wick's theorem applies and later take the limit of $\zeta \to 0$. The additional factor $1/\langle Q\rangle$ is treated differently depending on the system settings. In equilibrium and steady-state calculation, the problem reduces to a boundary value problem, and the value of $\langle Q\rangle$ must be considered explicitly. In general, non-equilibrium one solves an initial value problem, and it can be fixed via the initial conditions from the onset.

The projection procedure of taking $\zeta \to 0$ has various implications on field theoretical treatment. Firstly, all one-point averages of auxiliary particles must vanish $\langle d\rangle = 0$, which is a consequence of demanding that the density matrix factorises in different Q sectors and that $[\hat{H}, \hat{Q}] = 0$. Secondly, to perform the limit $\zeta \to 0$, we will need a way to make the leading order ζ scaling of the equations of motion explicit. This can most transparently be done using greater and lesser Green functions. Considering them at initial times, one can find the leading order

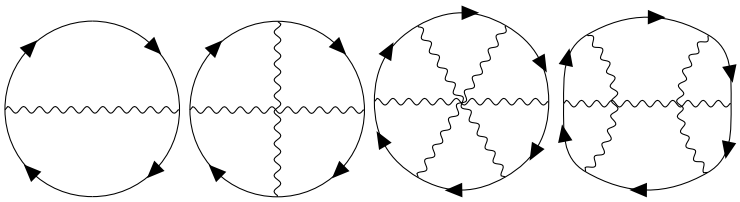

Figure 4.1: First diagrams contributing to the projected Luttinger-Ward functional. Solid lines represent auxiliary particles, and wiggly lines are physical particles.

scaling as

$$G^{>}(t_0,t_0) \propto \langle dd^\dagger \rangle = \mathrm{tr}(\rho\zeta^Q dd^\dagger) = \underset{Q=0}{\mathrm{tr}}(\rho dd^\dagger) + \mathcal{O}(\zeta) = \mathcal{O}(1) \tag{4.12}$$

$$G^{<}(t_0,t_0) \propto \langle d^\dagger d \rangle = \mathrm{tr}(\rho\zeta^Q d^\dagger d) = \underset{Q=0}{\mathrm{tr}}(\rho d^\dagger d) + \mathcal{O}(\zeta) = \mathcal{O}(\zeta)\,. \tag{4.13}$$

The leading order ζ scaling is preserved in the time-evolution since the constraint commutes with the Hamiltonian[1]. Therefore, we can get the scaling of diagrammatic contributions by counting the lesser functions contained after decomposing the Keldysh contour. The approximations to models must be obtained via conserving approximations to guarantee the constraint's preservation. We are using the 2-PI EA to generate these. Contributions from Γ^2 can be classified in terms of auxiliary particle loops. For simplicity, we focus on the 3−vertex theory, where two auxiliary particle operators connect to one physical particle operator. The general argument does not change for vertices with more operators since the number of auxiliary operators must still be two. Nevertheless, the topology of the resulting diagrams is more complicated and clutters up the diagrams.

We now organise Γ^2 in terms of auxiliary particle loops. First, we look at all diagrams with one auxiliary particle loop. The first order is the non-crossing approximation (NCA). The higher orders involve more crossing of propagators of physical particles. The first few contributions can be seen in Fig. 4.1. Let us consider a generic diagram from this class on the Schwinger-Keldysh contour. A diagram with N-vertices will contain N-auxiliary particle propagators connecting them in a loop. The vertices will also be connected by $N/2$ propagators of physical particles in various ways; all these possibilities can be collected in a function $\chi^c(t_1,t_2,...,t_N)$. We can write these diagrams as

$$\left[\prod_{i=1}^{N}\int_c dt_i\right] G^c(t_1,t_2)G^c(t_2,t_3)...G^c(t_{N-1},t_N)G^c(t_N,t_1)\chi^c(t_1,t_2,...,t_N)\,. \tag{4.14}$$

At this point, all propagators in the expression are contour-time-ordered and place for $G^c(t,t')$, a greater function is $t \succ t'$ and a lesser function if $t \prec t'$[60]. To obtain the leading order scaling in ζ, we must order the times t_1 to t_N in ascending order to pick up the least lesser functions. This results in $N-1$ greater functions and one lesser function from the Green function connecting the last to the first vertex $G^c(t_N,t_1)$. This shows that the lowest order contributions are of $\mathcal{O}(\zeta)$. The same argument can be applied to diagrams with more auxiliary particle loops, leading to another power of ζ for every auxiliary particle loop. This means that in the limit of $\zeta \to 0$, only the one-loop diagrams will contribute, and of these, only the subset

[1]Note that this implies that the spectral function is given only by the greater function. This means that the normalisation of the spectral function carries over to the greater function at equal time as $G^{>}_{i,j}(t,t) = -i\delta_{i,j}$.

with a single lesser function. [2]

The greater and lesser self-energies are now generated as

$$\Sigma^{>}(t,t') = i\frac{\delta\Gamma^2[G]}{\delta G^{<}(t',t)} \tag{4.15}$$

$$\Sigma^{<}(t,t') = i\frac{\delta\Gamma^2[G]}{\delta G^{>}(t',t)}\,. \tag{4.16}$$

Note that the ζ scaling of the Green functions is inherited by the self-energies and leads to a simplification of the equations of motion of the auxiliary Green functions, the Kadanoff-Baym equations (KB).
They are generally given by eq. (2.64) and (2.65) which are

$$\begin{aligned}(i\partial_t - h)G^{>}(t,t') = &\int_{t_0}^{t'} d\bar{t}\Sigma^{>}(t,\bar{t})G^{<}(\bar{t},t') - \int_{t_0}^{t} d\bar{t}\Sigma^{<}(t,\bar{t})G^{>}(\bar{t},t') \\ &+ \int_{t_0}^{t} d\bar{t}\Sigma^{>}(t,\bar{t})G^{>}(\bar{t},t') - \int_{t_0}^{t'} d\bar{t}\Sigma^{>}(t,\bar{t})G^{>}(\bar{t},t')\end{aligned} \tag{4.17}$$

$$\begin{aligned}(i\partial_t - h)G^{<}(t,t') = &\int_{t_0}^{t} d\bar{t}\Sigma^{>}(t,\bar{t})G^{<}(\bar{t},t') - \int_{t_0}^{t'} d\bar{t}\Sigma^{<}(t,\bar{t})G^{>}(\bar{t},t') \\ &+ \int_{t_0}^{t'} d\bar{t}\Sigma^{<}(t,\bar{t})G^{<}(\bar{t},t') - \int_{t_0}^{t} d\bar{t}\Sigma^{<}(t,\bar{t})G^{<}(\bar{t},t')\,.\end{aligned} \tag{4.18}$$

We now take the $\zeta \to 0$ limit on both sides and keep only the leading order contribution. Various terms on the rhs. vanish. In this way, one obtains simplified equations of motion for the auxiliary particle Green functions

$$(i\partial_t - h)G^{>}(t,t') = \int_{t_0}^{t} d\bar{t}\Sigma^{>}(t,\bar{t})G^{>}(\bar{t},t') - \int_{t_0}^{t'} d\bar{t}\Sigma^{>}(t,\bar{t})G^{>}(\bar{t},t') \tag{4.19}$$

$$(i\partial_t - h)G^{<}(t,t') = \int_{t_0}^{t} d\bar{t}\Sigma^{>}(t,\bar{t})G^{<}(\bar{t},t') - \int_{t_0}^{t'} d\bar{t}\Sigma^{<}(t,\bar{t})G^{>}(\bar{t},t')\,. \tag{4.20}$$

These equations have two essential properties at equal-time $t = t'$: They preserve the constraint encoded in the lesser component, and they preserve the commutator encoded in the greater component.

4.2 Renormalisation of physical particles

Another important aspect is the scaling of the self-energy of the physical particles, which are influenced by the auxiliary particles. Extracting it directly from Γ^2 leads to a scaling of $\mathcal{O}(\zeta)$ and vanishes therefore. As a result, Green functions of physical particles appearing in the auxiliary particle self-energies are not renormalized by them. Nevertheless, the observable physical Green functions get renormalized. This can be seen from the connection of the rhs. of the KB equation to expectation values, which we have shown before in eq. (3.91) to be

$$\Sigma_{x,1}G_{1,y} \propto \frac{\delta^3 S}{\delta\varphi_x\delta\varphi_1\delta\varphi_2}\frac{\delta^3 W}{\delta J_1'\delta J_2'\delta J_y'} \tag{4.21}$$

[2] Note that in the presence of dissipative interactions, the contour ordering argument must be modified since they allow to change the contour branch at an interaction point. It still holds that greater and lesser functions classify the scaling, but the contour-time ordering argument is not directly applicable. Nevertheless, generic dissipative interaction can be traced back to a Hamiltonian interaction with a bath, where the arguments presented hold. We will return to this point later when we discuss open system dynamics for auxiliary particles.

Here on the rhs. $\frac{\delta^3 W}{\delta J_1' \delta J_2' \delta J_y'}$ belongs to an expectation value of an auxiliary particle operator. We can now apply the projection procedure for expectation values eq. (4.11) as

$$\left[\frac{\delta^3 W}{\delta J_1' \delta J_2' \delta J_y'}\right]_{Q=1} = \lim_{\zeta\to 0} \frac{1}{\langle Q\rangle} \frac{\delta^3 W}{\delta J_1' \delta J_2' \delta J_y'} \,. \tag{4.22}$$

Using this in the KB equation, for the photon Green functions P, we obtain for the rhs. in the projecting limit

$$\left[\Sigma_{x,1} P_{1,y}\right]_{Q=1} = \lim_{\zeta\to 0} \frac{1}{\langle Q\rangle} \Sigma_{x,1} P_{1,y} = \lim_{\zeta\to 0} \frac{1}{\langle Q\rangle} \Sigma_{x,1} \left[(G_0)_{1,y} + (G_0)_{1,2}\Sigma_{2,3} P_{3,y}\right] \tag{4.23}$$

$$= \lim_{\zeta\to 0} \frac{\Sigma_{x,1}}{\langle Q\rangle} (G_0)_{1,y} \,. \tag{4.24}$$

Therefore, in self-energies of the physical particles coming from auxiliary particles, only terms linear in ζ are retained. The equations of motion are no longer of the usual Dyson form but obtain a T-matrix form $G_0^{-1} P = \delta + \lim_{\zeta\to 0} \frac{\Sigma}{\langle Q\rangle} G_0$.

As we have seen, the auxiliary particle lesser function vanishes in the limit of $\zeta \to 0$. But in all observables, it appears with an additional factor of $1/\langle Q\rangle$. This gives rise to a contribution of the finite part of the lesser functions. To isolate this part, we define a new auxiliary-particle lesser Green function through $G^< = \zeta \tilde{G}^<$. This way, the finite part of $G^<$ is retained, and the ζ scaling is explicitly performed on the equations. We will always use initial conditions with $\mathrm{tr}(\tilde{G}^<(t_0, t_0)) = -i$ so that $\langle Q(t_0)\rangle = \zeta$. In this way, we only need to change all $G^<$ into $\tilde{G}^<$ in the equations obtained before. In all following expressions, we will use the old symbol $G^<$ for $\tilde{G}^<$ to not clutter up the notation, but the difference should be kept in mind.
We can now write the equations of motion for the photon Green functions due to a single molecule as

$$\begin{aligned} G_0^{-1} P^>(t,t') = &\int_{t_0}^{t'} d\bar{t} \Sigma^>(t,\bar{t}) G_0^<(\bar{t},t') - \int_{t_0}^{t} d\bar{t} \Sigma^<(t,\bar{t}) G_0^>(\bar{t},t') \\ &+ \int_{t_0}^{t} d\bar{t} \Sigma^>(t,\bar{t}) G_0^>(\bar{t},t') - \int_{t_0}^{t'} d\bar{t} \Sigma^>(t,\bar{t}) G_0^>(\bar{t},t') \end{aligned} \tag{4.25}$$

$$\begin{aligned} G_0^{-1} P^<(t,t') = &\int_{t_0}^{t} d\bar{t} \Sigma^>(t,\bar{t}) G_0^<(\bar{t},t') - \int_{t_0}^{t'} d\bar{t} \Sigma^<(t,\bar{t}) G_0^>(\bar{t},t') \\ &+ \int_{t_0}^{t'} d\bar{t} \Sigma^<(t,\bar{t}) G_0^<(\bar{t},t') - \int_{t_0}^{t} d\bar{t} \Sigma^<(t,\bar{t}) G_0^<(\bar{t},t') \,. \end{aligned} \tag{4.26}$$

4.3 Lindblad dynamics with auxiliary particles

Including dissipation is essential for many systems of interest and can also be done in the auxiliary particle formulation. This can either be achieved by directly using the field theory generated by the corresponding Lindblad operators [34] [35] or by coupling a bath to the system and using Born and Markov approximation. Due to the constraint of the auxiliary particles, this procedure is not entirely straightforward. The class of allowed operators, which are coupled to the reservoir, must commute with the constraint so that it is conserved in the time evolution. This is naturally fulfilled if one starts with physical operators and writes these with their corresponding auxiliary particle representation. Starting with a Lindblad operator, therefore

a Markovian bath, generates interaction terms of fourth order in the auxiliary fields, which mix different branches of the Keldysh contour. The projection can still be done in terms of greater and lesser functions. A more transparent way is to consider the bath directly coupled to the system and investigate the field theory generated, bearing in mind the Born and Markov approximation. This also allows for a straightforward generalisation to general bath setups, e.g. coloured or thermal baths and coherent pumps. Here, we will need to keep track of the auxiliary particle indices. Note that every impurity operator A can be represented in the Hilbert space of interest in terms of auxiliary particle operators d_n as

$$A = \sum_n \Gamma_{n,m} d_n^\dagger d_m \,. \tag{4.27}$$

We now consider the coupling to a bath with bosonic operators b as

$$\Delta H = \gamma(A^\dagger b + b^\dagger A) = \gamma \sum_{n,m} \left[\Gamma^*_{m,n} b + \Gamma_{n,m} b^\dagger\right] d_n^\dagger d_m \tag{4.28}$$

with bath correlation functions $g(z,z') = -i\,\langle T_c(b(z)b^\dagger(z')\rangle$. The first contribution to Γ^2 is the NCA diagram with auxiliary particle Green functions G and is given as

$$\int dz dz' \sum_{n,m,k,l} \gamma^2 \Gamma_{n,m}\Gamma^*_{k,l} G_{m,l}(z,z') G_{k,n}(z',z) g(z',z)\,. \tag{4.29}$$

The contour-ordered self-energies follow as

$$\begin{aligned}\Sigma_{i,j}(t,t') &= i\gamma^2 \sum_{n,k} \left[\Gamma_{n,j}\Gamma^*_{k,i} G_{k,n}(t,t') g(t,t') + \Gamma_{i,k}\Gamma^*_{j,n} G_{k,n}(t,t') g(t',t)\right] \\ &= i\gamma^2 \left[g(t',t)\Gamma G(t,t')\Gamma^\dagger + g(t,t')\Gamma^\dagger G(t,t')\Gamma\right]_{i,j}\,. \end{aligned} \tag{4.30}$$

In the second line, we introduced a useful matrix notation.
To obtain the usual Lindblad form, we assume that the bath is not occupied ($g^<(t,t') = 0$), which leads us to the auxiliary particle self-energies as

$$\Sigma^>(t,t') = i\gamma^2 g^>(t,t')\Gamma^\dagger G^>(t,t')\Gamma \tag{4.31}$$

$$\Sigma^<(t,t') = i\gamma^2 g^>(t',t)\Gamma G^<(t,t')\Gamma^\dagger\,. \tag{4.32}$$

These are now used in the KB equations for auxiliary particles (4.20) and (4.19)

$$(i\partial_t - h)G^>(t,t') = \int_{t'}^t d\bar{t} i\gamma^2 g^>(t,\bar{t})\Gamma^\dagger G^>(t,\bar{t})\Gamma G^>(\bar{t},t') \tag{4.33}$$

$$\begin{aligned}(i\partial_t - h)G^<(t,t') = &\int_{t_0}^t d\bar{t} i\gamma^2 g^>(t,\bar{t})\Gamma^\dagger G^>(t,\bar{t})\Gamma G^<(\bar{t},t') \\ &- \int_{t_0}^{t'} d\bar{t} i\gamma^2 g^>(\bar{t},t)\Gamma G^<(t,\bar{t})\Gamma^\dagger G^>(\bar{t},t')\,. \end{aligned} \tag{4.34}$$

To perform the Markov approximation, we assume that the bath correlation function has vanishing time support on the characteristic time scales of the system so that the auxiliary

particle Green functions can be pulled out of the integral. This allows us to obtain

$$(i\partial_t - h)G^>(t,t') \approx \Gamma^\dagger G^>(t,t)\Gamma G^>(t,t')\int_{t'}^{t} d\bar{t} i\gamma^2 g^>(t,\bar{t}) \tag{4.35}$$

$$\begin{aligned}(i\partial_t - h)G^<(t,t') \approx &\Gamma^\dagger G^>(t,t)\Gamma G^<(t,t')\int_{t_0}^{t} d\bar{t} i\gamma^2 g^>(t,\bar{t}) \\ &- \Gamma G^<(t,t)\Gamma^\dagger G^>(t,t')\int_{t_0}^{t'} d\bar{t} i\gamma^2 g^>(\bar{t},t)\,.\end{aligned} \tag{4.36}$$

Due to the small time support of the bath correlation functions on the scale of the system, t and t' are always far separated on the time scale of the bath, and we can assume

$$\int_{t_0}^{t} d\bar{t} g(t,\bar{t}) = \int_{-\infty}^{t} d\bar{t} g(t-\bar{t}) = \int_0^\infty d\tau g(\tau)\,. \tag{4.37}$$

We can further simplify this by choosing the bath density of state symmetric $\rho(\epsilon) = \rho(-\epsilon)$, allowing us to show that the integrals are purely imaginary as

$$\begin{aligned}\int_0^\infty d\tau g(\tau) &= -i\int_{-\infty}^{\infty} d\epsilon\rho(\epsilon)\int_0^\infty d\tau e^{-i\epsilon\tau} = -\left[-i\int_{-\infty}^{\infty} d\epsilon\rho(\epsilon)\int_0^\infty d\tau e^{i\epsilon\tau}\right]^\dagger \\ &= -\left[-i\int_{-\infty}^{\infty} d\epsilon\rho(-\epsilon)\int_0^\infty d\tau e^{-i\epsilon\tau}\right]^\dagger \underbrace{=}_{\rho(\epsilon)=\rho(-\epsilon)} -\left[-i\int_{-\infty}^{\infty} d\epsilon\rho(\epsilon)\int_0^\infty d\tau e^{-i\epsilon\tau}\right]^\dagger \\ \Rightarrow \int_0^\infty d\tau g(\tau) &= -\left[\int_0^\infty d\tau g(\tau)\right]^\dagger \Rightarrow \mathrm{Re}\left(\int_0^\infty d\tau g(\tau)\right) = 0 \Rightarrow \int_0^\infty d\tau g(\tau) := if\end{aligned}$$

The other integrals can be computed by considering the cases of $t > t'$ and $t < t'$; note that we have chosen here a theta function convention $\theta(0) = 1/2$

$$\int_{t_0}^{t'} d\bar{t} g^>(t,\bar{t}) = \theta(t'-t)\int_{-\infty}^{\infty} d\tau g^>(\tau) = \theta(t'-t)2if \tag{4.38}$$

$$\int_{t}^{t'} d\bar{t} g^>(t-\bar{t}) = \mathrm{sign}(t-t')if \tag{4.39}$$

Using now $G^>_{i,j}(t,t) = -i\delta_{i,j}$ and defining the bath coupling $\kappa/2 = -\gamma^2 f$[2] we obtain the general form of a Lindblad contribution to auxiliary particles

$$(i\partial_t - h)G^>(t,t') = -i\frac{\kappa}{2}\mathrm{sign}(t-t')\Gamma^\dagger\Gamma G^>(t,t') \tag{4.40}$$

$$(i\partial_t - h)G^<(t,t') = -i\frac{\kappa}{2}\Gamma^\dagger\Gamma G^<(t,t') - \kappa\theta(t'-t)\Gamma G^<(t,t)\Gamma^\dagger G^>(t,t') \tag{4.41}$$

[2]The bath dos. is positive $\rho(\epsilon) > 0$ and therefore $f < 0$.

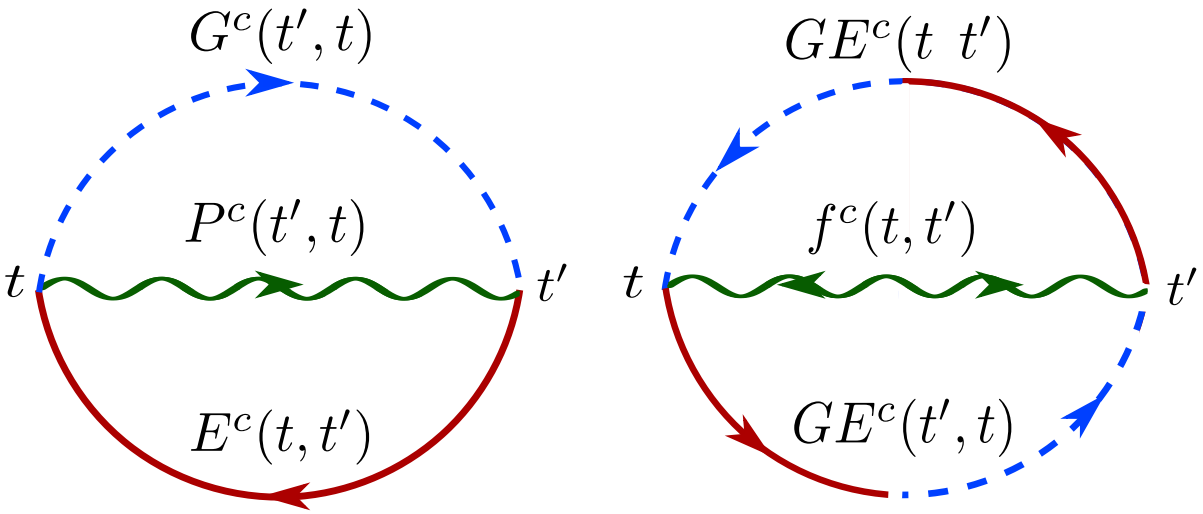

Figure 4.2: Diagramatic representation of the NCA approximation eq. (4.46). The left diagram generates the dynamics in the normal phase. The right diagrams only contributed in the condensed phase.

4.4 Equations of motion

We now define the correlation functions and equations of motion. We use the notation introduced in the Keldysh section eq.(2.53) for the photonic part. For the molecule part, we define

$$G^c_{n,m}(t,t') = -i\,\langle T_c(g_n(t)g^\dagger_m(t'))\rangle \tag{4.42}$$
$$E^c_{n,m}(t,t') = -i\,\langle T_c(e_n(t)e^\dagger_m(t')\rangle \tag{4.43}$$
$$EG^c_{n,m}(t,t') = -i\,\langle T_c(e_n(t)g^\dagger_m(t'))\rangle \tag{4.44}$$
$$GE^c_{n,m}(t,t') = -i\,\langle T_c(g_n(t)e^\dagger_m(t'))\rangle \tag{4.45}$$

The first contributions to the diagrammatic part are the NCA diagrams given by

$$\Gamma^2 = \frac{1}{2}\gamma^2\sum_{n,m}\int_c dtdt'\big[P^c(t',t)G^c_{n,m}(t',t)E^c_{m,n}(t,t') + h.c. \\ + GE^c_{n,m}(t,t')GE^c_{m,n}(t',t)f^c(t,t') + h.c.\big]\,. \tag{4.46}$$

Here, the first term will give the dynamics in the normal phase, whereas the second term only contributed in the condensed phase. The self-energies are extracted from this expression. Here, we are using the symbols P and f for the photon Green functions, but one must remember that they are the free photon propagator at this point. We come back to this in the next chapter. The molecule parts are given by

$$(\Sigma^>_G)_{n,m}(t,t') = i\gamma^2 E^>_{n,m}(t,t')P^<(t',t) \tag{4.47}$$
$$(\Sigma^<_G)_{n,m}(t,t') = i\gamma^2 E^<_{n,m}(t,t')P^>(t',t) \tag{4.48}$$
$$(\Sigma^>_E)_{n,m}(t,t') = i\gamma^2 G^>_{n,m}(t,t')P^>(t,t') \tag{4.49}$$
$$(\Sigma^<_E)_{n,m}(t,t') = i\gamma^2 G^<_{n,m}(t,t')P^<(t,t') \tag{4.50}$$
$$(\Sigma^>_{EG})_{n,m}(t,t') = i\gamma^2 GE^>_{n,m}(t,t')(f(t,t')+f(t',t))/2 \tag{4.51}$$
$$(\Sigma^<_{EG})_{n,m}(t,t') = i\gamma^2 GE^<_{n,m}(t,t')(f(t,t')+f(t',t))/2 \tag{4.52}$$

The photon self-energies generated are

$$(\Sigma_P^>)(t,t') = i\gamma^2 \sum_{n,m} E^>_{n,m}(t,t') G^<_{m,n}(t',t) \tag{4.53}$$

$$(\Sigma_P^<)(t,t') = i\gamma^2 \sum_{n,m} E^<_{n,m}(t,t') G^>_{m,n}(t',t) \tag{4.54}$$

$$(\Sigma_f^>)(t,t') = i\gamma^2 \sum_{n,m} EG^>_{n,m}(t,t') EG^<_{m,n}(t',t) \tag{4.55}$$

$$(\Sigma_f^<)(t,t') = i\gamma^2 \sum_{n,m} EG^<_{n,m}(t,t') EG^>_{m,n}(t',t) \tag{4.56}$$

We will collect all of these quantities in matrix structures and define the molecule Green functions as

$$\mathcal{G}_{n,m}(t,t') = -i \langle T_c \begin{pmatrix} g_n(t) g_m^\dagger(t') & g_n(t) e_m^\dagger(t') \\ e_n(t) g_m^\dagger(t') & e_n(t) e_m^\dagger(t') \end{pmatrix} \rangle \tag{4.57}$$

and similarly, collecting the self-energies and free propagators as

$$\Sigma_M(t,t') = \begin{pmatrix} \Sigma_G(t,t') & \Sigma_{GE}(t,t') \\ \Sigma_{EG}(t,t') & \Sigma_E(t,t') \end{pmatrix} \tag{4.58}$$

$$(\mathcal{G}^0)^{-1}_{n,m}(t) = \begin{pmatrix} i\partial_t \delta_{n,m} - h_g & -\gamma\varphi^*(t)\delta_{n,m} \\ -\gamma\varphi(t)\delta_{n,m} & i\partial_t \delta_{n,m} - h_e \end{pmatrix} \tag{4.59}$$

This notation allows us to use a matrix structure in the KB equation. Note that the "free" part of the molecule time evolution also contains contributions of the interaction term, namely the photon condensate $\varphi(t)$. It is the only point where the coherent photon field influences the molecules. These are obtained from the free propagators since it is defined as the second derivative of the action evaluated at the macroscopic field $\frac{\delta^2 S}{\delta \phi^2}\Big|_{\phi=\Phi}$.
Additionally, various Lindbladians need to be considered on the molecule side, which we will discuss now using the notation introduced in eq. (4.27).

The phonons are coupled to a bath due to collisions with other molecules in the dye solution. Here, vibrational excitations are exchanged with the bath. This is usually described by Lindblad operators b and $b^\dagger$. We decouple the vibrational bath for electronic ground and excited state here. Using the projection operator on electronic ground P_g and excited state P_e they can be written as bP_e, bP_g, $b^\dagger P_g$ and $b^\dagger P_e$. Additionally, it should be noted that we use the Hamiltonian in the original phonon basis, so without polaron transformation. Therefore, the oscillator equilibrium positions in the ground and excited state are not at the origin but shifted. This shift must be included in the dissipator to thermalise into the proper equilibrium distributions. In auxiliary particle representation, the corresponding coupling matrices are

$$(\Gamma_e^b)^{\sigma,\sigma'}_{n,m} = (\sqrt{n+1}\delta_{n+1,m} + s\delta_{n,m})\delta_{\sigma,e}\delta_{\sigma',e} \tag{4.60}$$

$$(\Gamma_e^{b^\dagger})^{\sigma,\sigma'}_{n,m} = (\sqrt{n+1}\delta_{n,m+1} + s\delta_{n,m})\delta_{\sigma,e}\delta_{\sigma',e} \tag{4.61}$$

$$(\Gamma_g^b)^{\sigma,\sigma'}_{n,m} = (\sqrt{n+1}\delta_{n+1,m} - s\delta_{n,m})\delta_{\sigma,g}\delta_{\sigma',g} \tag{4.62}$$

$$(\Gamma_g^{b^\dagger})^{\sigma,\sigma'}_{n,m} = (\sqrt{n+1}\delta_{n,m+1} - s\delta_{n,m})\delta_{\sigma,g}\delta_{\sigma',g}\,. \tag{4.63}$$

We will use λ as the bath coupling strength and $\bar{n}$ as the average phonon occupation in the bath. This leads us to Lindblad couplings in the KB eq. of $\lambda(\bar{n}+1)$ and $\lambda\bar{n}$ respectively.
The collisions between the dye and other molecules in the solution also lead to decoherence in the electronic state, which has the effect of dephasing. It is described by a Lindblad operator σ_z with coupling constant γ_ϕ leading us in auxiliary particle representation to

$$(\Gamma^{\sigma_z})^{\sigma,\sigma'}_{n,m} = \delta_{n,m}(\delta_{\sigma,e}\delta_{\sigma',e} - \delta_{\sigma,g}\delta_{\sigma',g})\,. \tag{4.64}$$

Also, the electronic states can be de-excited without producing a cavity photon. Two distinct processes can lead to this. Firstly, the electronic excitation can be exchanged in a collision between molecules, and the collision partner might not be radiatively coupled to the cavity mode. This effect is highly suppressed due to the high quantum efficiency of the dye solution. The second process is spontaneous emission into photon modes, which are not trapped in the cavity, mainly the free space modes at the open sides of the cavity. These two processes can be described by a Lindbladian σ^- with coupling constant $\Gamma_\downarrow$ and matrix elements

$$(\Gamma^{\sigma^-})^{\sigma,\sigma'}_{n,m} = \delta_{n,m}\delta_{\sigma,g}\delta_{\sigma',e}\,. \tag{4.65}$$

The external pump laser can be described in different ways. Experimentally, it is strongly blue detuned wrt. the zero phonon line and does not couple directly to the cavity modes. Technically, this can be included in the model via an external photon propagator. However, the energy is quickly dissipated due to the rapid relaxation of the vibrational states. Therefore, another way to model the pumping is via a Lindblad operator σ^+ with coupling $\Gamma_\uparrow$ as

$$(\Gamma^{\sigma^+})^{\sigma,\sigma'}_{n,m} = \delta_{n,m}\delta_{\sigma,e}\delta_{\sigma',g}\,. \tag{4.66}$$

What is still left are the equations of motion for the photon condensate $\varphi(t)$ for which we obtain

$$(i\partial_t - h + \frac{i}{2}\kappa)\varphi(t) = i\gamma\sum_n EG^<_{n,n}(t,t)\,. \tag{4.67}$$

As in the case of the photon self-energy, also here, the rhs. of the equation of motion vanishes in the limit $\zeta \to 0$, and only an unrenormalised photon condensate is seen by the molecules. Therefore, starting without a condensate, only a trivial condensate from the initial off-diagonal electronic correlation EG will be generated. This results from the fact that we only considered a single molecule until now, which will not be able to form a macroscopic coherent photon state. This will change when we include the macroscopic dye reservoir.

Chapter 5

Dynamical Mean-Field Theory

The effect of large molecule reservoirs can be included via a variation of Dynamical-Mean-Field-Theory (DMFT), which induces renormalisation of the photons due to the other molecules. The literature on DMFT in lattice systems, in and out of equilibrium, is vast, and we refer the interested reader to [61] [62]. Here, we will outline only the main train of thought of the cavity construction of DMFT.

Let us begin by considering a liquid of N_{mol} dye molecules, with positions i, in a cavity with modes k. The action in auxiliary particle representation and local constraints[1] reads:

$$S = \sum_i e_i^\dagger (G^0_{e,i})^{-1} e_i + \sum_i g_i^\dagger (G^0_{g,i})^{-1} g_i + \sum_k (G^0_\gamma)^{-1}_k a_k^\dagger a_k + \gamma \sum_i (a_i^\dagger g_i^\dagger e_i + a_i g_i e_i^\dagger) \tag{5.1}$$

We did not write time arguments and internal phonon quantum numbers here to avoid further cluttering the notation. Here, γ is the local coupling strength of the photon to the molecule. To obtain the coupling to the mode, the interaction can be transformed by considering the overlap of cavity wave function $\chi_k(i)$ with the local wavefunction of the molecule states. This generally produces a space- and mode-dependent coupling, reflecting the different mode profiles inside the cavity $\gamma \sum_i a_i = \sum_{k,i} \gamma_{i,k} a_k$. We will assume that this coupling can be represented uniformly. This means we assume that all photon modes have the same overlap with all molecules we are describing.[2]

The DMFT is now constructed as follows. First, we single out a molecule at position 0 and integrate out all other molecules and local photon states. This involves certain approximations in the coupling of this local problem to the rest we have integrated out. Namely, that the photon self-energy is local. This reduces the problem to a single impurity problem, which we will solve afterwards. In the second step, we set up the formalism for the full system, which we will call the lattice problem, also assuming the locality of the self-energies and derive the equations of motion. This is done in the mode representation of the cavity photons. We then assume that the local Green's functions and the local self-energies are the same for both approaches, closing the self-consistency loop. In a local basis, we may write the action as

$$S = \sum_i e_i^\dagger (G^0_{e,i})^{-1} e_i + \sum_i g_i^\dagger (G^0_{g,i})^{-1} g_i + \sum_{i,j} t_{i,j} a_i^\dagger a_j + \gamma \sum_i (a_i^\dagger g_i^\dagger e_i + a_i g_i e_i^\dagger) \tag{5.2}$$

$$\text{with} \qquad t_{i,j} = \sum_k \chi_k^*(i) \chi_k(j) (G^0_\gamma)^{-1}_k$$

[1] Note that the auxiliary particle representation has various subtleties when multiple impurities are represented in this way. Nevertheless, these issues will not change the construction of the DMFT in the case presented here.

[2] The ideas presented here can be extended to include the spatial dependence of the mode profile, but it is computationally rather expensive. For the system in question, one would consider a spatial dependent but still local self-energy.

We now separate the action into a local part S_0, the coupling between the local system and rest ΔS, as well as the rest of the system S_B.

$$S_0 = t_{0,0} a_0^\dagger a_0 + e_0^\dagger (G_{e,0}^0)^{-1} e_0 + g_0^\dagger (G_{g,0}^0)^{-1} g_0 + \gamma (a_0^\dagger g_0^\dagger e_0 + a_0 g_0 e_0^\dagger) = t_{0,0} a_0^\dagger a_0 + S_S \tag{5.3}$$

$$\Delta S = \sum_i (t_{i,0} a_i^\dagger a_0 + t_{0,i} a_0^\dagger a_i) \tag{5.4}$$

$$S_B = \sum_{i,j\neq 0} t_{i,j} a_i^\dagger a_j + \sum_{i\neq 0} e_i^\dagger (G_{e,i}^0)^{-1} e_i + \sum_{i\neq 0} g_i^\dagger (G_{g,i}^0)^{-1} g_i + \sum_{i\neq 0} \gamma (a_i^\dagger g_i^\dagger e_i + a_i g_i e_i^\dagger) \tag{5.5}$$

The partition function is expanded in terms of coupling between the local system and the rest as

$$Z = \int \mathcal{D}[a_0, e_0, g_0] e^{iS_0} \int \mathcal{D}[a_i, e_i, g_i] e^{iS_B} e^{i\Delta S} \tag{5.6}$$

$$= \int \mathcal{D}[a_0, e_0, g_0] e^{iS_0} \int \mathcal{D}[e_i, g_i] e^{iS_B} \left[1 + i\Delta S - \Delta S^2/2 + ...\right] \tag{5.7}$$

$$= \int \mathcal{D}[a_0, e_0, g_0] e^{iS_0} Z_B \left[1 + i \langle \Delta S \rangle_B - \langle \Delta S^2 \rangle_B /2 + ...\right] . \tag{5.8}$$

The first two terms are given by

$$\langle \Delta S \rangle_B = \sum_i (t_{i,0} \langle a_i^\dagger \rangle_B a_0 + t_{0,i} a_0^\dagger \langle a_i \rangle_B) \tag{5.9}$$

$$\begin{aligned} \langle \Delta S^2 \rangle_B = \sum_{i,j\neq 0} \big[& t_{i,0} t_{j,0} a_0 a_0 \langle a_i^\dagger a_j^\dagger \rangle_B + t_{0,i} t_{0,j} a_0^\dagger a_0^\dagger \langle a_i a_j \rangle_B \\ & + t_{i,0} t_{0,j} a_0 a_0^\dagger \langle a_i^\dagger a_j \rangle_B + t_{0,i} t_{j,0} a_0^\dagger a_0 \langle a_i a_j^\dagger \rangle_B \big] \end{aligned} \tag{5.10}$$

Note here that different times are involved in the correlation functions in the second line and that the averages are taken wrt. to the rest of the system. The averages in the second line can be written as connected Green's functions plus disconnected parts. We assume now that all connected correlation functions of higher order than quadratic are negligible. This assumption is equivalent to local photon self-energies since only the photon couples different positions. Afterwards, we can use the link cluster theorem to re-exponentiate the expression and get the connected correlation functions in the action. Writing now the new local action with explicit time arguments, we obtain

$$S' = \int_c dt \int_c dt' \psi^\dagger(t) M^{-1}(t,t') \psi(t') + \int_c dt (\Phi^\dagger(t) \psi(t) + h.c.) + S_S \, . \tag{5.11}$$

Here $\psi(t) = (a_0(t), a_0^\dagger(t))^T$ is the Nambu representation of the photon fields and $M^{-1}(t,t')$ collects all contributions to the two-point correlation functions. In the same way, $\Phi(t)$ collects all contributions to the one-point correlations. The explicit form of these terms M^{-1} and Φ appearing in the action is straightforward but also not important for a diagrammatic approach. We will start to discuss the now changed local problem and give the connection to the "lattice" problem afterwards to close the set of equations. In the local problem, the free photon propagator is now given by the Weissfield $M(t,t')$ and appears as the photon Green function in the auxiliary particle self-energies. The field Φ appears as a source term in the equation of motion of the condensate as

$$\int_c dt' M^{-1}(t,t') \Psi(t') = i\gamma \sum_n \begin{pmatrix} E G_{n,n}^<(t,t) \\ G E_{n,n}^<(t,t) \end{pmatrix} - \Phi(t) \tag{5.12}$$

The first term on the rhs. does vanish in the limit of $\zeta \to 0$, as we have shown earlier. Therefore, the condensate which the molecule sees Ψ_0 is determined by

$$\Psi_0(t) = -\int_c dt' M(t,t')\Phi(t') \tag{5.13}$$

Nevertheless, as physical observable, the local condensate is by the same arguments as in the case of two-point functions given by

$$\Psi(t) = i\gamma \sum_n \int_c dt' M(t,t') \begin{pmatrix} EG^<_{n,n}(t',t') \\ GE^<_{n,n}(t',t') \end{pmatrix} - \int_c dt' M(t,t')\Phi(t') \tag{5.14}$$

We now close the set of equations and obtain equations for M and Ψ_0. For this, we need to extract the local Green functions from the local problem and from the "lattice" problem. This requires the knowledge of the local self-energy of the photons Σ_{loc}. As we have shown in the single molecule case, we obtained a T-matrix equation for the photon two-time functions, where the T-matrix is given by naively generated self-energy of Γ^2. Now we need to extract the physical self-energy of the photons due to a single molecule $\bar{\Sigma}$ from it using the definition of the self-energy via the Dyson equation as

$$\int_c dt_1 \Sigma(t,t_1) M(t_1,t') \stackrel{!}{=} \int_c dt_1 \bar{\Sigma}(t,t_1) P(t_1,t') \tag{5.15}$$

$$\Rightarrow \bar{\Sigma}(t,t') = \Sigma(t,t') - \int_c dt_1 \int_c dt_2 \Sigma(t,t_1) M(t_1,t_2) \bar{\Sigma}(t_2,t') \tag{5.16}$$

In steady state calculation, this can conveniently be solved in frequency space using, for the spectral components, $\bar{\Sigma}(\omega) = \Sigma(\omega)\left(1 + M(\omega)\Sigma(\omega)\right)^{-1}$[3], but for general non-equilibrium calculation, this is not possible. The local self-energy we obtained is due to a single molecule and must be scaled by the molecule density N_{mol} to obtain the local self-energy in mode space. Therefore, the local self-energy in the "lattice" problem is $\Sigma_{loc} = N_{mol}\bar{\Sigma}$. The "lattice" KB equation for each mode is then

$$(i\partial_t - h_k) P_k(t,t') = \delta_c(t,t') + \int_C dt_1 \, \Sigma_{loc}(t,t_1) P_k(t_1,t') \, . \tag{5.17}$$

In equilibrium calculations, this equation can be solved using the spectral components of the Green functions since the distribution function is fixed to the Bose function, and the problem can be converted to solving a single density of states integral. This is not the case anymore in non-equilibrium. Here, every mode has to evolve individually. Using now our assumption that the overlap of the spatial profiles of the modes with the molecule wave functions is the same everywhere, we can extract the local Green function as $P_{loc} = \sum_k P_k$. The two-point Weissfield is then calculated as

$$M(t,t') = P_{loc}(t,t') - \int_C dt_1 dt_2 P_{loc}(t,t_1) \bar{\Sigma}(t_1,t_2) M(t_2,t') \tag{5.18}$$

The condensate in the "lattice" system for each mode is obtained from the equation of motion as

$$(G_0^{-1})_k \Psi_k(t) = i\gamma N_{mol} \sum_n \begin{pmatrix} EG^<_{n,n}(t,t) \\ GE^<_{n,n}(t,t) \end{pmatrix} \tag{5.19}$$

$$\Rightarrow \Psi_k(t) = i\gamma N_{mol} \int_c dt' (G_0)_k(t,t') \sum_n \begin{pmatrix} EG^<_{n,n}(t',t') \\ GE^<_{n,n}(t',t') \end{pmatrix} \tag{5.20}$$

[3]The Keldysh component can be extracted in a similar way.

The local condensate is again obtained via $\Psi_{loc} = \sum_k \Psi_k$. The effective condensate seen by the molecules Ψ_0 from eq. (5.13) is then given as

$$\Psi_0(t) = i\gamma \int_c dt' \left[N_{mol} \sum_k (G_0)_k(t,t') - M(t,t') \right] \sum_n \begin{pmatrix} EG^<_{n,n}(t',t') \\ GE^<_{n,n}(t',t') \end{pmatrix} . \tag{5.21}$$

For a complete DMFT treatment, one now needs to time evolve the local problem and (5.16), (5.17), (5.18), (5.19) and (5.21). Some of the additional equations can not be transformed into a KB form since some of the objects involved do not have an inverse connected to time derivatives. They must be solved in Dyson form, which is numerically demanding and leads to various difficulties.

Nevertheless, for the system in mind, tremendous simplifications can be achieved by noting that N_{mol} is large, of the order $10^6 - 10^9$, and the local coupling constant γ is small compared to the intrinsic energy scales of the molecule. Therefore, the contribution of a single molecule $\bar{\Sigma}$ is small so that we can obtain from eq. (5.18) that $M(t,t') \approx G_{loc}(t,t')$. Then from eq. (5.16) it follows that the local self-energy is given as $\Sigma_{loc}(t,t') = N_{mol}\Sigma(t,t')$. By the same reasoning in eq. (5.21) Ψ_0 is just given by $\Psi_0(t) = \sum_k \Psi_k(t)$. Therefore, the set of equations can be reduced significantly to only the ones which possess KB form, namely

$$(i\partial_t - h_k)\Psi_k(t) = i\gamma N_{mol} \sum_n \begin{pmatrix} EG^<_{n,n}(t,t) \\ GE^<_{n,n}(t,t) \end{pmatrix} \tag{5.22}$$

$$(i\partial_t - h_k)P_k(t,t') = \delta_c(t,t') + \int_c dt_1 \, \Sigma_{loc}(t,t_1)P_k(t_1,t') \, . \tag{5.23}$$

Within this approximation, the photon propagator in the auxiliary particle self-energies is the renormalised local Green function $G_{loc} = \sum_k G_k$ and the condensate in the free part of the molecule equation is given by $\Psi_0 = \sum_k \Psi_k$.

Chapter 6

Ward Identity and $U(1)$ Symmetry

The Hamiltonian is invariant under two phase transformation. One is associated with the conservation of the constraint Q and is in equilibrium used to perform the projection. Here, we want to investigate the second invariance under $a^\dagger \to a^\dagger e^{-i\theta}$ and $e^\dagger \to e^\dagger e^{-i\theta}$, which is a result from the rotating wave approximation used to obtain the Jaynes-Cummings interaction. It is connected to the total number of excitations in the cavity $a^\dagger a + P_e$ or in auxiliary particle representation $a^\dagger a + \sum_n e_n^\dagger e_n$. The symmetry is not fully broken by the inclusion of dissipation but needs to be extended along the Keldysh contour. In the following, we want to explore the consequences of this symmetry. Firstly, we note that the auxiliary particle must have a vanishing one-point average $\langle e_n \rangle = 0$ at the physical point due to the strongly imposed particle number constraint Q. Therefore, the first order 1-PI Ward-identity will only contain information about the photonic part. We explicitly include the open system case, leading us to

$$\begin{aligned} &{G^{-1}}^{+,-}_{k,i} T^{-,-}_{i,j} \Phi^-_j - {G^{-1}}^{+,+}_{k,i} T^{+,+}_{i,j} \Phi^+_j = \\ &= \int dt' ({G^{-1}}^T_{aa}(t,t') - {G^{-1}}^<_{a,a}(t,t'))\Phi(t') - \int dt' ({G^{-1}}^T_{aa^\dagger}(t,t') - {G^{-1}}^<_{aa^\dagger}(t,t'))\Phi^*(t') \end{aligned} \tag{6.1}$$

We now separate the inverse Green functions into the free part and self-energies as

$$\begin{aligned} \int dt' ({G_0^{-1}}^T_{aa^\dagger}(t,t') - {G_0^{-1}}^<_{aa^\dagger}(t,t'))\Phi^*(t') = &\int_{t_0}^t dt' (\Sigma^>_{aa^\dagger}(t,t') - \Sigma^<_{aa^\dagger}(t,t'))\Phi^*(t') \\ &- \int_{t_0}^t dt' (\Sigma^>_{aa}(t,t') - \Sigma^<_{a,a}(t,t'))\Phi(t') \end{aligned} \tag{6.2}$$

We obtain here the dissipative analogue of the Hugenholtz-Pines relation

$$\begin{aligned} \left(i\partial_t + h + \frac{i}{2}(\kappa_\downarrow - \kappa_\uparrow) \right) \Phi^*(t) = &\int_{t_0}^t dt' (\Sigma^>_{aa^\dagger}(t,t') - \Sigma^<_{aa^\dagger}(t,t'))\Phi^*(t') \\ &- \int_{t_0}^t dt' (\Sigma^>_{aa}(t,t') - \Sigma^<_{a,a}(t,t'))\Phi(t') \end{aligned} \tag{6.3}$$

Note that his condition still fixes the pole position of the Green functions, but now the imaginary part of the self-energies must also compensate for the Lindbladian dissipation [34]. This might be understood from the coupled system and bath Hamiltonian perspective. Here, the symmetry transformation would also include the bath, and the self-energies would include explicit bath contributions. But in deriving the Lindblad form, we made certain assumptions about the bath density of states and distribution, which now imposes the occupations via the relations between dissipative coupling constants κ. We choose a symmetric bath density of states such that no

real part is obtained, which would shift the chemical potential in a steady-state approach. Therefore, only the imaginary part of the bath contributions must be accounted for through the relation between the pure system self-energies. In practice, the main point of this result is the energy shift due to the real part of the self-energies and a phase shift to compensate for the dissipation.
Nevertheless, this result looks rather different from the equation of motion we obtain from the variational principle of the 2PI EA. The equation of motion of the condensate is the same as the 2PI Ward identity. The main caveat is that the NCA self-energies in the condensed phase do not fulfil the consistency condition (3.94). This can be seen by expansion (3.94) in terms of the derivative of the self-energy, which results in ladder-like resummation. Therefore, the energy of the condensate is not necessarily forced to the pole of the Green function. This can lead to inconsistencies between the fluctuation spectrum and the phase coherent contribution.

Chapter 7

Relation to Cumulant Expansion

In this section, we look into the similarities and differences between the approach put forward here and the often-used master equation approach. To this end, we first show the connection to the Markovian rate equations. Secondly, we will show how cumulant expansions relate to the approach used here.

We consider the case where the phonon spectra are static equilibrium spectra, so the photon interaction does not influence them. Furthermore, we drop the symmetry-breaking terms for the moment. We can isolate the specific electronic dissipative contribution to the spectra by using the relative time dynamics. We obtain via the Lindbladian with loss $\Gamma_\downarrow$ and pump $\Gamma_\uparrow$ to equations of motion as

$$i\partial_\tau G^>(t,t') = -i\frac{\Gamma_\uparrow}{2}\mathrm{sign}(t-t')G^>(t,t') \tag{7.1}$$

$$i\partial_\tau G^<(t,t') = \frac{\Gamma_\downarrow}{2}\left(\theta(t-t')E^<(t',t') - \theta(t'-t)E^<(t,t)\right)G^>(t,t') \tag{7.2}$$

$$i\partial_\tau E^>(t,t') = -i\frac{\Gamma_\downarrow}{2}\mathrm{sign}(t-t')E^>(t,t') \tag{7.3}$$

$$i\partial_\tau E^<(t,t') = \frac{\Gamma_\uparrow}{2}\left(\theta(t-t')G^<(t',t') - \theta(t'-t)G^<(t,t)\right)E^>(t,t') \tag{7.4}$$

These relative time contributions can be incorporated by substituting

$$G^<(t,t') \to G^<(t,t')e^{-\frac{\Gamma_\uparrow}{2}|t-t'|} \quad , \quad E^<(t,t') \to E^<(t,t')e^{-\frac{\Gamma_\downarrow}{2}|t-t'|} \tag{7.5}$$

$$G^>(t,t') \to G^>(t,t')e^{-\frac{\Gamma_\uparrow}{2}|t-t'|} \quad , \quad E^>(t,t') \to E^>(t,t')e^{-\frac{\Gamma_\downarrow}{2}|t-t'|}\,. \tag{7.6}$$

We are ultimately interested in the photon number. Therefore, we take a look at the equation of motion of the lesser function at equal time. These are constructed from

$$\begin{aligned}(i\partial_t - h)P^<(t,t') = &\int_{t_0}^{t} d\bar{t}\Sigma^>(t,\bar{t})P^<(\bar{t},t') - \int_{t_0}^{t'} d\bar{t}\Sigma^<(t,\bar{t})P^>(\bar{t},t') \\ &+ \int_{t_0}^{t'} d\bar{t}\Sigma^<(t,\bar{t})P^<(\bar{t},t') - \int_{t_0}^{t} d\bar{t}\Sigma^<(t,\bar{t})P^<(\bar{t},t')\end{aligned} \tag{7.7}$$

$$\begin{aligned}(i\partial_{t'} + h)P^<(t,t') = &\int_{t_0}^{t'} d\bar{t}P^<(t,\bar{t})\Sigma^>(\bar{t},t') - \int_{t_0}^{t} d\bar{t}P^>(t,\bar{t})\Sigma^<(\bar{t},t') \\ &+ \int_{t_0}^{t} d\bar{t}P^<(t,\bar{t})\Sigma^<(\bar{t},t') - \int_{t_0}^{t'} d\bar{t}P^<(t,\bar{t})\Sigma^<(\bar{t},t')\,.\end{aligned} \tag{7.8}$$

Adding them at equal time leads us to the Boltzmann equation for the photon number

$$i\partial_T P^<(t,t) = \int_{t_0}^{t} d\bar{t}\left[\Sigma^>(t,\bar{t})P^<(\bar{t},t) + P^<(t,\bar{t})\Sigma^>(\bar{t},t)\right] - \int_{t_0}^{t} d\bar{t}\left[P^>(t,\bar{t})\Sigma^<(\bar{t},t) + \Sigma^<(t,\bar{t})P^>(\bar{t},t)\right] . \tag{7.9}$$

The photon self-energies in NCA and simplified DMFT approximation are

$$\Sigma^>(t,t') = iN_{mol}\gamma^2 \sum_{n,m} E^>_{n,m}(t,t')G^<_{m,n}(t',t) \tag{7.10}$$

$$\Sigma^<(t,t') = iN_{mol}\gamma^2 \sum_{n,m} E^<_{n,m}(t,t')G^>_{m,n}(t',t)\,. \tag{7.11}$$

We now look at the self-energy integrals and go into an interaction picture, factoring out photon detuning and electronic dissipation and assuming that photon occupation changes are slow on the molecule time scales. This allows us to write the first integral as

$$\int_{t_0}^{t} d\bar{t}\Sigma^>(t,\bar{t})P^<(\bar{t},t) = iN_{mol}\int_{t_0}^{t} d\bar{t}\sum_{n,m} E^>_{n,m}(t,\bar{t})G^<_{m,n}(\bar{t},t)P^<(\bar{t},t) \tag{7.12}$$

$$\approx iN_{mol}P^<(t,t)\int_{t_0}^{t} d\bar{t}\gamma^2 e^{-\frac{\Gamma_\uparrow+\Gamma_\downarrow}{2}|t-\bar{t}|}e^{-i\delta(\bar{t}-t)}\sum_{n,m} E^>_{n,m}(t,\bar{t})G^<_{m,n}(\bar{t},t)\,. \tag{7.13}$$

Assuming that molecule spectra are static and not renormalized by the photons, we can factorise the molecule Green functions in electronic occupations and phonon spectra as

$$E^>_{n,m}(t,t') = -ip^>_{n,m}(t-t') \qquad G^<_{n,m}(t,t') = -ix_g(T)p^<_{n,m}(t-t')\,. \tag{7.14}$$

The molecule spectra are broad compared to the electronic dissipation processes, and we may write

$$-n(t)M_g(t)\int_0^\infty d\tau\gamma^2 e^{-\frac{\Gamma_\uparrow+\Gamma_\downarrow}{2}\tau}e^{-i\delta\tau}\sum_{n,m} p^>_{n,m}(\tau)p^<_{m,n}(-\tau) = -n(t)M_g(t)K(\delta)\,. \tag{7.15}$$

The second integral is treated in the same way, and we obtain the contribution from the greater self-energy part as

$$-n(t)M_g(t)\mathrm{Re}\left[2\gamma^2\int_0^\infty d\tau e^{-\frac{\Gamma_\uparrow+\Gamma_\downarrow}{2}\tau}e^{-i\delta\tau}\sum_{n,m} p^>_{n,m}(\tau)p^<_{m,n}(-\tau)\right] := -n(t)M_g(t)B_{abs}\,. \tag{7.16}$$

For the lesser contribution, we find with analogous definitions

$$\int_{t_0}^{t} d\bar{t}\,\Sigma^<(t,\bar{t})P^>(\bar{t},t) = iN_{mol}\int_{t_0}^{t} d\bar{t}\sum_{n,m}\gamma^2 E^<_{n,m}(t,t')G^>_{m,n}(t',t)P^>(\bar{t},t) \tag{7.17}$$

$$\approx iN_{mol}P^>(t,t)\int_{t_0}^{t} d\bar{t}\gamma^2 e^{-\frac{\Gamma_\uparrow+\Gamma_\downarrow}{2}|t-\bar{t}|}e^{-i\delta(\bar{t}-t)}\sum_{n,m} E^<_{n,m}(t,t')G^>_{m,n}(t',t) \tag{7.18}$$

$$\approx -M_e(n(t)+1)\int_0^\infty d\tau e^{-\frac{\Gamma_\uparrow+\Gamma_\downarrow}{2}\tau}e^{-i\delta\tau}\sum_{n,m} p^<_{n,m}(\tau)p^>_{m,n}(-\tau) \tag{7.19}$$

$$= -M_e(n(t)+1)H(\delta)\,. \tag{7.20}$$

The contribution from the lesser self-energy part is

$$M_e(n(t)+1)\mathrm{Re}\left[2\int_0^\infty d\tau\gamma^2 e^{-\frac{\Gamma_\uparrow+\Gamma_\downarrow}{2}\tau}e^{-i\delta\tau}\sum_{n,m}p^<_{n,m}(\tau)p^>_{m,n}(-\tau)\right] = M_e(n(t)+1)B_{em}\,. \quad (7.21)$$

The relation between the integrals can be obtained by complex conjugation

$$\left[K(\delta)\right]^\dagger = \left[\gamma^2\int_0^\infty d\tau e^{-\frac{\Gamma_\uparrow+\Gamma_\downarrow}{2}\tau}e^{-i\delta\tau}\sum_{n,m}p^>_{n,m}(\tau)p^<_{m,n}(-\tau)\right]^\dagger \quad (7.22)$$

$$= \gamma^2\int_0^\infty d\tau e^{-\frac{\Gamma_\uparrow+\Gamma_\downarrow}{2}\tau}e^{i\delta\tau}\sum_{n,m}p^<_{n,m}(\tau)p^>_{m,n}(-\tau) = H(-\delta) \quad (7.23)$$

which are the same relations as we have found from the operator approach.
We obtain the contribution of the molecules to the equations of motion of the photon number as

$$\partial_t n(t) = B_{em}M_e(n+1) - B_{abs}M_g n\,. \quad (7.24)$$

The equation of motion for the excited molecules $M_e(t)$ can be obtained in the same way as shown here by considering the Boltzmann equation of the molecules. This shows that our approach reduces to the rate equations in the Markovian limit.

Another interesting aspect is the origin of the Kennard-Stepanov relation for the absorption and emission coefficient in this approach. This can most easily be seen in a steady state where the photon self-energies can be Fourier-transformed as

$$\Sigma^>(\omega) = iN_{mol}\gamma^2\int d\nu E^>(\omega+\nu)G^<(\nu) \quad , \quad \Sigma^<(\omega) = iN_{mol}\gamma^2\int d\nu E^<(\omega+\nu)G^>(\nu) \quad (7.25)$$

In thermal equilibrium, the greater and lesser functions are connected via the fluctuation-dissipation theorem[1] $G^<(\omega) = e^{-\beta\omega}G^>(\omega)$. The photon self-energies will inherit this relation if the molecule is in thermal equilibrium as

$$\Sigma^>(\omega) = iN_{mol}\gamma^2\int d\nu E^>(\omega+\nu)G^<(\nu) = iN_{mol}\gamma^2\int d\nu e^{\beta(\omega+\nu)}E^<(\omega+\nu)e^{-\beta\nu}G^>(\nu) \quad (7.26)$$

$$= e^{\beta\omega}iN_{mol}\gamma^2\int d\nu E^<(\omega+\nu)G^>(\nu) = e^{\beta\omega}\Sigma^<(\omega)\,. \quad (7.27)$$

We now take a look at another kind of approximation, which is, in spirit, closer to the approach we are following. In [63] the phonon modes are not averaged out, but the system is mapped to a 2N-level system, which is also effectively done in our approach. Afterwards, a cumulant expansion up to the second order is employed to close the set of equations of motion. Here, we want to explore the difference in the approximation schemes. To this end, we can focus on a greatly simplified model of a two-level system, which will show different physics but nevertheless make the comparison of the approximations more clear. In [63], the coherent photon part was neglected, which we will also do here for comparison's sake.

We start with a Hamiltonian of a two-level system coupled to a photon mode

$$H = \delta a^\dagger a + g(a\sigma^+ + a^\dagger\sigma^-)\,. \quad (7.28)$$

[1] It is equivalent to the KMS boundary condition.

The equation of motion for the photon number with the ground/excited state projectors $P_{g/e}$ are given by

$$i\partial_t \langle a^\dagger a\rangle = g\langle a^\dagger \sigma^-\rangle - g\langle \sigma^+ a\rangle \tag{7.29}$$

$$i\partial_t(\langle a^\dagger\sigma^-\rangle - \langle a\sigma^+\rangle) = -\delta(\langle a^\dagger\sigma^-\rangle + \langle a\sigma^+\rangle) + 2g\langle a^\dagger a P_g\rangle - 2g\langle aa^\dagger P_e\rangle \tag{7.30}$$

We now truncate in second cumulant order, neglecting symmetry broken terms, simplifying the second equation of motion to

$$i\partial_t(\langle a^\dagger\sigma^-\rangle - \langle a\sigma^+\rangle) = -\delta(\langle a^\dagger\sigma^-\rangle + \langle a\sigma^+\rangle) + 2g\langle a^\dagger a\rangle\langle P_g\rangle - 2g\langle aa^\dagger\rangle\langle P_e\rangle \tag{7.31}$$

We again look at the Boltzmann eq. to compare with the field theory approach

$$\begin{aligned} i\partial_T P^<(t,t) = &\int_{t_0}^t d\bar{t}\left[\Sigma^>(t,\bar{t})P^<(\bar{t},t) + P^<(t,\bar{t})\Sigma^>(\bar{t},t)\right] \\ &- \int_{t_0}^t d\bar{t}\left[P^>(t,\bar{t})\Sigma^<(\bar{t},t) + \Sigma^<(t,\bar{t})P^>(\bar{t},t)\right]. \end{aligned} \tag{7.32}$$

The rhs. of the KB eq. gives the approximation of the average generated by the Heisenberg equation. Therefore, to compare the results, we take a time derivative of the rhs. of the Boltzman eq. to get the approximation of the second equation of motion. We obtain via chain rule:

$$\left[\Sigma^>(t,t)P^<(t,t) + P^<(t,t)\Sigma^>(t,t)\right] - \left[P^>(t,t)\Sigma^<(t,t) + \Sigma^<(t,t)P^>(t,t)\right] \tag{7.33}$$

$$+\int_{t_0}^t d\bar{t}\left[\Sigma^>(t,\bar{t})\partial_t P^<(\bar{t},t) + \partial_t P^<(t,\bar{t})\Sigma^>(\bar{t},t)\right] \tag{7.34}$$

$$-\int_{t_0}^t d\bar{t}\left[\partial_t P^>(t,\bar{t})\Sigma^<(\bar{t},t) + \Sigma^<(t,\bar{t})\partial_t P^>(\bar{t},t)\right] \tag{7.35}$$

$$+\int_{t_0}^t d\bar{t}\left[\partial_t\Sigma^>(t,\bar{t})P^<(\bar{t},t) + P^<(t,\bar{t})\partial_t\Sigma^>(\bar{t},t)\right] \tag{7.36}$$

$$-\int_{t_0}^t d\bar{t}\left[P^>(t,\bar{t})\partial_t\Sigma^<(\bar{t},t) + \partial_t\Sigma^<(t,\bar{t})P^>(\bar{t},t)\right] \tag{7.37}$$

The NCA self-energies of the Hamiltonian are given by

$$\Sigma^>(t,t') = ig^2E^>(t,t')G^<(t',t) \quad , \quad \Sigma^<(t,t') = ig^2E^<(t,t')G^>(t',t)\,. \tag{7.38}$$

Therefore, from the first line (7.33) we obtain

$$2ig^2\left[E^>(t,t)G^<(t,t)P^<(t,t) - E^<(t,t)G^>(t,t)P^>(t,t)\right] = 2g^2\left[M_e(n+1) - M_g n\right]. \tag{7.39}$$

This already recovers the interacting part of the second-order cumulant expansion. Note that the time-evolution with δ, which would also be true for all free molecule contributions, is recovered via chain rule from the derivatives of the self-energies. Here, the derivatives acting on the Green functions in it can be written through the KB. eq., and the free part supplements these contributions. The difference between the approaches is the self-energy integrals in eq. (7.34-7.37) . We will later show their importance specifically for the Kennard-Stepanov relation of the molecule spectra.

Part IV

Dynamics in Multi-Mode Cavities

Chapter 8

Summary of the Model

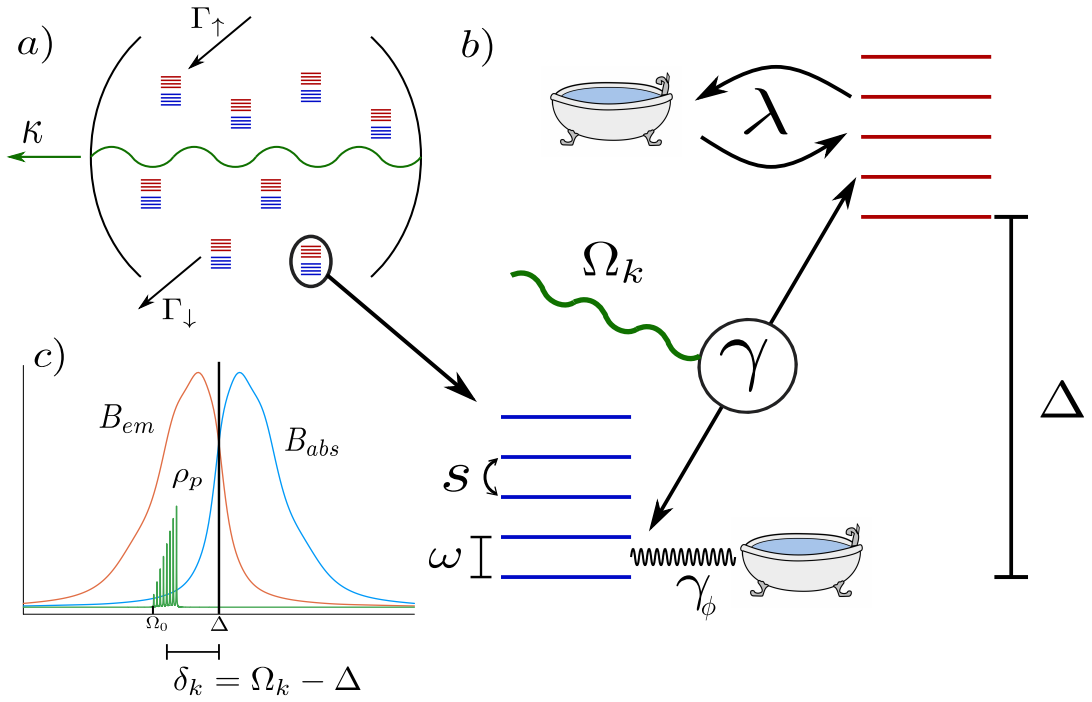

Figure 8.1: Schematic representation of the model used to describe the system. a) Cavity system with dye molecule solution. b) Model of the dye molecules. c) Molecule spectra and photon density of states. Details are discussed in the text.

In the previous chapters, we derived all the tools needed to tackle the coherence of the photons. After this rather technical part, it is worthwhile to recapitulate the essential processes captured in our approach. As shown in Fig. 8.1 a), we consider a cavity with a photon loss rate κ filled with a dilute dye molecule solution, pumped via an external laser source with a rate $\Gamma_\uparrow$. Molecules also lose excitation with a rate $\Gamma_\downarrow$, either due to radiationless decay or emission into non-trapped cavity modes. These three contributions are modelled via incoherent Lindblad processes as

$$\kappa\mathcal{L}[a_k] \quad , \quad \Gamma_\uparrow\mathcal{L}[\sum_n e_n^\dagger g_n] \quad , \quad \Gamma_\downarrow\mathcal{L}[\sum_n g_n^\dagger e_n]\,. \tag{8.1}$$

The dye molecules Fig. 8.1 b), are modelled as two electronic states with an energy difference of Δ, dressed with harmonic oscillator states with a spacing of ω, representing the vibrational

excitations of the molecules. The displacement between the equilibrium positions of these oscillators due to the Frank-Condon principle is incorporated via a hopping in the oscillator states with the Huang-Rhys parameter s^2.

$$h_e + h_g = \Delta \sum_n e_n^\dagger e_n + \omega \sum_n n \left[e_n^\dagger e_n + g_n^\dagger g_n \right] + \omega s \sum_n \sqrt{n+1} (e_{n+1}^\dagger e_n - g_{n+1}^\dagger g_n + h.c.) \quad (8.2)$$

Relaxation of the vibrations due to collisions is modelled with a coupling to a bath with a coupling rate λ and thermal occupation $\bar{n}$. This will lead to the thermalisation of the vibrational states to the bath temperature implicit in $\bar{n}$.

$$\lambda \left((\bar{n}+1)\mathcal{L} \left[\sum_n \sqrt{n+1} e_n^\dagger e_{n+1} + s e_n^\dagger e_n \right] + \bar{n}\mathcal{L} \left[\sum_n \sqrt{n+1} e_{n+1}^\dagger e_n + s e_n^\dagger e_n \right] \right) \quad (8.3)$$

$$+\lambda \left((\bar{n}+1)\mathcal{L} \left[\sum_n \sqrt{n+1} g_n^\dagger g_{n+1} - s g_n^\dagger g_n \right] + \bar{n}\mathcal{L} \left[\sum_n \sqrt{n+1} g_{n+1}^\dagger g_n - s g_n^\dagger g_n \right] \right) \quad (8.4)$$

We will also explore the differences between a thermal and the Markovian Lindblad bath for the phonon relaxation. The same collisions also lead to dephasing with a rate γ_ϕ as

$$\gamma_\phi \mathcal{L} \left[\sum_n e_n^\dagger e_n - g_n^\dagger g_n \right] . \quad (8.5)$$

The interaction between the molecules and the cavity photons is modelled via a Jaynes-Cummings interaction with coupling strength γ, which we consider the same for all cavity modes with energy Ω_k. The molecule number is incorporated via the simplified DMFT.

$$H_p + H_I = \sum_k \Omega_k a_k^\dagger a_k + \gamma \sum_{n,k} \left[a_k^\dagger g_n^\dagger e_n + a_k g_n e_n^\dagger \right] \quad (8.6)$$

This setup leads to generic absorption B_{abs} and emission B_{em} spectra, as seen in Fig. 8.1 c). They cross at the energy difference of the electronic states Δ, also called the zero-phonon line. Due to the rotating wave approximation used to arrive at the Jaynes-Cummings interaction, only the energy difference between the photon energy Ω_k and the molecule energy Δ is relevant. Therefore, we use the detuning $\delta_k = \Omega_k - \Delta$ from the zero-phonon line as the energy of the photon modes. The curvature of the mirror maps the cavity states to an effective two-dimensional harmonic oscillator. This means that the photon states above the ground mode δ_0 are linearly spaced with a difference $\Delta\delta_k$ and linearly degenerate, as indicated by the density of states ρ_p.

Chapter 9

Molecule Spectra

Reconstructing the appropriate molecule parameters is one of the most challenging tasks when applying the methods introduced here. The guiding principle is to reproduce the measured emission and absorption spectra. One should keep in mind that these spectra are experimentally dependent, among others, on temperature, solvents, and concentration. Therefore, we limit ourselves here to the most simple reference model, which is the one introduced in the previous sections. More complex molecule dynamics might lead to better agreement in the spectra but will involve more constants to be fixed. As we have shown in the previous chapter, the molecule spectra can be computed from the photon self-energies in a steady state as

$$B_{em}(\omega) = \lim_{t\to\infty} \frac{\Sigma^<(t,\omega)}{N_{mol}\mathrm{tr}(E^<(t,t))} \quad \text{and} \quad B_{abs}(\omega) = \lim_{t\to\infty} \frac{\Sigma^>(t,\omega)}{N_{mol}\mathrm{tr}(G^<(t,t))}\,. \tag{9.1}$$

To analyse the underlying structure of the molecule states, it is helpful to look at a particular property of the lesser Green function of the auxiliary particles. In the auxiliary particle method, the lesser functions at equal time contain information about the reduced density matrix of the molecule system. This can be seen by using the cyclic property of the trace in the not projected Green function as

$$G^<_{n,m}(t,t) = -i\mathrm{tr}(\rho\zeta^Q d^\dagger_m(t) d_n(t)) = -i\mathrm{tr}(d_n(t)\rho\zeta^Q\, d^\dagger_m(t)) \tag{9.2}$$

We can trace the different Q sectors separately and take the $\zeta \to 0$ limit. The trace over the physical particle states $|n_p\rangle$ is the same in each Q sector so that we can write

$$\begin{aligned}
\lim_{\zeta\to 0} G^<_{n,m}(t,t)/\zeta &= \lim_{\zeta\to 0} -i/\zeta \sum_{n_p} \langle n_p| \left[\langle vac|\, d_n(t)\rho\zeta^Q d^\dagger_m(t)\,|vac\rangle + \sum_{Q=1}^{\infty} \mathrm{tr}_Q\left(d_n(t)\rho\zeta^Q d^\dagger_m(t)\right)\right] |n_p\rangle \\
&= \lim_{\zeta\to 0} -i/\zeta \sum_{n_p} \langle n_p| \left[\langle d_n(t)|\, \rho\zeta^Q\,|d_m(t)\rangle + \sum_{Q=1}^{\infty} \mathrm{tr}_Q\left(d_n(t)\rho\zeta^Q d^\dagger_m(t)\right)\right] |n_p\rangle \\
&= \lim_{\zeta\to 0} -i/\zeta \sum_{n_p} \langle n_p| \left[\zeta\, \langle d_n(t)|\, \rho\,|d_m(t)\rangle + \mathcal{O}(\zeta^2)\right] |n_p\rangle \\
&= \lim_{\zeta\to 0} -i \sum_{n_p} \langle n_p, d_n|\, \rho(t)\,|n_p, d_m\rangle = -i\mathrm{tr}_{n_p}\left(\langle d_n|\, \rho(t)\,|d_m\rangle\right)
\end{aligned} \tag{9.3}$$

Therefore we can obtain the reduced molecule density matrices as $\lim_{\zeta\to 0} iG^<_{n,m}(t,t)/\zeta = \rho^{red}_{n,m}(t)$.

9.1 Molecule spectra with Lindblad bath

We analyse the spectra separately first, focusing on the molecules' dynamics generated by eq. (8.2 - 8.5). As a first step, we look at the spectra obtained by coupling the molecules only to Lindblad baths. We need to determine here the molecule vibration frequency ω, the Huang-Rhys factor s^2, the phonon relaxation rate λ with the average phonon bath occupation $\bar{n}$ as well as the dephasing rate γ_ϕ. Temperature will enter here through the average phonon bath occupation $\bar{n}$. Afterwards, the coherent coupling γ can be determined by comparison with the measured amplitude of absorption and emission coefficient. As a reference for the Rhodamin 6G spectra, we follow [24], [64] and [65]. The spectra cover a spectral range of roughly 180 THz with a Stokes shift of 13 THz. We determine the bath occupation from $\bar{n} = b(\beta\omega)$ with room temperature at $T = 300\,\mathrm{K}(\approx 6.25\,\mathrm{THz})$. Considering four phonon states, a reasonable spectrum can already be obtained, but more realistic spectra usually require more states. In Fig. 9.1, spectra are shown for six phonon states using the parameters in the caption of the figure.

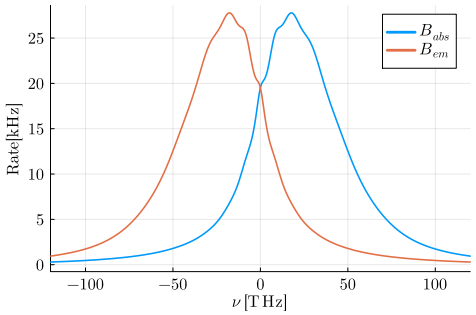

Figure 9.1: Absoprtion and emission spectra obtained with $N = 6$, $\bar{n} = 0.385$,$\lambda = 2.9$ THz ,$\omega = 8$ THz ,$s = 0.92$,$\gamma_\phi = 2.5$ THz ,$\gamma = 550$ MHz. Note all parameters are given in frequency, not angular frequency.

We first take a look at the state distribution of the phonons. Previously, we already argued that the bath must couple to the shifted phonon operators $b + s\sigma_z$ to thermalise the system to the minima of the respective potentials. To quantify if the system relaxes to the correct minimum of the shifted oscillators, we compute the eigenvectors of the molecule Hamiltonian and the lesser Green functions for the truncated phonon space from

$$G^<(t,t)\,|g_i(t)\rangle = \rho_i\,|g_i(t)\rangle \quad \text{and} \quad h_g\,|v_i^g\rangle = \epsilon_i^g\,|v_i^g\rangle\ . \tag{9.4}$$

The idea is if the system thermalises to the correct minimum of the respective oscillator, the density matrix should be diagonal in the eigenbasis of this oscillator. The diagonal entries for the electronic ground state lesser function at equal-time are shown in Fig. 9.2. Here Fig. 9.2a is obtained directly from the time evolution and Fig. 9.2b is rotated into the eigenbasis of the shifted molecule oscillator via its eigenvector matrix R. The lesser Green function in the steady state is strongly diagonal in this basis. If we compare the eigenvectors of the lesser Green function in the long-time steady state $|g_i(t \to \infty)\rangle$, to the eigenvectors of the molecule Hamiltonian $|v_i^g\rangle$, we obtain an overlap of

$$|1 - \sum_{i=1}^{N} \langle v_i^g | g_i(t \to \infty)\rangle\ /N| = 1.3 \cdot 10^{-2}\,. \tag{9.5}$$

In Fig. 9.3a, the steady-state distribution of the diagonal elements of the rotated lesser function is shown. They are the diagonal elements of the reduced density matrix and give the occupation probability of the phonon states. We also show a Boltzmann factor of the shifted molecule Hamiltonian at room temperature. The same temperature imprinted by the $\bar{n}$ factor in the phonon Lindbladians. They are in good agreement. As we will see, this result is rather deceiving. Since the states follow a Boltzmann distribution of the molecule Hamiltonian, one might now

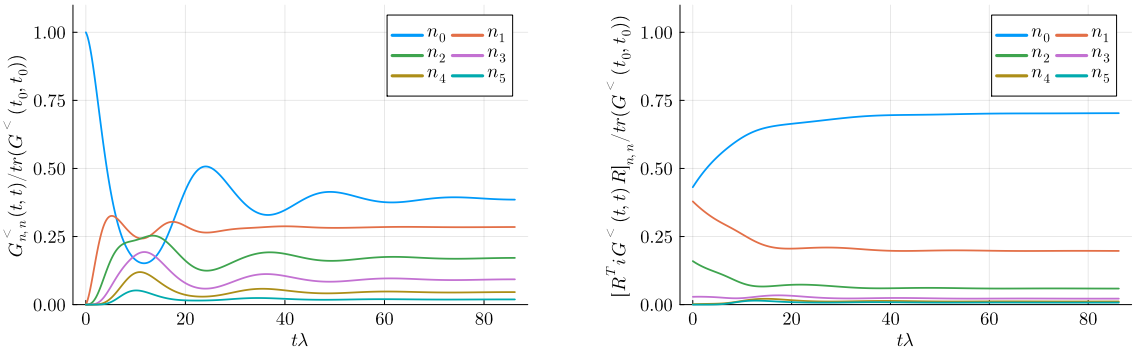

(a) Original basis of molecule Hamiltonian

(b) Eigenbasis of molecule Hamiltonian

Figure 9.2: Ground state phonon occupation of the molecule states during non-interacting time evolution. a) Diagonal elements in the original basis; b) Diagonal elements in the eigenbasis of the molecule Hamiltonian

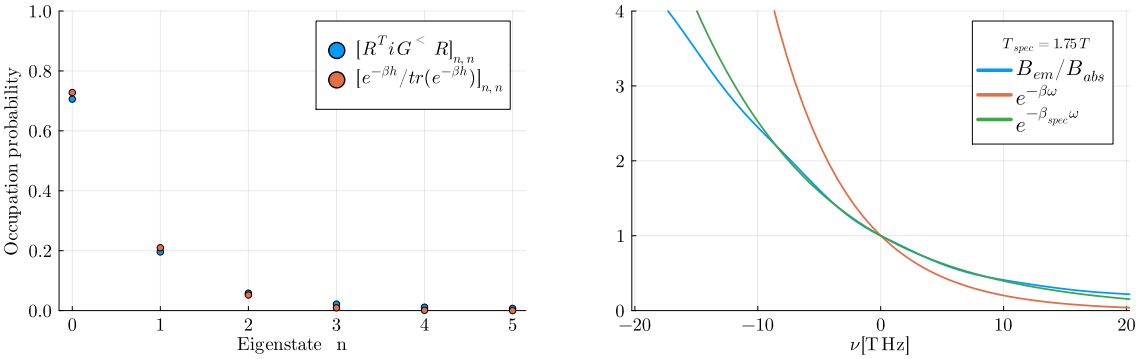

(a) Steady state distribution of the molecule states

(b) Kennard–Stepanov relation

Figure 9.3: a) Diagonal elements of the steady-state lesser functions and the thermal density matrix of the shifted molecule Hamiltonian for $T = 300K$. The system thermalises to the shifted Hamiltonian. b) Ratio of the emission and absorption spectra as a function of frequency measured from the zero phonon lines. Exponential behaviour is expected following the Kennard–Stepanov relation. A fit shows a higher temperature in the spectra.

expect to find the Kennard–Stepanov relation between the emission and absorption spectra. Their ratio should follow a Boltzmann factor and is shown in Fig. 9.3b. The behaviour around the zero phonon line is exponential but with a higher temperature. Further away from the zero-phonon line, the exponential behaviour quickly breaks down.

This can be traced back to the Lindblad coupling of the phonon bath. Due to the Markovian assumption in the derivation of the Lindbladian, the spectral information about the temperature of the bath is lost. In this approximation, the retarded and lesser functions in the long time steady state can be computed from

$$G^R(\omega) = \left[\omega - h - i\sum_i \kappa_i \Gamma_i^\dagger \Gamma_i\right]^{-1} \quad , \quad G^<(\omega) = G^R(\omega)\left[\sum_i \kappa_i \Gamma_i G^<(t,t)\Gamma_i^\dagger\right] G^A(\omega)\,. \quad (9.6)$$

The coefficients κ_i are the respective coupling constants of the Lindbladian and Γ_i the matrix

elements of the operators in auxiliary particle representation. Here, $G^<(t,t)$ encodes the long-time steady-state occupations determined by the coefficients κ_i. For general greater and lesser functions in a steady state, a similar formula hold, where the Lindblad part between retarded and advanced functions is replaced by the frequency-dependent self-energy [30]

$$G^{\gtrless}(\omega) = G^R(\omega)\Sigma^{\gtrless}(\omega)G^A(\omega)\,. \tag{9.7}$$

Using the Markovian approximation, the self-energy part loses its frequency dependence and does not imprint the fluctuation-dissipation theorem onto the relation between greater and lesser functions. But as we have seen in the previous chapter, the Kennard–Stepanov relation is a direct consequence of it. Therefore, a Lindblad bath fails to capture the Kennard–Stepanov relation. Nevertheless, it is possible to generate spectra which fulfil an exponential behaviour over the spectral range of some photon states, but usually at a higher temperature as used in the bath occupation $\bar{n}$. The same shortcoming also limits the applicability at large detunings where the ratio of emission and absorption becomes large. These regimes can not be reached since the exponentials necessary for the strong decay do not govern the long tails of the spectra but rather Lorentzians, as seen from eq. (9.6).

9.2 Molecule spectra with thermal bath

As in the rate equation approach, we expect the emission and absorption spectra's statistical distribution to be imprinted onto the photons. Therefore, it is imperative to obtain these correctly. To achieve this, we must implement the fluctuation-dissipation relation on the auxiliary particle Green functions. We have shown that this will not be possible with a Markovian bath, as assumed in the Lindblad construction. Therefore, we go back to the construction of the dissipation before the Markov approximation was performed. We obtained the auxiliary particle self-energy due to a bath as

$$\Sigma^{bath}_{i,j}(t,t') = i\lambda\left[g(t',t)\Gamma G(t,t')\Gamma^\dagger + g(t,t')\Gamma^\dagger G(t,t')\Gamma\right]_{i,j}\,. \tag{9.8}$$

We now couple the phonons to an Ohmic bath in the usual linear way via the exchange of oscillator quanta. The coupling matrix Γ is then given by the auxiliary particle representation of the shifted harmonic oscillator destruction operator from eq. (4.60) and (4.62). The density of states of the bath is chosen as linear with an exponential cut-off $\rho(\epsilon) = \frac{\epsilon}{\rho_0}e^{-D\epsilon}$. The temperature is imprinted onto the bath via its occupation function, the Bose function. Numerically, the bath must be discretised, and we compute the greater and lesser Green functions of it as

$$g^>(t,t') = -i\sum_k \rho(\epsilon_k)e^{-i\epsilon_k(t-t')}\left[\frac{1}{e^{\beta\epsilon_k}-1}+1\right] \tag{9.9}$$

$$g^<(t,t') = -i\sum_k \rho(\epsilon_k)e^{-i\epsilon_k(t-t')}\frac{1}{e^{\beta\epsilon_k}-1}\,. \tag{9.10}$$

Care must be taken in the bath discretisation to avoid spurious signatures in the correlation functions. The mode spacing $\Delta\epsilon$ of the bath must be smaller than the reciprocal of the maximum time the system is evolved to, $\Delta\epsilon < \frac{2\pi}{t_{max}}$. Otherwise, Poincaré recurrence leads to periodic peaks appearing at long times. Therefore, a large number of bath modes need to be taken into account to cover the spectral range of the bath. The exponential cutoff D mainly controls the long-time behaviour of the greater function and dampens oscillations.

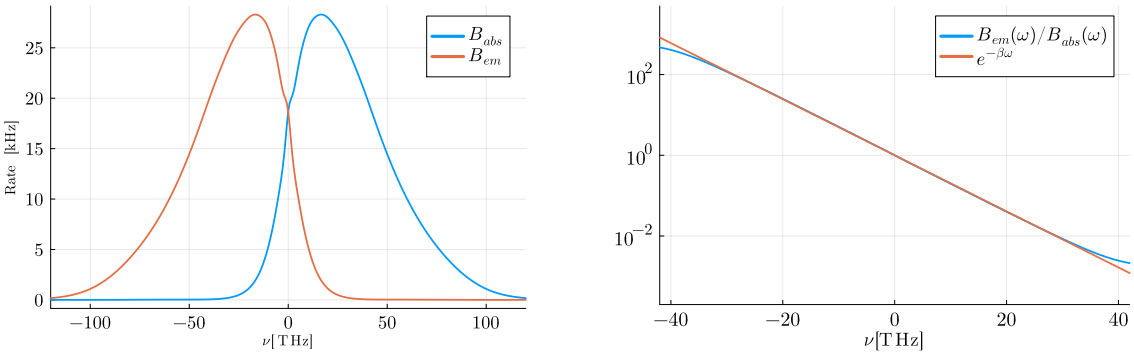

(a) Absorption and emission spectra

(b) Kennard-Stepanov relation

Figure 9.4: a) Absorption and emission spectra obtained with a finite temperature bath. The parameter are $N = 8$,$\lambda = 3.85$ THz ,$\omega = 6.6$ THz ,$s = 1.05$,$\gamma_\phi = 1$ THz ,$\gamma = 520$ MHz with a bath determined by , $T = 300$ K, $\Delta\epsilon = \frac{2\pi}{60}$ THz, $D/\Delta\epsilon = 150$ and 2000 bath modes. ; b) Ratio of emission and absorption in logarithmic scale. The Kennard-Stepanov relation is fulfilled over a large frequency range with the temperature of the bath.

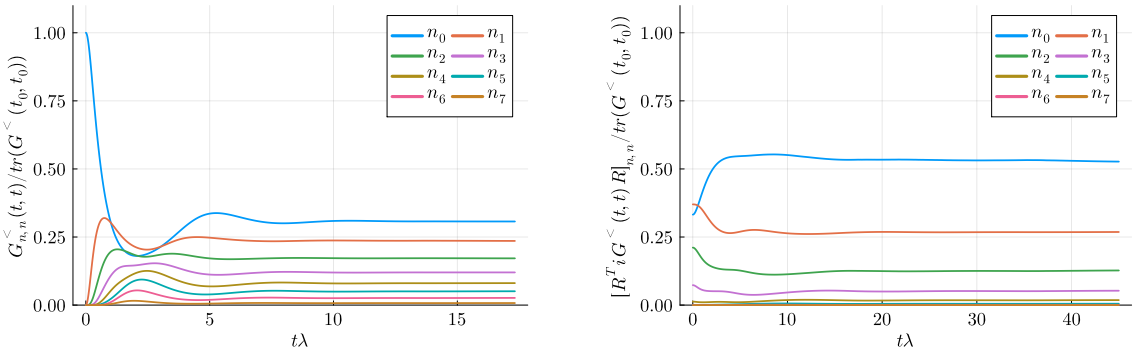

(a) Original basis of molecule Hamiltonian

(b) Eigenbasis of molecule Hamiltonian

Figure 9.5: Ground state phonon occupation of the molecule states during time evolution with a thermal bath. a) Diagonal elements in the original basis; b) Diagonal elements in the eigenbasis of the molecule Hamiltonian

A spectrum obtained this way and the corresponding Kennard-Stepanov relation can be seen in Fig. 9.4. The Kennard-Stepanov relation is now fulfilled for a larger frequency band, such that the ratio of emission and absorption can be tuned over a large range. Two effects dominantly produce deviations. Firstly, finite truncations of the phonon space. Here, enough modes must be considered to represent all occupied states at the temperature T in the shifted basis. Secondly, the dephasing parameter γ_ϕ. It introduces the same issue encountered in the purely Markovian bath case. One should also keep in mind that these spectra are generated from a time evolution with finite accuracy on a non-equidistant time grid, then interpolated onto an equidistant grid, and Fourier transformed on a finite domain. This also introduces defects, which are most prominent in the ratio at the boundaries of the spectra.

In Fig. 9.5, the evolution of the diagonal elements of the lesser functions at equal-time are shown. As in the previous case, the lesser functions become diagonal in the shifted oscillator basis. Here, the overlap of the eigenvectors in the long-time steady state is

$$|1 - \sum_{i=1}^{N} \langle v_i^g | g_i(t \to \infty) \rangle / N| = 2 \cdot 10^{-3} \,. \tag{9.11}$$

Nevertheless, the eigenvalues for the lesser function do not follow a Boltzmann distribution of the molecule Hamiltonian. Only in the limit of vanishing bath coupling, the system would thermalise to this distribution [28]. In our case, the systems spectra are strongly influenced by the bath, so the dynamics are also strongly governed by the bath coupling.

Another important aspect concerns the dephasing of the electronic states. In the collisions, which lead to the exchange of phonons with the bath, also phase information between the electronic states should be lost. In Fig. 9.6, the equal time dynamics of the off-diagonal auxiliary particle lesser function $EG^<$ is shown. It represent in the physical operator basis the expectation value $\langle \sigma^-(t) \rangle = i\mathrm{tr}(EG^<(t,t))$. This expectation value measures the coherence between the electronic ground and excited state. In the master equation approach, it decays with the dephasing rate γ_ϕ. Therefore, one might expect that the decay of the correlations should be dominated by the dephasing parameter γ_ϕ. But they decay much quicker due to the additional dephasing induced by the phonon relaxation λ.

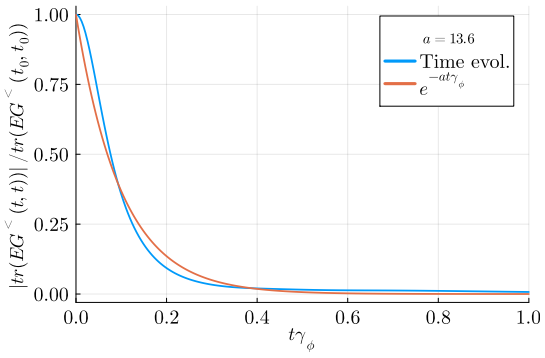

Figure 9.6: Decay of the equal-time, phonon summed, Green function $\mathrm{tr}(EG^<(t,t))$. It describes the molecule coherence and shows decoherence effects due to bath coupling far larger than the expected dephasing rate γ_ϕ.

Chapter 10

Normal Phase Dynamics

Before diving into the photon dynamics inside the cavity, let us briefly explain the numerical details of all systems discussed in the following. As initial conditions, we will always start with an empty photon system. This means all photon Green functions are zeros at initial times except the greater components being $-i$ due to the commutation relation. We must imprint a phase into the system to obtain a symmetry-broken phase. This is done by a small value of the off-diagonal molecule correlator $i\mathrm{tr}\left[GE^{<}(t_0,t_0)\right] \approx 1/N_{mol}$, of the order of the inverse molecule number. In the normal phase, this correlation will further decay, and, in the condensate phase, grow. We also start with a finite number of excited molecules inside the cavity, here 5%. This number must be chosen to be significantly smaller depending on the system's parameters. We will show results in a dissipative regime close to the zero phonon line. Here, most excitations in the cavity are contained in the molecule system and due to the large dissipation, the number of excited molecules is relatively high. The systems are solved with the KB solver introduced earlier with $\texttt{atol} = 10^{-5}$ and $\texttt{rtol} = 10^{-4}$. The memory integrals are cut following the decay of the self-energy eq.(2.84) at $t_\Sigma \cdot \lambda = 8$.

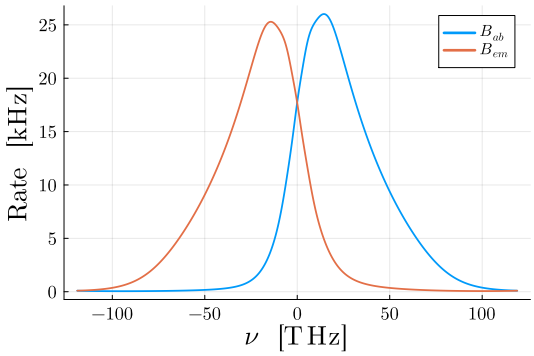

Figure 10.1: Molecule spectra used in the interacting case. We use a energy scale of 10 THz and consider $N = 4$ phonon states with $s = 1.05$, $\omega = 0.75$, $\lambda = 0.6$, $\gamma_\varphi = 0.1$, $\Gamma_\downarrow = 5 \cdot 10^{-2}$, $\gamma = 5 \cdot 10^{-5}$, $N_{mol} = 10^8$.

We now turn to the photon dynamics in the normal phase. This means in the following parameter regime, no coherent field is supported. Due to the numerical complexity and the available computational power, we need to make some concessions in the system's parameters. We consider a smaller number of phonon states, as shown previously, and enlarge the molecule dissipative couplings. This results in the spectra seen in Fig. 10.1. The parameters can be found in the caption. For these spectra, the Kennard-Stephanov relation is not fulfilled in such a large range as in Fig. 9.4b. We consider 10 modes in the cavity, with a large trapping frequency of $\Delta\delta_k = 1.5$ THz, which are linearly degenerate. This resolves a temperature range of around $2k_BT$. Due to the small number of modes and the large trapping frequencies, the critical particle number is very small. This makes the system sensitive to tremendously small changes in the pump rate. To counteract this, we work with rather large cavity loss. We first look at large dissipation with $\kappa = 500$ GHz and electronic loss $\Gamma_\downarrow = 500$ GHz.

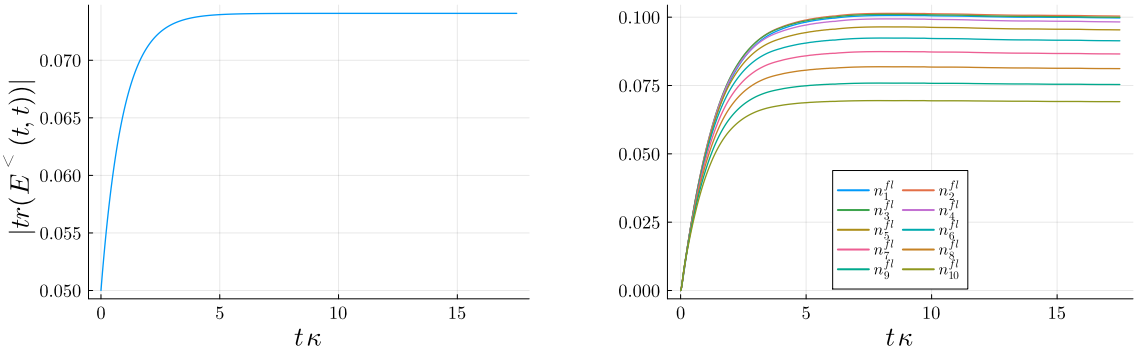

(a) Fraction of excited molecules

(b) Photon number without degenerasis.

Figure 10.2: Time-evolution of the fraction of excited molecules and photons to a steady state in the non-symmetry broken regime.

We use a detuning close to the zero phonon line $\delta_0 = -20\,\mathrm{THz}$ and a pump rate of $\Gamma_\uparrow = \frac{2}{25}\kappa$. This results in moderate ratios of absorption and emission rates.
In Fig. 10.2, we show the relaxation of the photon number and the excited molecules. These quantities are obtained from the two-time correlators, the Green functions and self-energies. Fig. 10.3a shows the self-energies from which the emission and absorption spectra are extracted. They are strongly confined to the equal time diagonal, which allows us to cut the memory integrals in the KB eq. following eq. (2.84). This is not the case for the photon Green functions themselves. The imaginary part of lesser functions of the ground mode and the fifth excited mode can be seen in Fig. 10.3b. At small cavity losses κ, they have support on most of the two-time grid. The spectra are obtained from these two-time data. The absorption and emission spectra are obtained as slices in the centre of motion (com.) time $T = (t + t')/2$ of the spectra Fig. 10.3c.

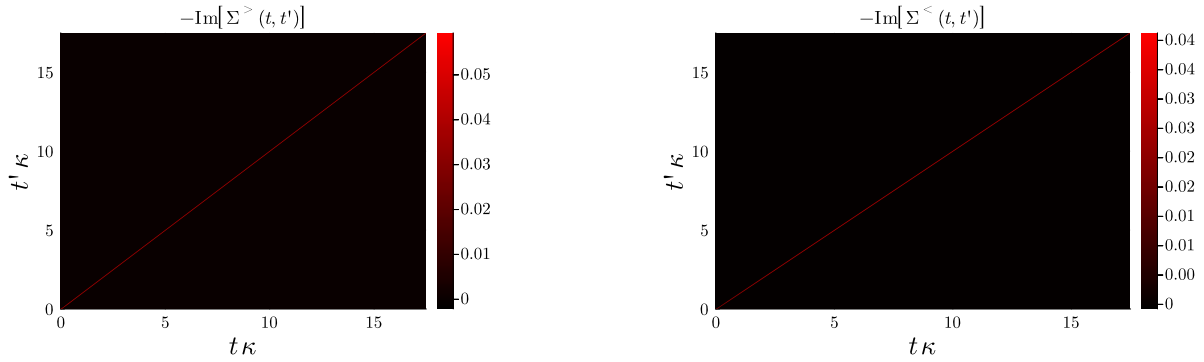

(a) Imaginary part of the normal photon self-energies in the two-time plane. They are strongly confined to the equal time diagonal as anticipated in eq. (2.84) .

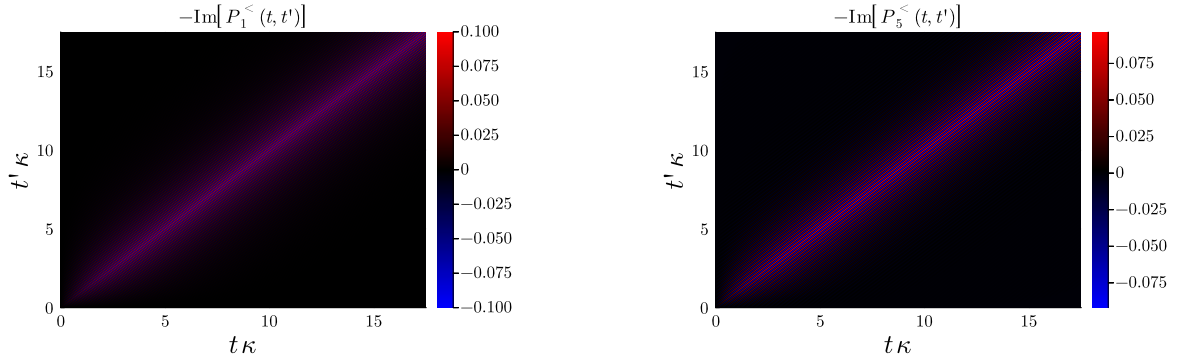

(b) Imaginary part of the lesser function of the ground- and fifth cavity mode in the two-time plane.

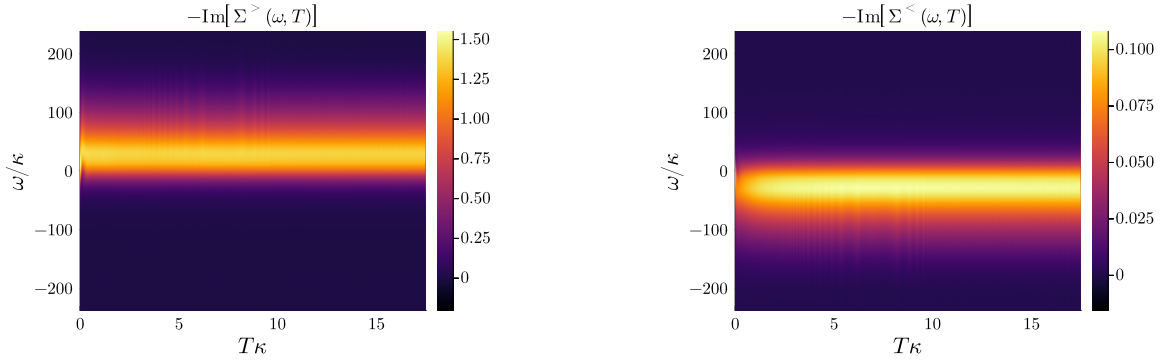

(c) Fourier transform of the photon self-energies in Wigner coordinates, so as a function of com. T and frequency as Fourier transform wrt. to relative time $\tau = t - t'$. Left: The greater self-energy leads to the absorption coefficient. Right: The lesser self-energy leads to the emission coefficient.

Figure 10.3: Example of the two-time functions computed in this approach.

We now turn to the thermalisation of the photon spectra in the normal state. For this, we compare the fluctuation-dissipation relation between the greater and lesser functions in equilibrium. We consider the mode summed functions

$$N_p(\nu) = -\sum_k \mathrm{Im}\left(P_k^<(T_\infty, \nu)\right) \tag{10.1}$$

$$N_h(\nu) = -\sum_k \mathrm{Im}\left(P_k^>(T_\infty, \nu)\right) . \tag{10.2}$$

In thermal equilibrium, they should be related by

$$N_p(\nu) = e^{-\beta(\nu-\mu)} N_h(\nu) . \tag{10.3}$$

In Fig. 10.4, a fit of this relation is shown, and the parameters are given in the caption. The fit reveals that the spectra are thermal, but the temperature is higher than in the phonon bath. This can be traced back to two phenomena. Firstly, as previously discussed, the large Lindblad couplings in the molecules lead to a higher temperature in the spectra. The main contribution comes from the large dephasing parameter γ_ϕ. But more importantly, the large mode spacing and small number of modes lead to small photon numbers. In this regime, spontaneous emission dominates. Due to the comparably large number of excited molecules but small emission coefficient, it competes with the cavity decay κ. This issue was essentially already found in the phenomenological rate equation approach in the introduction eq. (1.6). But here, it manifests in a higher temperature and the spectral functions of the photons. Nevertheless, the spectra follow the fluctuation-dissipation theorem rather well. Therefore, the photon correlations can be expected to be thermal even if the spectra do not directly indicate this when constructed from the free cavity density of states. This effect is significantly reduced at smaller dissipative couplings. In Fig. 10.5, the relation for a system with smaller dissipation is shown. The system has not reached its steady state at the point where the spectra are obtained. But already at this stage, the photon spectrum shows a temperature close to the phonon bath temperature. Here, we again compare with the bath temperature and not the temperature of the molecule spectra, which is higher due to the dissipative coupling γ_ϕ. The spikes in the spectrum Fig. 10.5 arise due to the smaller time domain for the Fourier transformation at the end of the time evolution. They are numerical and decrease for longer time evolutions.

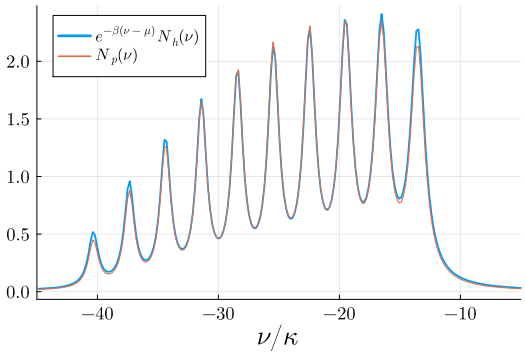

Figure 10.4: Test of the fluctuation-dissipation theorem for the photon spectra. The spectra thermalise, but due to the large dissipation at a larger temperature $T_{fit} = 5.2\,T$ and chemical potential $\mu = -132\,\kappa$.

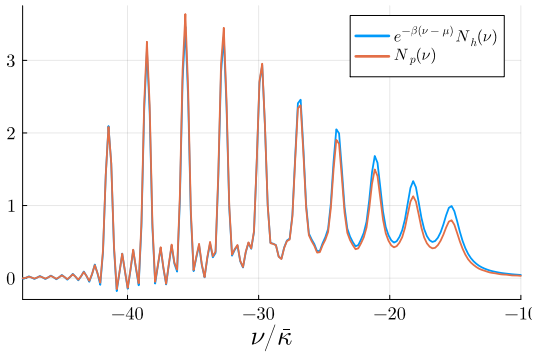

Figure 10.5: Fluctuation-dissipation theorem for the photon spectra at significantly smaller dissipative coupling $\kappa = 20$ GHz, $\Gamma_\uparrow = \kappa/4$, $\gamma_\phi = 250$ GHz. The frequency axis is scaled with the cavity loss used in fig. (10.3c). The system has not fully reached a steady state, and the spectra are not fully thermalised. A fit shows a temperature $T_{fit} = 1.1\,T$ and a chemical potential $\mu = -71\bar{\kappa}$.

Chapter 11

Condensed Phase Dynamics

We now turn to the condensation of the photons. The critical region is tremendously small since the photon number in the phase incoherent fluctuations is small. This leads to a strong sensitivity of the condensate fraction with the pump rate. Therefore, one quickly reaches a regime where the coherent field dominates the system. This is also the regime where we will show results here. We increased the pump rate to $\Gamma_\uparrow = \frac{1}{5}\kappa$ and left the other parameter as in the first example. In Fig. 11.1, the time evolution of the fraction of excited molecules and the photon fluctuations can be seen. Their drop coincides with the emergence of the phase coherent condensate, as seen in Fig. 11.2. Here, multiple modes contribute to the condensate. In Fig. 11.3, the real part of these fields is shown as a function of time in a small time interval.

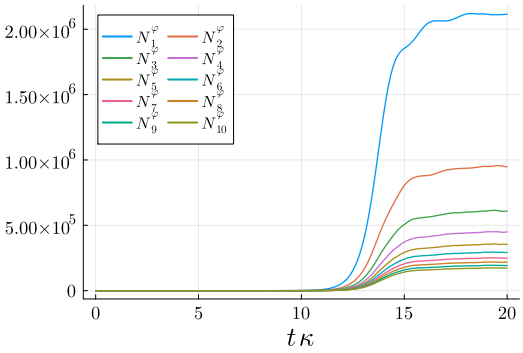

Figure 11.2: Density of phase-coherent photons in the transversal cavity modes, including degeneracies.

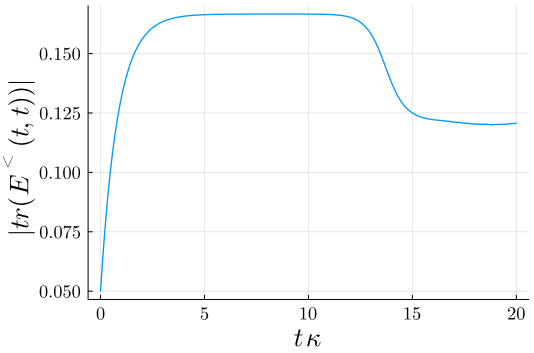

(a) Fraction of excited molecules

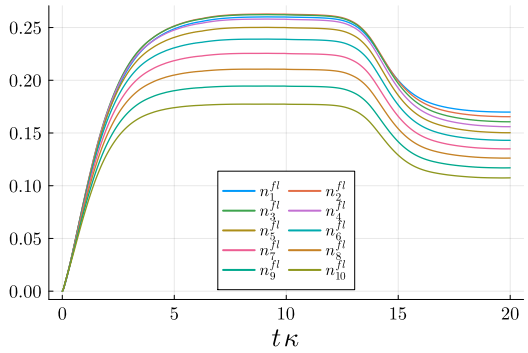

(b) Fluctuating photon number without degeneracy

Figure 11.1: Time-evolution of the fraction of excited molecules and photon fluctuations to a steady state in the symmetry broken regime.

They evolve with the same frequency. This is a manifestation of the macroscopic wavefunction of the photon system. To understand this behaviour, let us, for a moment, turn to cold-atom experiments on BECs. Let us assume we have massive bosons in a trap, which interact with a contact interaction. Furthermore, let us assume that the description via the Gross-Pitaevskii equation is valid. In the real space representation, we can write it as

$$i\partial_t \Psi(x,t) = h_0(x)\Psi(x,t) + g|\Psi(x,t)|^2\Psi(x,t)\,.$$

Here, h_0 is the single particle Hamiltonian containing kinetic energy, the trapping potential, and the chemical potential. When the BEC is formed in a steady state, the wavefunction evolves in time with its energy as $\Psi(x,t) = e^{-iEt}\Psi(x)$. The density profile follows then from

$$E\Psi(x) = h_0(x)\Psi(x) + g|\Psi(x)|^2\Psi(x)\,.$$

But we can also look at this problem in the basis of the eigenfunctions $\phi_n(x)$ of the single particle Hamiltonian h_0. If we decompose the fields into this basis as $\Psi(x) = \sum_n \phi_n(x)\Psi_n$ we end up with

$$E\Psi_n = \epsilon_n\Psi_n + \sum_{p,q,k} U_{n,p,q,k}\Psi_q^*\Psi_k^*\Psi_p$$

$$\text{with} \quad U_{n,p,q,k} = g\int dx \phi_n(x)\phi_p(x)\phi_q^*(x)\phi_k^*(x)$$

The solution will be some distribution of the Ψ_n. But all these contributions still time-evolve with the same energy E. This effect is essentially what happens with the cavity modes in Fig. 11.3. Experimentally, this manifests in a deviation of the density profile from the profile of the trap ground mode. This is an effect of the interaction. In [2], a broadening of the spatial distribution was reported as the condensate fraction is increased. Our result here does not necessarily explain this broadening. Here, even though the interaction strength is realistically small, the condensate fraction is unreasonably large due to the small number of modes, the large trapping frequency and the limitation on how close the critical point can be approached in the time evolution. Also, other processes contribute to the broadening, which are not contained in the treatment presented here. One possibility is the heating of the solvent. The heating effects result in a thermo-optic interaction considered in [66]. This effect is on a tremendously long time scale compared to the molecule time scales considered here. Therefore, it is hard to incorporate into the presented formulation. Another contribution could come from the pump spot size. It usually exceeds the mode profile of the ground mode. At small pump rates, the molecule solution is in a global equilibrium in the

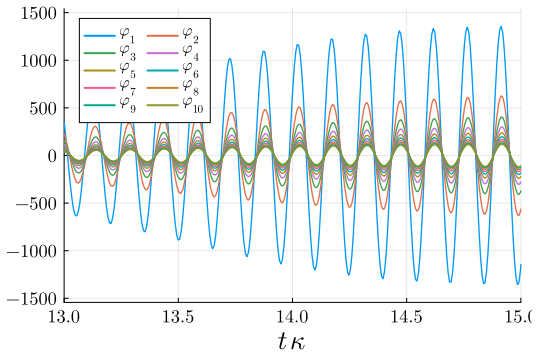

Figure 11.3: Mode resolved real part of the condensates in a small time interval.

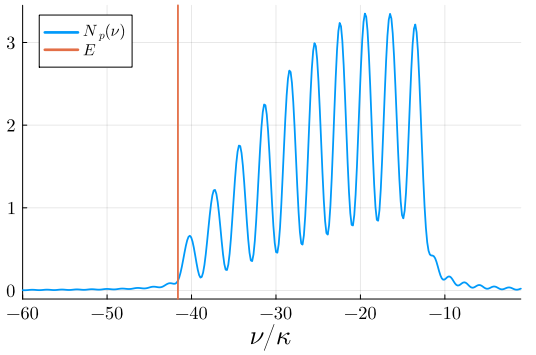

Figure 11.4: Photon number spectrum of the fluctuations and the energy of condensate $E = -41.6\kappa$ obtained from fitting the phase oscillation of the condensate. The spectrum fulfils the fluctuation-dissipation theorem but at a higher temperature.

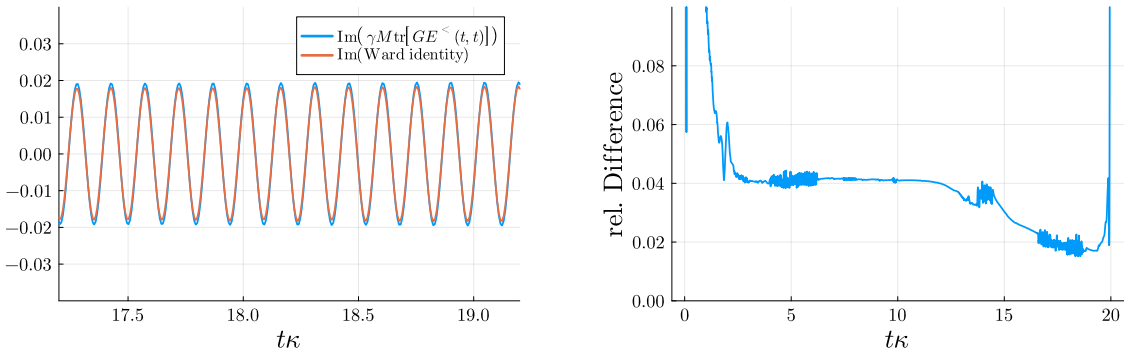

(a) Time evolution of the imaginary part.

(b) Relative Difference of the signals in a)

Figure 11.5: Comparison of the equation of motion of the condensate with the Ward identity. a) The imaginary part evolves with the same phase and phase velocity. b) Relative difference of the relations.

cavity. However, after the BEC is formed and the pump rate is increased, the external regions, not contained in the spatial profile of the BEC, accumulate molecule excitation. This might lead to a broadening of the spatial profile. Studying this scenario by considering the molecule solutions inhomogeneous would be tremendously insightful. Here, an interesting point is that the different mode distributions inside the cavity can lead to mode competition and loss of coherence [67]. Unfortunately, the available computational power does not allow us to study this.

As we have seen, we can obtain the energy of the condensate from its phase oscillation. In Fig. 11.4, its position relative to the spectrum of the fluctuation is shown. It emerges closely below the ground mode of the cavity as expected. The fluctuation spectrum follows the fluctuation-dissipation theorem in the sense of the first example in the normal phase we showed. Here again, the temperature is larger than that of the phonon bath. To test if condensate's energy fits the fluctuation spectrum, we look at the Ward identity obtained earlier. We compare the Ward identity eq. (6.3) with the mode summed equations of motion of the condensate eq. (5.22). This is the equation of motion of the local condensate, for which eq. (6.3) should hold. It implies that

$$\sum_k \left[\int_{t_0}^{t} dt' (\Sigma^{>}_{aa^\dagger}(t,t') - \Sigma^{<}_{aa^\dagger}(t,t'))\varphi^*_k(t') - \int_{t_0}^{t} dt' (\Sigma_{aa}(t,t') - \Sigma_{aa}(t',t))\varphi_k(t') \right] \tag{11.1}$$

$$\stackrel{!}{=} i\gamma N_{mol} \mathrm{tr}\left[GE^{<}(t,t)\right] \tag{11.2}$$

In Fig. 11.5a, we show their imaginary part in a small time window to resolve the oscillation. The agreement is surprisingly good as shown by computing the relative error of the eq. (11.2) as $|\text{lhs.} - \text{rhs.}|/|\text{rhs.}|$. Here Fig. 11.5b shows an agreement of around $2\% - 4\%$. This agreement is striking, considering we use a simplified DMFT formulation with a lowest-order approximation for the impurity solver.

We want to show another aspect that is unfortunately only hardly visible in the current parameter range, but might be more important when the cavity parameters are taken to the experimental region. In Fig. 11.3, the oscillation of the condensate in the cavity modes looks in-phase. This is not the case. The equation of motion leads to a necessary phase shift of the modes depending on their detuning. As shown from the Hugenholtz-Pines theorem for open systems, this phase shift is crucial to cancel the dissipation due to κ and obtain a stable condensate. The phase shift can be calculated from the equation of motion of the phase coherent condensate

$$\partial_t \varphi_k(t) = -i\delta_k \varphi_k(t) - \frac{\kappa}{2}\varphi_k(t) + \gamma N_{mol} \mathrm{tr}\left[EG^<(t,t)\right] . \quad (11.3)$$

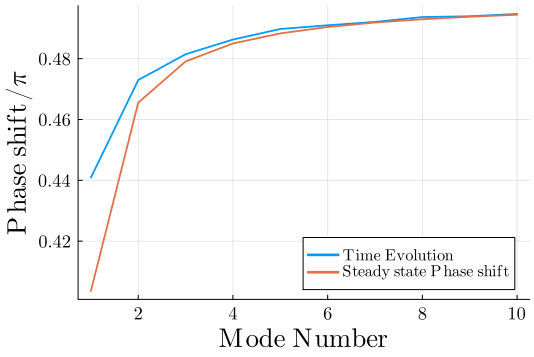

Figure 11.6: Phase shift between the off-diagonal molecule correlators and the coherent fields in the modes. In blue is the numerical result of the time evolution, and in orange, eq. (11.4) with the condensate energy $E = -41.6\kappa$.

In the steady-state the coherent part of the photons and molecules evolve with the same phase evolution $\varphi_k(t) = e^{-iEt}e^{-i\theta_k}\phi_k$ and $\mathrm{tr}\left[EG^<(t,t)\right] = e^{-iEt}e^{-i\nu}g$ with $g = |\mathrm{tr}\left[EG^<(t,t)\right]|$ and $\phi_k = |\varphi_k(t)|$. This allows us to write

$$-i(E-\delta_k)\phi_k = -\frac{\kappa}{2}\phi_k + \gamma N_{mol} g e^{i(\theta_k-\nu)} \Rightarrow \frac{E-\delta_k}{\kappa/2} = \tan(\nu-\theta_k) \quad (11.4)$$

A comparison of this steady-state formula to the numerically obtained phase shift is shown in Fig. 11.6. The relation seems already to hold for the higher modes, but the low-lying modes still deviate. This could also be anticipated from Fig. 11.2. The density of the lower modes still shows dynamics and has not reached a steady state yet. The phase shift to the molecule plays here the role of stabilising the condensate against the cavity decay κ. This gives us another perspective on the multiple modes contributing in Fig. 11.2. In the absence of the cavity loss, we expect a decay of the occupations in the modes as $1/(E-\delta_k)^2$. This decay is slowed down by dissipation κ to a Lorentzian shape $1/(\kappa^2/4 + (E-\delta_k)^2)$. We use a large dissipation κ. Therefore, also modes that are further away energetically contribute to the phase coherent part. This is the main reason why we obtain large occupations for the higher modes. Similar behaviour due to finite cavity loss has also been reported in [68].

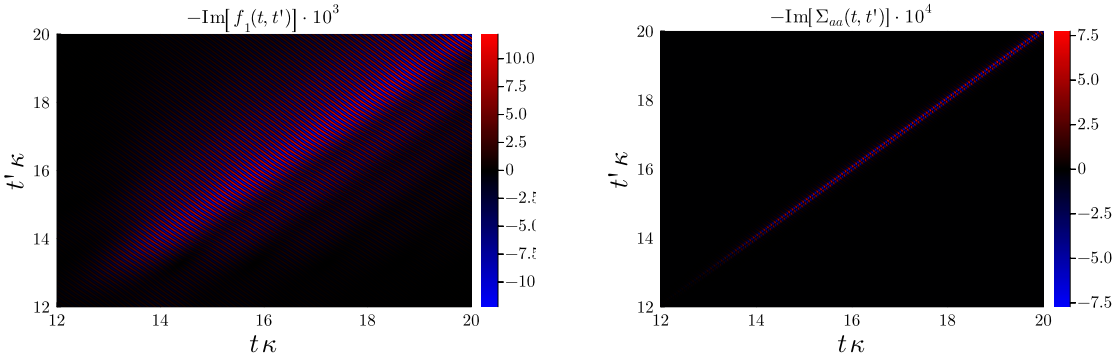

Figure 11.7: Imaginary part of $f_1(t,t')$ and the $\Sigma_{aa}(t,t')$ in the two-time plane.

Additionally to the photon condensate, the anomalous photon propagators are also present in this phase. Fig. 11.8 shows the absolute values on the time diagonal, and Fig. 11.9 shows the imaginary part compared to the evolution of the (scaled) square of the condensate. They all evolve with the same phase factor as the square of the condensate. This indicates that all these anomalous propagators are a property of the condensate. In Fig. 11.7, the anomalous propagator for the ground mode and the anomalous self-energy are shown in the two-time plane. The absolute values of the anomalous propagators are surprisingly large compared to the number of fluctuating photons. In the context of atomic BEC's, these correlators are usually interpreted as a result of two-body scattering [37]. They are necessary to implement the symmetry relation between the 1-particle and 2-particle observables. Here, they fulfil a similar role, as they are necessary to implement the relation between the condensate and the Green functions in Fig. 11.5a. It is unclear if this would also hold with more realistic cavity parameters or if this is a consequence of the large condensate fraction. Nevertheless, a comparison to atomic BEC's [69] indicates that at smaller mode spacing, these effects are enhanced. From the quantum optics perspective, they tell us about squeezing of the light. We want to emphasise that the results presented here do not provide any information about multi-mode squeezing. However, these correlators might be especially interesting in micro-structured cavities. By imprinting additional structures onto the surface of the mirrors, different potential landscapes can be engineered. In this way, a double well was realised in

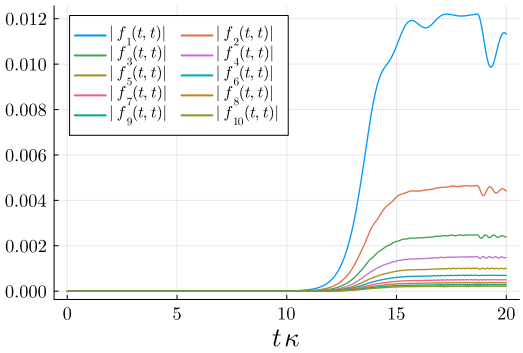

Figure 11.8: Absolute value of the anomalous photon propagators, including the degeneracies of the modes in com. time.

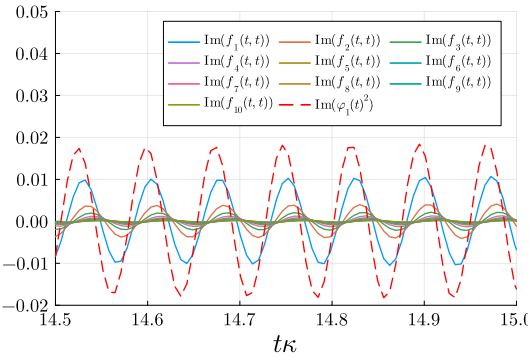

Figure 11.9: Phase evolution of the anomalous propagators on the time diagonal compared with the condensate phase evolution.

[70]. Here, a direct tunnelling couples neighbouring sites due to the spatial overlap of the mode. In this setup, the anomalous propagator between the sites can give information about the entanglement of the sites [71]. Numerically, this system is demanding not only because of the larger molecule space, which needs to be considered but especially because the local modes have a smaller mode volume. This leads to fewer molecules in their profile, drastically increasing the thermalisation time. On the upside, this makes the system even more interesting since the tunnelling rate is on the time scale of the thermalisation.

11.1 Strong-coupling regime

The strong-coupling regime can be reached by increasing the molecule density N_{mol} or the photon-molecule coupling γ. Even though they are formally similar, they influence the system differently. This can most transparently be seen when eliminating the explicit dependence on the molecule number from the equations. This can be achieved by mapping $\gamma \to \gamma\sqrt{N_{mol}}$ and simultaneously scaling the photon correlators as $\varphi \to \varphi/\sqrt{N_{mol}}$ and $P^{\gtrless} \to P^{\gtrless}/N_{mol}$. After this transformation, the equations of motion do not have any explicit dependence on N_{mol} anymore. The molecule number now only appears in the initial conditions of the photon correlator. For an empty cavity, the greater functions at initial time are $P^{>}(t_0, t_0) = -i/N_{mol}$. This specifically scales the contribution of the commutator by a factor of $1/N_{mol}$. From another perspective, the molecule number controls the contribution of spontaneous emission. This scaling behaviour is a consequence of the simplified DMFT. We will show here some results for a coupling γ twice as large as before $\gamma = 1$ GHz. At larger couplings, various phases are expected, and the many dissipative couplings make this method rather versatile. We do not aim here to claim any specific physical behaviour or phase. This presentation aims to emphasise certain aspects which hint at inconsistencies and should be checked when results are interpreted. Firstly, we show the total photon number in the phase-coherent part against the off-diagonal molecule Green function in Fig. 11.11a . The large value of the off-diagonal molecule correlator hints at the formation of excitons, and the comparable size to the photon condensate suggests a polariton condensate. This view is supported by the molecule spectra showing a strong peak emerging at the energy of the condensate. They are shown in Fig. 11.11b with a scaled reference of the photon number spectrum. The photon fluctuations are not vastly changed. They get shifted and broadened by the larger photon self-energies. The energy of the condensate is gapped wrt. to the fluctuation spectrum, which is a key feature of exciton-polariton condensates [5]. If we consider the Ward identity, we find a large deviation as shown in Fig. 11.10. The exciton is a highly entangled molecule state, which can here only emerge due to the strong interaction with the photons. Therefore, we can expect to need more than the NCA diagrams to describe this state. This discrepancy manifests here in an inconsistency between the fluctuations and the condensate. Therefore, conclusions drawn on the state of the system and the signatures manifesting in the light should be taken with a grain of salt.

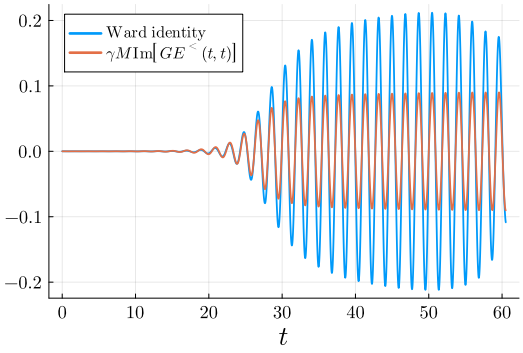

Figure 11.10: Test of the Ward identity.

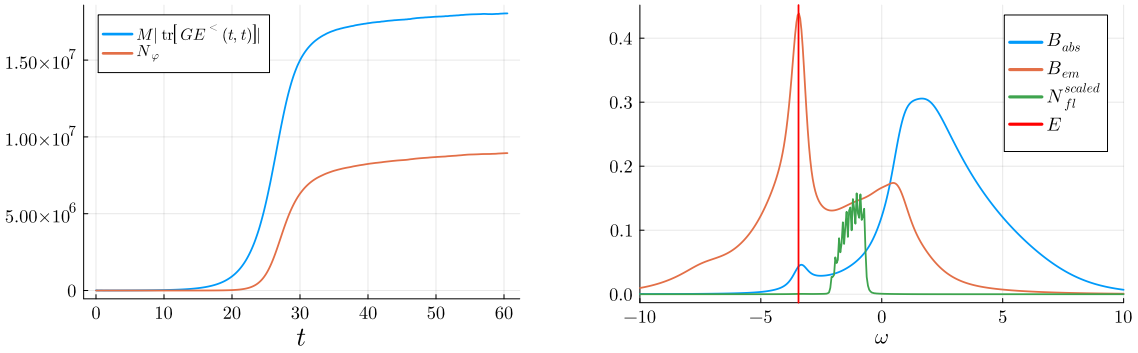

(a) (b)

Figure 11.11: a) Condensed photons and molecule coherence $N_{mol}|\langle\sigma^+(t)\rangle|$. b) Molecule spectrum with photon fluctuations as a reference to the energy of the condensate E.

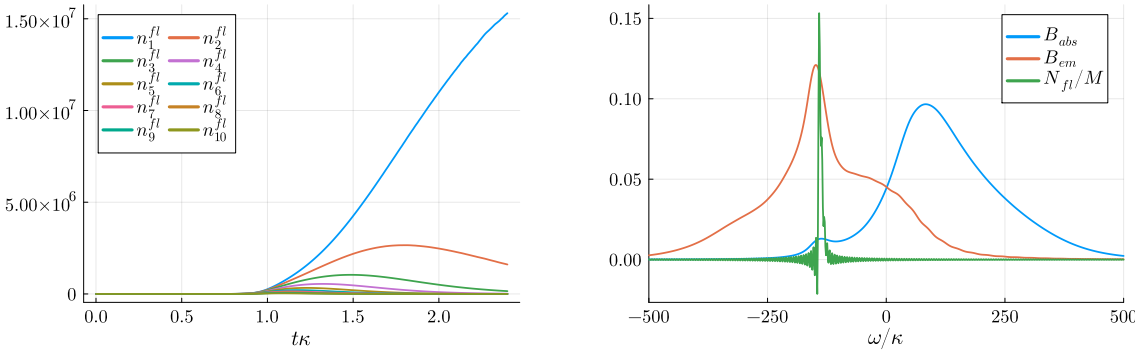

(a) Incoherent photon number (b) Molecule spectra

Figure 11.12: Loss of coherence in strong-coupling regime. a) Photon number accumulates in the ground mode. b) Molecule and photon number spectrum at $T\kappa = 1.8$: Parameters in units of 10 THz given by $\gamma = 2 \cdot 10^{-4}$, $\Delta\delta_k = 0.1$, $\kappa = 2 \cdot 10^{-2}$, $\Gamma_\downarrow = 10^{-3}$, $\Gamma_\uparrow = \kappa/4$.

Increasing the coupling strength further, the system loses its coherence and only the fluctuating part of the photons contributes Fig. 11.12a. The photon numbers show similar dynamics as expected from the rate equation approach. The molecule spectra get strongly renormalised and a peak at the ground mode energy emerges as the mode accumulates photons Fig. 11.12b. The photon spectral function Fig. 11.13 develops a slight negative part at the ground mode to accommodate the large photon numbers, and a faint high energy tail or side peak emerges. The high energy behaviour was reported in a mean-field study [72] and interpreted as a strong coupling signature attributed to an upper polariton band. Coherence is recovered at large pump rates, but the molecule spectra get so strongly renormalised that they are hardly recognisable as molecule spectra and are far from thermal.

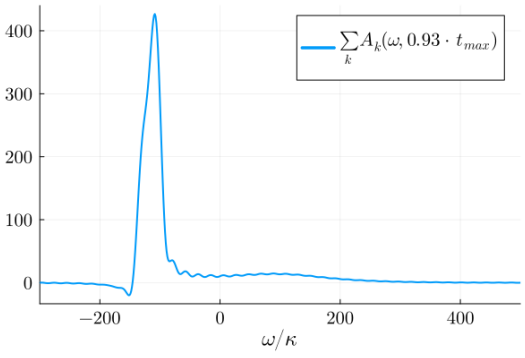

Figure 11.13: Photon spectral function.

Conclusion

Incorporating a coherent photon field, which leads to a classical phase coherent wave emitted from the cavity, turned out to be complicated. In a rate equation approach, one quickly concludes that it requires a lasing state, which is distinct from the BEC state. To remedy this, we developed a formalism to describe the molecule dynamics in a field theory setting. This auxiliary particle representation, in combination with the spontaneously broken $U(1)$ symmetry in an open-driven quantum system, requires a variety of different theory tools. We gave an introduction to the Schwinger-Keldysh formalism and the approximation method of the 2-PI EA. From this, we developed the auxiliary particle theory for an open-driven system and incorporated large molecule reservoirs with a simplified DMFT. This leads us to a crucial consistency requirement between the fluctuation spectrum and condensate. The time-evolution of the coupled two-time Green functions and condensate is performed with an adaptive order and step size method.

It turned out that a non-Markovian thermal bath for the vibrations is needed to obtain physical spectra following the Kennard-Stepanov relation. We could show that the light thermalises in the cavity and pre-thermal states could be observed. We presented results in the symmetry-broken phase and could show that for realistic molecule parameters, a phase-coherent condensate emerges at the bottom of the fluctuation spectrum. Our approximation fulfils the Ward identity at this point, revealing the importance of the anomalous propagators to obtain consistent energies for the condensate. This allows us to conclude that we observed a photon condensate in this parameter regime. What still remains is the question of whether what we observe is a BEC or a laser. The presented parameter regime has a tremendously small number of fluctuating photons, such that the condensate fraction is close to one. It results from the combination of a small number of modes, the large mode spacing and the strong cavity loss. With only the information of the g_1 function of the light, this state should be experimentally indistinguishable from a lasing state. At the present stage, we can not make reliable predictions for the g_2 function. However, the state has two-photon correlations manifesting in the anomalous propagators in a similar order to the fluctuations. From atomic BEC, we can expect that this correlation grows as the mode spacing is reduced [69], as we also expect from the photon fluctuations. Additionally, the occurrence of the anomalous self-energy is crucial to maintain the Ward identity. This would not be expected in a lasing state.

In the presentation of the result, we have already hinted at various points that need further investigation. These were mainly concerned with numerical improvements to reach the experimental parameter of the cavity and tackle various effects from the cavity geometry. We want to expand this list here on a few fronts;

Second order coherence

These properties of the photon fluctuations have been investigated experimentally and theoretically using the rate equation approach [25] as well as the auxiliary particle method without symmetry breaking [58]. In the symmetry-broken phase, the path to obtain these contributions is unclear. That we needed to check the Ward identity already hinted to the fact that these correlation functions are manifestly not uniquely defined when approximations to the self-energies in the symmetry broken phase are applied. A first principle calculation would, in any case, result in coupled Bethe-Salpeter equations. At the present time, they are numerically too expensive to solve in non-equilibrium. The most promising path to obtain these in the symmetry-broken phase seems to be response theory, as applied without symmetry breaking in [58]. Here, two main questions need to be answered. Firstly, in the Green function setup, the response is usually calculated from the linear response of the two-time Green function [30]. How this concept generalises to a simultaneous change of the coherent field is not explored. Secondly, in this system, the light response will always be accompanied by a matter response. Their correlation will mix on the level of KB equations. Extracting the photon correlations from these signals requires an understanding of the underlying symmetries between these different responses. Here, the analysis of the higher-order Ward identities might lead to some insight into this problem. To the best of the author's knowledge, the study of these connections has only recently been started [73]. Nevertheless, in the context of the photon BEC, these corrections can be expected to be small. Another unexplored aspect is that the two-time Green function formulation of linear response theory can also provide additional information from the two-time nature of the correlation functions. This might also be a pathway to obtain more exotic correlation functions like out-of-time-ordered correlators.

Non-Markovian Molecule bath

In the approach put forward here, we included all internal molecule states, which makes it numerically expensive. Therefore, it might not be applicable to large structured cavity systems. But as we have seen, molecule spectra are largely unperturbed by the photon interaction in the region where the photon BEC is studied. We have shown that the Markovian master equation does not support a phase-coherent BEC state and that the Kennard-Stepanov relation can not be obtained from a Lindblad bath. This means that also multi-level approximation in a cumulant expansion as used in [63] will not show an actual Kennard-Stepanov relation. Therefore, the most promising approach to minimize the computation cost seems to treat the phonon system as a non-Markovian bath. Technically, this can be achieved using the Polaron transformation and only applying the auxiliary particle representation to the electronic states. The phonon bath can then be integrated out in the path integral formulation. This leads, in NCA approximation, in the normal state effectively to a non-Markovian variant of the master equation used in [22]. In the condensed phase, the anomalous parts also contribute as a non-Markovian variant of eq. (1.25).

By now, a hallmark of condensed matter physics is that the experimentalists are quite ahead of the theory, and the photon BEC is no exception. The micro-structuring of cavities opens up entirely new possibilities, from studying the Kibble-Zurek mechanism in continuous rings, over topology of open-driven systems in discrete arrays to entanglement in discrete lattice structures. In the light of these developments, there is still much work ahead of theorists.

Bibliography

[1] F. Schäfer et al., *Dye lasers*, Enlarged 3rd, Topics in Applied Physics (Springer Berlin Heidelberg, 1990).

[2] J. Klaers et al., "Bose–Einstein condensation of photons in an optical microcavity", Nature **468**, 545–548 (2010).

[3] B. T. Walker et al., "Driven-dissipative non-equilibrium Bose–Einstein condensation of less than ten photons", Nature Physics **14**, 1173–1177 (2018).

[4] A. Redmann et al., "Bose-Einstein Condensation of Photons in a Four-Site Quantum Ring", arXiv.2312.14741 (2023).

[5] J. Keeling and S. Kéna-Cohen, " Bose–Einstein Condensation of Exciton-Polaritons in Organic Microcavities ", Annual Review of Physical Chemistry **71**, 435–459 (2020).

[6] T. Khazanov et al., "Embrace the darkness: An experimental perspective on organic exciton–polaritons", Chemical Physics Reviews **4**, 041305 (2023).

[7] C. Clear et al., "Phonon-Induced Optical Dephasing in Single Organic Molecules", Phys. Rev. Lett. **124**, 153602 (2020).

[8] J. Schmitt et al., "Spontaneous Symmetry Breaking and Phase Coherence of a Photon Bose-Einstein Condensate Coupled to a Reservoir", Phys. Rev. Lett. **116**, 033604 (2016).

[9] A. Einstein, "Quantentheorie des einatomigen idealen Gases", Sitzungsberichte der Preussischen Akademie der Wissenschaften. B. 1. S. 3 (1925).

[10] M. H. Anderson et al., "Observation of Bose-Einstein Condensation in a Dilute Atomic Vapor", Science **269**, 198–201 (1995).

[11] K. Davis et al., "Bose-Einstein Condensation in a Gas of Sodium Atoms", Phys. Rev. Lett. **75**, 3969 (1995).

[12] M. W. Zwierlein et al., "Formation Dynamics of a Fermion Pair Condensate", Phys. Rev. Lett. **94**, 180401 (2005).

[13] F. Dalfovo et al., "Theory of Bose-Einstein condensation in trapped gases", Rev. Mod. Phys. **71**, 463–512 (1999).

[14] E. P. Gross, " Structure of a quantized vortex in boson systems", Nuovo Cimento **20**, 454–477 (1961).

[15] L. Pitaevskii, "Vortex Lines in an Imperfect Bose Gas ", JETP **13**, 451 (1961).

[16] M. Planck, "Über das Gesetz der Energieverteilung im Normalspectrum", Annalen der Physik **309**, 553–563 (1901).

[17] O. Gabriel, *Franck-Condon-Prinzip.svg*, (2007) https://commons.wikimedia.org/wiki/File:Franck-Condon-Prinzip.svg.

[18] M. Sakai et al., "Chapter 12 - Two-color picosecond time-resolved infrared super-resolution microscopy", in *Nano biophotonics*, Vol. 3, edited by H. Masuhara et al., Handai Nanophotonics (Elsevier, 2007), pp. 189–195.

[19] M. Kasha, "Characterization of electronic transitions in complex molecules", Discuss. Faraday Soc. **9**, 14–19 (1950).

[20] J. Klaers, "The thermalization, condensation and flickering of photons", Journal of Physics B: Atomic, Molecular and Optical Physics **47**, 243001 (2014).

[21] S. Weinberg, *The Quantum Theory of Fields, Volume 1: Foundations* (Cambridge University Press, 1995).

[22] P. Kirton and J. Keeling, "Thermalization and breakdown of thermalization in photon condensates", Phys. Rev. A **91**, 033826 (2015).

[23] P. Kirton and J. Keeling, "Nonequilibrium Model of Photon Condensation", Phys. Rev. Lett. **111**, 100404 (2013).

[24] M. Radonjić et al., "Interplay of coherent and dissipative dynamics in condensates of light", New Journal of Physics **20**, 055014 (2018).

[25] F. E. Öztürk et al., "Observation of a non-Hermitian phase transition in an optical quantum gas", Science **372**, 88–91 (2021).

[26] N. Karve and R. Loganayagam, "Heisenberg Picture for Open Quantum Systems.", arXiv:2011.15118 (2020).

[27] R. Kubo, "Generalized Cumulant Expansion Method", Journal of the Physical Society of Japan **17**, 1100–1120 (1962).

[28] A. Kamenev, *Field Theory of Non-Equilibrium Systems* (Cambridge University Press, 2011).

[29] J. Rammer, *Quantum Field Theory of Non-equilibrium States* (Cambridge University Press, 2007).

[30] G. Stefanucci and R. van Leeuwen, *Nonequilibrium Many-Body Theory of Quantum Systems: A Modern Introduction* (Cambridge University Press, 2013).

[31] E. A. Calzetta and B.-L. B. Hu, *Nonequilibrium Quantum Field Theory* (Oxford University Press, 2009).

[32] J. Berges, "Nonequilibrium Quantum Fields: From Cold Atoms to Cosmology", arXiv:1503.02907 (2015).

[33] J. Berges, "Introduction to nonequilibrium quantum field theory", AIP Conf. Proc. **739**, edited by M. Bracco et al., 3–62 (2004).

[34] L. M. Sieberer et al., "Keldysh field theory for driven open quantum systems", Reports on Progress in Physics **79**, 096001 (2016).

[35] C.-H. Huang et al., "Modeling particle loss in open systems using Keldysh path integral and second order cumulant expansion", Phys. Rev. Res. **5**, 043192 (2023).

[36] A. McDonald and A. A. Clerk, "Exact Solutions of Interacting Dissipative Systems via Weak Symmetries", Phys. Rev. Lett. **128**, 033602 (2022).

[37] A. Griffin et al., *Bose-Condensed Gases at Finite Temperatures* (Cambridge University Press, 2009).

[38] F. Meirinhos et al., "Adaptive numerical solution of Kadanoff-Baym equations", SciPost Phys. Core **5**, 030 (2022).

[39] E. Hairer et al., *"Solving Ordinary Differential Equations: Vol.~I Nonstiff Problems"*, Vol. 8, Springer Series in Computational Mathematics (Springer, 1987).

[40] J. Stoer and R. Bulirsch, *Introduction to Numerical Analysis*, 3rd ed., Vol. 12, Texts in applied mathematics (Springer, New York, 2002).

[41] G. Baym and L. P. Kadanoff, "Conservation Laws and Correlation Functions", Phys. Rev. **124**, 287–299 (1961).

[42] T. D. Lee and C. N. Yang, "Many-Body Problem in Quantum Statistical Mechanics. IV. Formulation in Terms of Average Occupation Number in Momentum Space", Phys. Rev. **117**, 22–36 (1960).

[43] J. M. Luttinger and J. C. Ward, "Ground-State Energy of a Many-Fermion System. II", Phys. Rev. **118**, 1417–1427 (1960).

[44] G. Baym, "Self-Consistent Approximations in Many-Body Systems", Phys. Rev. **127**, 1391–1401 (1962).

[45] C. De Dominicis, "Variational Formulations of Equilibrium Statistical Mechanics", Journal of Mathematical Physics **3**, 983–1002 (1962).

[46] C. de Dominicis and P. C. Martin, "Stationary Entropy Principle and Renormalization in Normal and Superfluid Systems. I. Algebraic Formulation", J. Math. Phys. **5**, 14–30 (1964).

[47] J. M. Cornwall et al., "Effective Action for Composite Operators", Phys. Rev. D **10**, 2428–2445 (1974).

[48] A. Vasiliev, *Functional Methods in Quantum Field Theory and Statistical Physics* (Taylor & Francis, Jan. 2019).

[49] G. Aarts et al., "Far from equilibrium dynamics with broken symmetries from the 2PI - 1/N expansion", Phys. Rev. D **66**, 045008 (2002).

[50] H. van Hees and J. Knoll, "Renormalization in self-consistent approximation schemes at finite temperature: Theory", Phys. Rev. D **65**, 025010 (2001).

[51] H. van Hees and J. Knoll, "Renormalization of self-consistent approximation schemes at finite temperature. II. Applications to the sunset diagram", Phys. Rev. D **65**, 105005 (2002).

[52] H. van Hees and J. Knoll, "Renormalization in selfconsistent approximation schemes at finite temperature. 3. Global symmetries", Phys. Rev. D **66**, 025028 (2002).

[53] J. Berges et al., "Nonperturbative renormalization for 2PI effective action techniques", Annals Phys. **320**, 344–398 (2005).

[54] A. Pilaftsis and D. Teresi, "Symmetry Improved CJT Effective Action", Nuclear Physics B **874**, 594–619 (2013).

[55] G. Markó et al., "Loss of solution in the symmetry improved Φ-derivable expansion scheme", Nuclear Physics B **913**, 405–424 (2016).

[56] M. Kajan, "Slave-Particle representation of Jaynes-Cummings Models", MA thesis (Rheinische Friedrich-Wilhelms-Universität Bonn, Mar. 2019).

[57] Tim Lappe, "Non-Markovian Dynamics of Open Bose-Einstein Condensates", PhD thesis (Rheinische Friedrich-Wilhelms-Universität Bonn, Mar. 2021).

[58] T. Bode et al., "Non-markovian dynamics of open quantum systems via auxiliary particles with exact operator constraint", Phys. Rev. Res. **6**, 013220 (2024).

[59] P. Coleman, "New approach to the mixed-valence problem", Phys. Rev. B **29**, 3035–3044 (1984).

[60] M. Eckstein and P. Werner, "Nonequilibrium dynamical mean-field calculations based on the noncrossing approximation and its generalizations", Phys. Rev. B **82**, 115115 (2010).

[61] H. Aoki et al., "Nonequilibrium dynamical mean-field theory and its applications", Rev. Mod. Phys. **86**, 779–837 (2014).

[62] H. U. R. Strand et al., "Nonequilibrium Dynamical Mean-Field Theory for Bosonic Lattice Models", Phys. Rev. X **5**, 011038 (2015).

[63] A. J. Moilanen et al., "Mode switching dynamics in organic polariton lasing", Phys. Rev. B **106**, 195403 (2022).

[64] *Pypbec*, https://github.com/photonbec/PyPBEC, 2020.

[65] R. A. Nyman, *Absorption and Fluorescence spectra of Rhodamine 6G* (Zenodo, Apr. 2017).

[66] E. Stein and A. Pelster, "Photon BEC with thermo-optic interaction at dimensional crossover", New Journal of Physics **24**, 023032 (2022).

[67] Y. Tang et al., "Breakdown of Temporal Coherence in Photon Condensates", Phys. Rev. Lett. **132**, 173601 (2024).

[68] J. Marelic et al., "Spatiotemporal coherence of non-equilibrium multimode photon condensates", New Journal of Physics **18**, 103012 (2016).

[69] V. V. Kocharovsky et al., "Fluctuations in Ideal and Interacting Bose–Einstein Condensates: From the Laser Phase Transition Analogy to Squeezed States and Bogoliubov Quasiparticles", in , Vol. 53, edited by G. Rempe and M. Scully, Advances In Atomic, Molecular, and Optical Physics (Academic Press, 2006), pp. 291–411.

[70] C. Kurtscheid et al., "Thermally condensing photons into a coherently split state of light", Science **366**, 894–897 (2019).

[71] B. Li et al., "On the equivalence between squeezing and entanglement potential for two-mode Gaussian states", Scientific Reports **13**, 11722 (2023).

[72] P. Fowler-Wright et al., "Efficient Many-Body Non-Markovian Dynamics of Organic Polaritons", Phys. Rev. Lett. **129**, 173001 (2022).

[73] V. Rokaj et al., "Free electron gas in cavity quantum electrodynamics", Phys. Rev. Res. **4**, 013012 (2022).

[74] M. Wagner, "Exakte Berechnung von Franck-Condon-Integralen", Zeitschrift für Naturforschung A **14**, 81–91 (1959).

[75] S. Koide, "Über die Berechnung von Franck-Condon-Integralen", Zeitschrift für Naturforschung A **15**, 123–128 (1960).

Appendix

Correlation functions of the polaron transform

We want to show here how the polaron correlation function can be calculated assuming a thermal phonon state. This can be done using the Schwinger-Keldysh formalism introduced in chapter 2. We take a rather general approach here and only assume non-interacting thermal phonons so that the bath density of state $\rho(\omega)$ can be easily changed afterwards. This allows us to write the phonon greater and lesser Green functions in frequency space as

$$G^{>}(\omega) = -i\rho(\omega)b(\beta\omega) \quad , \quad G^{<} = -i\rho(\omega)(b(\beta\omega)+1)\,.$$

The action can then be written in frequency space as

$$S = \int d\nu \sum_{\sigma,\sigma'\in\pm} \vec{\phi}^*_\sigma(\nu) G^{-1}_{\sigma,\sigma'}(\nu)\vec{\phi}_{\sigma'}(\nu) = \int d\nu \vec{\phi}^*(\nu) G^{-1}(\nu)\vec{\phi}(\nu)$$

The average of $\langle D(t)\rangle$ is the same on both branches and time independent, due to thermal equilibrium. It can directly be computed from the path integral using $\eta_+ = (1,0)^T$

$$\langle D(t)\rangle = \int \frac{D[\phi]}{\sqrt{\det(G^{-1})}} \exp(i\int d\nu \left(\vec{\phi}^*(\nu)G^{-1}(\nu)\vec{\phi}(\nu) + 2s\left(e^{i\nu t}\phi^*_+(\nu) - \phi_+(\nu)e^{-i\nu t}\right)\right)$$

$$= \int \frac{D[\phi]}{\sqrt{\det(G^{-1})}} \exp(i\int d\nu \left((\vec{\phi}^*(\nu) + 2se^{-i\nu t}\eta_+^T G(\nu))G^{-1}(\nu)(\vec{\phi}(\nu) - 2sG(\nu)\eta_+ e^{i\nu t}) + 4S\eta_+^T G(\nu)\eta_+\right)$$

$$= \exp\left[i4s^2\int d\nu G^T(\nu)\right] = \exp\left[-2s^2\int d\nu\rho(\nu)(1+2b(\beta\nu))\right] \qquad \text{with} \quad b(x) = \frac{1}{e^x-1}\,.$$

For the two-time correlator we obtain in the same fashion

$$\langle D_-(t)D^\dagger_+(t')\rangle = \int \frac{D[\phi]}{\sqrt{\det(G^{-1})}} \exp(i\int d\nu\Big(\vec{\phi}^*(\nu)G^{-1}(\nu)\vec{\phi}(\nu)$$
$$+ 2s\Big(e^{i\nu t}\phi^*_-(\nu) - \phi_-(\nu)e^{-i\nu t} - e^{i\nu t'}\phi^*_+(\nu) + \phi_+(\nu)e^{-i\nu t'}\Big)\Big)$$

$$= \int \frac{D[\phi]}{\sqrt{\det(G^{-1})}} \exp\big[i\int d\nu\big\{(\vec{\phi}^*(\nu) + 2s(e^{-i\nu t'},-e^{-i\nu t})G(\nu))G^{-1}(\nu)(\vec{\phi}(\nu) - 2sG(e^{i\nu t'},-e^{i\nu t})^T)$$
$$+ 4s^2(e^{-i\nu t'},-e^{-i\nu t})G(\nu)(e^{i\nu t'},-e^{i\nu t})^T\big\}\big]$$
$$= \exp\big[4is^2\int d\nu\left(G^T(\nu) + G^{\tilde{T}}(\nu) - e^{-i\nu(t-t')}G^{>}(\nu) - e^{i\nu(t-t')}G^{<}(\nu)\right)\big]$$
$$= \exp\big[4is^2\int d\nu\left((G^{>}(\nu)+G^{<}(\nu))(1-\cos(\nu(t-t')) + i\sin(\nu(t-t'))(G^{>}(\nu)-G^{<}(\nu))\right)\big]$$
$$= \exp\big[4is^2\int d\nu\left((G^{>}(\nu)+G^{<}(\nu))2\sin^2(\nu(t-t')) + i\sin(\nu(t-t'))(G^{>}(\nu)-G^{<}(\nu))\right)\big]$$
$$= \exp\big[-4s^2\int d\nu\rho(\nu)\left(2(1+2b(\beta\nu))\sin^2(\nu(t-t')) + i\sin(\nu(t-t'))\right)\big]$$

$$\langle D_-^\dagger(t')D_+(t)\rangle = \int \frac{D[\phi]}{\sqrt{\det(G^{-1})}} \exp(i\int d\nu\Big(\vec{\phi}^*(\nu)G^{-1}(\nu)\vec{\phi}(\nu) + 2s\Big(e^{i\nu t}\phi_+^*(\nu) - \phi_+(\nu)e^{-i\nu t} - e^{i\nu t'}\phi_-^*(\nu) + \phi_-(\nu)e^{-i\nu t'}\Big)\Big)$$

$$= \int \frac{D[\phi]}{\sqrt{\det(G^{-1})}} \exp\big[i\int d\nu\big\{(\vec{\phi}^*(\nu) + 2s(e^{-i\nu t}, -e^{-i\nu t'})G(\nu))G^{-1}(\nu)(\vec{\phi}(\nu) - 2sG(e^{i\nu t}, -e^{i\nu t'})^T) + 4s^2(e^{-i\nu t}, -e^{-i\nu t'})G(\nu)(e^{i\nu t}, -e^{i\nu t'})^T\big\}\big]$$

$$= \exp\big[4is^2\int d\nu\,\Big(G^T(\nu) + G^{\tilde{T}}(\nu) - e^{i\nu(t-t')}G^>(\nu) - e^{-i\nu(t-t')}G^<(\nu)\Big)\,\big]$$

$$= \exp\big[-4s^2\int d\nu\rho(\nu)\,\Big(2(1+2b(\beta\nu))\sin^2(\nu(t-t')) - i\sin(\nu(t-t'))\Big)\,\big]$$

The symmetry properties are $\big[\mathcal{D}^>(\tau)\big]^* = \mathcal{D}^>(-\tau) = \mathcal{D}^<(\tau) = \big[\mathcal{D}^<(-\tau)\big]^*$
The two-time correlators $\mathcal{F}$ are given by

$$\langle D_-(t)D_+(t')\rangle = \int \frac{D[\phi]}{\sqrt{\det(G^{-1})}} \exp(i\int d\nu\Big(\vec{\phi}^*(\nu)G^{-1}(\nu)\vec{\phi}(\nu) + 2s\Big(e^{i\nu t}\phi_-^*(\nu) - \phi_-(\nu)e^{-i\nu t} + e^{i\nu t'}\phi_+^*(\nu) - \phi_+(\nu)e^{-i\nu t'}\Big)\Big)$$

$$= \int \frac{D[\phi]}{\sqrt{\det(G^{-1})}} \exp\big[i\int d\nu\big\{(\vec{\phi}^*(\nu) - 2s(e^{-i\nu t'}, e^{-i\nu t})G(\nu))G^{-1}(\nu)(\vec{\phi}(\nu) + 2sG(e^{i\nu t'}, e^{i\nu t})^T) + 4s^2(e^{-i\nu t'}, e^{-i\nu t})G(\nu)(e^{i\nu t'}, e^{i\nu t})^T\big\}\big]$$

$$= \exp\big[4is^2\int d\nu\,\Big(G^T(\nu) + G^{\tilde{T}}(\nu) + e^{-i\nu(t-t')}G^>(\nu) + e^{i\nu(t-t')}G^<(\nu)\Big)\,\big]$$

$$= \exp\big[4is^2\int d\nu\,\big((G^>(\nu) + G^<(\nu))(1+\cos(\nu(t-t')) - i\sin(\nu(t-t'))(G^>(\nu) - G^<(\nu))\big)\,\big]$$

$$= \exp\big[4is^2\int d\nu\,\Big((G^>(\nu) + G^<(\nu))2\cos^2(\nu(t-t')) - i\sin(\nu(t-t'))(G^>(\nu) - G^<(\nu))\Big)\,\big]$$

$$= \exp\big[-4s^2\int d\nu\rho(\nu)\,\Big(2(1+2b(\beta\nu))\cos^2(\nu(t-t')) - i\sin(\nu(t-t'))\Big)\,\big] \qquad (11.5)$$

This lets us conclude the symmetry property as $\big[\mathcal{F}(\tau)\big]^\dagger = \mathcal{F}(-\tau)$. Another interesting property of these correlators is the product of them follows $\langle D_-(t)D_+^\dagger(t')\rangle\,\langle D_-(t)D_+(t')\rangle = \langle D\rangle^4$.

Polaron transformation in auxiliary particle representation

Most of the following section was used in the master thesis of the author [56].

The coupling matrix $\gamma_{n,m}$ is composed of the unitary transformations, which diagonalizes the excited and ground state Hamiltonian. We want to find an analytic form for the structure of the matrix. Our starting point, before the auxiliary particle transformation, was a Hamiltonian containing operators of harmonic oscillators. Here, the coupling term comes from a position shift of the oscillators to $\pm x_0$ in excited and ground state. The transformation diagonalizing the molecule part should be a translation back to the original position. We now use results obtained from the real space representation of the harmonic oscillator problem and apply these properties to the auxiliary particle problem. To this end, we recapitulate here various results of [74] [75]. The unitary transformation is the shift operator and can be considered in a matrix form connecting the wavefunction in the two representations. Its entries are the overlap integrals of the shifted oscillator wavefunction with the unshifted ones.

$$U^{\pm}_{n,m} = \int dx \Psi_n(x \pm x_0)\Psi_m(x)\,. \tag{11.6}$$

These elements are called the Franck-Condon coefficients or integrals.
The route we want to take is to derive symmetry and addition properties for these elements, which allows us to show that the transformation needed to diagonalise the Hamiltonian has the same properties.
We first consider the action of an exponential of creation and destruction operators of the harmonic oscillator on a function composed of these:

$$e^{\pm x_0 a^\dagger} f(a^\dagger, a) = f(a^\dagger, a \mp x_0) e^{\pm x_0 a^\dagger} \qquad e^{\pm x_0 a} f(a^\dagger, a) = f(a^\dagger \pm x_0, a) e^{\pm x_0 a} \tag{11.7}$$

From here, it directly follows that

$$U = \exp(x_0(a - a^\dagger)) \qquad U a^\dagger a = (a^\dagger + x_0)(a + x_0)U = (a^\dagger a + x_0(a^\dagger + a) + x_0^2)U\,.$$

This can be used to find relations between the matrix elements of U as

$$\begin{aligned}
\Rightarrow n U_{m,n} &= n \int dx \Psi_m(x) U \Psi_n(x) = \int dx \Psi_m(x) U a^\dagger a \Psi_n(x) \\
&= \int dx \Psi_m(x)(a^\dagger a + x_0(a^\dagger + a) + x_0^2) U \Psi_n(x) \\
&= m U_{m,n} + x_0\sqrt{m} U_{m-1,n} + x_0\sqrt{m+1} U_{m+1,n} + x_0^2 U_{m,n} \\
\Rightarrow \sqrt{n+1} U_{m,n+1} &= \int dx \Psi_m(x) U a^\dagger \Psi_n(x) = \int dx \Psi_m(x)(a^\dagger + x_0) U \Psi_n(x) \\
&= \sqrt{m} U_{m-1,n} + x_0 U_{m,n}
\end{aligned}$$

Considering now the with ω scaled Hamiltonian of our auxiliary particles under this unitary transformation:

$$\begin{aligned}
&\sum_n n d_n^\dagger d_n + s\sqrt{n+1}(d_{n+1}^\dagger d_n + d_n^\dagger d_{n+1}) \\
&= \sum_{n,k,l} n d_k^\dagger d_l U_{k,n}^\dagger U_{n,l} + s\sqrt{n+1}(d_k^\dagger d_l U_{k,n+1}^\dagger U_{n,l} + d_k^\dagger d_l U_{k,n}^\dagger U_{n+1,l})
\end{aligned}$$

We separate the operator content from the matrix elements of the unitary transformation and evaluate the sum over the index n with the properties found earlier.

$$\sum_{n,k,l} nU^\dagger_{k,n}U_{n,l} + s\sqrt{n+1}(U^\dagger_{k,n+1}U_{n,l} + U^\dagger_{k,n}U_{n+1,l})$$
$$= \sum_{n,k,l} kU^\dagger_{k,n}U_{n,l} - s\sqrt{k}U^\dagger_{k-1,n}U_{n,l} - s\sqrt{k+1}U^\dagger_{k+1,n}U_{n,l} + s^2U^\dagger_{k,n}U_{n,l}$$
$$+ s\sqrt{k}U^\dagger_{k-1,n}U_{n,l} + s\sqrt{k+1}U^\dagger_{k+1,n}U_{n,l} - 2s^2U^\dagger_{k,n}U_{n,l} = \sum_{n,k,l}(k-s^2)U^\dagger_{k,n}U_{n,l} = \sum_{k,l}(k-s^2)\delta_{k,l}$$

Therefore, the transformation diagonalises also the auxiliary particle Hamiltonian. Note here that the unitary transformations for both oscillators are complex conjugates of each other, which is equivalent to a shift by $+s$ and $-s$.
The matrix elements can be obtained with the wavefunctions of the harmonic oscillators in dimensionless units

$$\Psi_n(x) = \frac{1}{\sqrt{\sqrt{\pi}2^n n!}} e^{-\frac{x^2}{2}} H_n(x)$$

here $H_n(x)$ are the Hermite polynomials with the properties,

$$H_n(x+a) = \sum_{i=0}^{n} \binom{n}{i} H_i(x)(2a)^{n-i} \tag{11.8}$$

$$\int dx H_n(x)H_m(x)e^{-x^2} = \sqrt{\pi}2^n n!\delta_{n,m} \tag{11.9}$$

The overlap integrals can be calculated as

$$\frac{1}{\sqrt{\pi 2^{n+m}m!n!}} \int dx e^{-\frac{(x-a)^2}{2}} H_n(x-a)e^{-\frac{x^2}{2}} H_m(x)$$
$$= \frac{1}{\sqrt{\pi 2^{n+m}m!n!}} \int dx e^{-\frac{(x-a/2)^2}{2}} H_n(x-a/2)e^{-\frac{(x+a/2)^2}{2}} H_m(x+a/2)$$
$$= \frac{1}{\sqrt{\pi 2^{n+m}m!n!}} e^{-\frac{a^2}{4}} \sum_{i=0}^{n}\sum_{j=0}^{m} \binom{n}{i}\binom{m}{j}(-a)^{n-i}(a)^{m-j} \int dx e^{-x^2} H_i(x)H_j(x)$$
$$= \frac{1}{\sqrt{\pi 2^{n+m}m!n!}} e^{-\frac{a^2}{4}} \sum_{i=0}^{n}\sum_{j=0}^{m} \binom{n}{i}\binom{m}{j}(-a)^{n-i}(a)^{m-j}\sqrt{\pi}2^i i!\delta_{j,i}$$
$$= \frac{1}{\sqrt{2^{n+m}m!n!}} e^{-\frac{a^2}{4}} \sum_{i=0}^{\min(n,m)} \binom{n}{i}\binom{m}{i}(-a)^{n-i}(a)^{m-i}2^i i!$$
$$= \frac{1}{\sqrt{m!n!}} e^{-\frac{a^2}{4}} (-1)^n (\frac{a}{\sqrt{2}})^{m+n} \sum_{i=0}^{\min(n,m)} \binom{n}{i}\binom{m}{i}(-a^2/2)^{-i} i!$$
$$= \frac{1}{\sqrt{m!n!}} e^{-\frac{a^2}{4}} (-1)^{n-\min(n,m)} (\frac{a}{\sqrt{2}})^{m+n} (\frac{a}{\sqrt{2}})^{-2\min(n,m)} U[-\min(n,m), |n-m|+1, a^2/2]$$

Here $U[a,b,x]$ is Krummers function of second kind, which is connected to the generalised Laguerre polynomials through

$$L^\alpha_n(x) = \frac{(-1)^n}{n!} U[-n, \alpha+1, x]\,. \tag{11.10}$$

With this, we find

$$U_{n,m} = e^{-\frac{a^2}{4}} \begin{cases} \left(\frac{a}{\sqrt{2}}\right)^{m-n} \sqrt{\frac{n!}{m!}} L_n^{m-n}\left(\frac{a^2}{2}\right) & m > n \\ \left(\frac{-a}{\sqrt{2}}\right)^{n-m} \sqrt{\frac{m!}{n!}} L_m^{n-m}\left(\frac{a^2}{2}\right) & n > m \end{cases} \tag{11.11}$$

Under the transformation, the interaction with the photons transforms as

$$\begin{aligned} \sum_n \gamma a^\dagger d_{g,n}^\dagger d_{e,n} &= \sum_{n,l,k} \gamma a^\dagger d_{g,k}^\dagger d_{e,l} U_{k,n}^\dagger(x_0) U_{n,l}(-x_0) = \sum_{n,l,k} \gamma a^\dagger d_{g,k}^\dagger d_{e,l} U_{k,n}^\dagger(x_0) U_{n,l}^\dagger(x_0) \\ \Rightarrow \gamma_{k,l} &= \sum_n \gamma U_{g,k,n}^\dagger(x_0) U_{g,n,l}^\dagger(x_0) = \gamma U_{g,k,l}^\dagger(2x_0) \\ &= \gamma e^{-x_0^2} \begin{cases} \left(x_0\sqrt{2}\right)^{l-k} \sqrt{\frac{k!}{l!}} L_k^{l-k}\left(2x_0^2\right) & l > k \\ \left(-x_0\sqrt{2}\right)^{k-l} \sqrt{\frac{l!}{k!}} L_l^{k-l}\left(2x_0^2\right) & k > l \end{cases} \end{aligned}$$

As already mentioned, we will not use this representation further since, in the fully interacting theory, the phonon quantum numbers will mix due to the photon interaction anyway.